Defense Threat Reduction Agency
8725 John J. Kingman Road, MS-6201
Fort Belvoir, VA 22060-6201

TECHNICAL REPORT

Medical Modeling of Particle Size Effects for CB Inhalation Hazards

Distribution A. Approved for public release; distribution is unlimited.

September 2015

Kyle K. Millage et al.

Prepared by:
Applied Research Associates, Inc.
Health Effects and Medical
Response Group
801 N. Quincy St. STE 700
Arlington, VA 22060

DESTRUCTION NOTICE:

REPORT DOCUMENTATION PAGE

Form Approved
OMB No. 0704-0188

1. REPORT DATE *(DD-MM-YYYY)* 00-09-2015	2. REPORT TYPE Technical	3. DATES COVERED *(From - To)* April 9, 2007 - March 9, 2009
4. TITLE AND SUBTITLE Medical Modeling of Particle Size Effects for CB Inhalation Hazards		**5a. CONTRACT NUMBER** DTRA01-03-D-0014-0025
		5b. GRANT NUMBER
		5c. PROGRAM ELEMENT NUMBER
6. AUTHOR(S) Kyle K. Millage, Gene E. McClellan, Bahman Asgharian, Joshua J. Bergman, Darren R. Oldson, and Sharon A. Watson		**5d. PROJECT NUMBER**
		5e. TASK NUMBER
		5f. WORK UNIT NUMBER
7. PERFORMING ORGANIZATION NAME(S) AND ADDRESS(ES) Applied Research Associates, Inc. Health Effects and Medical Response Group 801 N. Quincy St. STE 700 Arlington, VA 22203		**8. PERFORMING ORGANIZATION REPORT NUMBER**
9. SPONSORING / MONITORING AGENCY NAME(S) AND ADDRESS(ES) Defense Threat Reduction Agency 8725 John J. Kingman Road, STOP 6201 Fort Belvoir, VA 22060-6201		**10. SPONSOR/MONITOR'S ACRONYM(S)** DTRA
		11. SPONSOR/MONITOR'S REPORT NUMBER(S) DTRA-TR-15-10

12. DISTRIBUTION / AVAILABILITY STATEMENT

Approved for public release; distribution is unlimited.

13. SUPPLEMENTARY NOTES

The work was sponsored by the Defense Threat Reduction Agency.

14. ABSTRACT

In this project, Applied Research Associates, Inc. (ARA) developed the Deposition And Response in the Respiratory Tract (DARRT) model; an improved medical model of particle size effects for inhalation hazards from chemical and biological (CB) agents. This project was initiated to improve modeling of the variation in human response caused by differences in particle sizes, in particular, for coarse particles that may be present near a dissemination source and may remain suspended long enough in an urban environment to expose large numbers of people. Plume dispersion calculations with the Defense Threat Reduction Agency's (DTRA's) Hazard Prediction and Assessment Capability (HPAC) show that, contrary to common beliefs, particles as large as 20 to 40 microns in diameter can be a significant hazard tens of kilometers downwind of a release. DARRT predicts the probability of infection or injury from inhalation exposure to aerosol hazards of CB agents with aerodynamic diameters between 0.01 and 100 microns and describes the resulting medical impact. Many current models assume that only the 1 to 5 micron "respirable" particles capable of reaching the pulmonary region of the respiratory system are of concern; however, we find that inclusion of coarse (greater than 5 micron) particle deposition is important, as well.

15. SUBJECT TERMS

Inhalation mechanics, FXCODA, DARRT, bioagent, aerosol, particle size, particle deposition, biological agents, ricin, tularemia

16. SECURITY CLASSIFICATION OF:			17. LIMITATION OF ABSTRACT	18. NUMBER OF PAGES	19a. NAME OF RESPONSIBLE PERSON Dr. Chris Kiley
a. REPORT Unclassified	**b. ABSTRACT** Unclassified	**c. THIS PAGE** Unclassified	UU		**19b. TELEPHONE NUMBER** *(include area code)* 703-767-3460

Standard Form 298 (Rev. 8-98)
Prescribed by ANSI Std. Z39.18

Preface

The research and development work described in this report was conducted for Project CB06MSB096 of the Joint Science and Technology Office (JSTO) of the Department of Defense (DoD) Chemical and Biological Defense (CBD) Program. JSTO is also the Chemical/Biological Technologies Directorate (RD-CB) in the Research and Development Enterprise of the Defense Threat Reduction Agency (DTRA). Project CB06MSB096 is titled *Medical Modeling of Particle Size Effects for Inhalation Hazards*.

The first year of this project was initiated by Mr. Charles Fromer of the Information Systems Capability Development Division (RD-CBI). It was funded as an option under DTRA Contract Number DTRA01-03-D-0014-0015 with Contract Officer's Representative (COR) Mr. Eric Nelson of the Modeling Division (RD-NTM) in DTRA's Nuclear Technologies Directorate. The second and third years of the project were funded under DTRA Contract Number DTRA01-03-D-0014-0025. The CORs for this contract were Mrs. Stephanie Hamilton of RD-CBI and, subsequently, Dr. Christopher Kiley, also of RD-CBI. This final report covers all of Project CB06MSB096.

In addition to the support and guidance provided by the above mentioned DTRA personnel, the authors thank Dr. Louise Pitt, Director of the Center for Aerobiological Sciences at the U.S. Army Medical Research Institute of Infectious Diseases, for initial encouragement and direction.

Table of Contents

Attachment 1 - A Review of Inhalability Fraction Models: Discussion and Recommendations

Attachment 2 - Comparison of Stochastic, Symmetric and 5-Lobe Asymmetric Lung Models in MPPD

Attachment 3 - Effects of Particle Size on Physiological Responses to BW Agent Aerosols

Attachment 4 - FXCODA: Tularemia and Ricin Models with Regional Particle Deposition

Attachment 5 - Respiratory Effects of HD Exposure in Humans

List of Figures

List of Tables

1. Executive Summary

In this project, Applied Research Associates, Inc. (ARA) developed the Deposition And Response in the Respiratory Tract (DARRT) model; an improved medical model of particle size effects for inhalation hazards from chemical and biological (CB) agents. This project was initiated to improve modeling of the variation in human response due to differences in particle sizes, in particular, for coarse particle sizes that may be present near a dissemination source and may remain suspended long enough in an urban environment to expose large numbers of people. In addition, plume dispersion calculations with the Defense Threat Reduction Agency's (DTRA's) Hazard Prediction and Assessment Capability (HPAC) show that, contrary to common wisdom, particles as large as 20 to 40 microns in diameter can be a significant hazard for tens of kilometers downwind of a release. DARRT predicts the probability of infection or injury from exposure to aerosol hazards of CB agents with aerodynamic diameters between 0.01 and 100 microns and describes the resulting medical impact. Many current models assume that only the 1 to 5 micron "respirable" particles capable of reaching the pulmonary region of the respiratory system are of concern; however, we find that inclusion of coarse (greater than 5 micron) particle deposition is important, as well. Coarse particle deposition in the nose, mouth and throat can pose a substantial health risk, particularly for infectious agents.

The DARRT model uses the Multiple Path Particle Dosimetry (MPPD) model to estimate the deposited (retained) doses of inhaled aerosols by region of the respiratory tract. Several modifications were made to MPPD to improve its applicability to particle size distributions of interest to the CB defense community and provide a solid foundation for improving associated human response models. An improved model of inhalability, a measure of the fraction of the ambient concentration of particles that actually enter the head through the nose or mouth during inspiration, was developed and implemented with MPPD. In addition, the particle size range was extended to include particle sizes from 10 nanometer (nm) to 100 microns (μm) and an improved clearance model for the extrathoracic region was implemented. The MPPD model was also modified to accept input based on particle size bins to be consistent with data transfer from transport and dispersion models such as the SCIPUFF (Second-Order Closure Integrated PUFF) model in HPAC. The DARRT model requires material property data for the CB agent of interest, such as material density and organism concentration. In the current software implementation of the DARRT model for HPAC and the Joint Effects Model (JEM), this information is read from the material file. With the new DARRT model, the user can now also control some inhalation variables such as breathing rate. Details of the MPPD model and its implementation are contained in Section 3, *Implementation of a Particle Deposition Model for the Respiratory Tract.*

Models of human response to biological agents previously implemented in HPAC and JEM all assume that the presented dose (the time-integrated, ambient agent concentration multiplied by the breathing rate) is completely effective in producing disease or injury. To support this assumption, the material property files for dry agents specify only a single particle size bin of 4.9-5.1 micron. As noted above, this simplifying assumption was based on the understanding that most effects, particularly for biological agents, are associated with pulmonary deposition of "respirable" particles of the agent. Although some of the source modules in HPAC and JEM, such as CBWPN, allow the user to set a particle size distribution in the form of a lognormal distribution for the released biological agent, the transport and dispersion calculation performed by SCIPUFF has only the single particle size bin provided by the material file to work with and so puts all the material in that bin, resulting in a mono-dispersed aerosol of 5 microns in diameter. As part of the DARRT implementation, we added size bins to the material files for the dry particulate form of ricin and tularemia to allow realistic particle size distributions. As a result, not only will the implementation of DARRT improve the human response modeling of ricin and tularemia, but additionally, the improvement in the associated material files will improve the transport and dispersion modeling of these two agents.

The current implementation of the DARRT model includes human response models for *F. tularensis* (the organism causing tularemia), ricin, and sulfur mustard (HD); data for additional agents have been reviewed in this project and models can be developed in the future. The DARRT human response model predicts the differences in disease manifestation for tularemia depending on the particle deposition location. Historical data indicates the probability of infection for tularemia is a function of the number of agent-containing particles deposited in the extrathoracic (ET) or pulmonary (P) regions. Extrathoracic deposition results in an upper respiratory infection, while pulmonary deposition results in a pneumonic infection. Details of the model are contained in Section 4, *Development of a Human Response Model Accounting for Aerosol Size – Prototype Agent Francisella tularensis.*

As noted, the probability of tularemia infection is a function of the number of deposited agent-containing particles (ACPs). During this project we developed a method for assessing the probability that a particle of a given size is actually an ACP. Particles can consist of carrier material as well as *F. tularensis* organisms. Larger particles will often contain multiple organisms and the smaller particles can contain no organisms. As the particle size decreases toward that of an organism (~1 micron for *F. tularensis* bacteria), some particles may contain no cells and simply consist of carrier material. Obviously, these particles cannot cause an infection. Our method of calculating the probability of a particle being an ACP is described in Section 3.4, *Agent Containing Particle Calculation.* This calculation is essential when evaluating the potential hazard of threats developed at varying levels of sophistication.

The DARRT model of human response to ricin, a toxin of biological origin, is based on the mass of ricin deposited in the pulmonary region and correlates the human response with pulmonary deposition of the particles. While ricin can be lethal by other routes of exposure such as injection, aerosolized ricin has been shown to be lethal only by pulmonary deposition. Details of the pulmonary ricin model are contained in Section 5.1, *Development of Additional Models for Particle Size-Dependent Health Effects, Ricin*.

The DARRT model was also developed for inhalation of droplets associated with liquid chemical agents. Some chemical agents, such as HD can cause ocular, cutaneous and respiratory responses. Typically one considers inhaled vapor as the only respiratory hazard; however, under certain environmental conditions aerosolized liquid agent that has not yet evaporated can also be inhaled, an effect not currently modeled in HPAC and JEM. We developed a method for calculating the dosage taken into the body through inhalation of liquid droplets and combining it with the vapor dosage. The total combined dosage is passed to the existing inhaled HD model in FXCODA, the CB human response component of HPAC and JEM. Due to current limitations in the communication between SCIPUFF and FXCODA, the new DARRT HD model can be run only in post-processing mode in conjunction with a sampler output file. Details regarding the liquid droplet inhalation model for HD are contained in Section 5.2, *Development of Additional Models for Particle Size-Dependent Health Effects, Mustard.*

The DARRT model provides a much needed improvement in understanding the physical location of the deposition of solid and liquid aerosols in the respiratory tract and correlates the biological effects with the deposition location. This project and its various aspects have been presented at numerous conferences and workshops during the course of development. A listing of these presentations is contained in Appendix 4. In addition, one paper, *A Review of Inhalability Fraction Models: Discussion and Recommendations*, has been published in the peer-reviewed journal *Inhalation Toxicology* (Millage *et al.*, 2009); a preprint of the article is included as Attachment 1.

2. Project Overview: Objective and Results

The Deposition And Response in the Respiratory Tract (DARRT) model was developed to improve inhalation and biological response models by including the influence of aerosol particle size. The project (CB06MSB096) was performed for DTRA/CBI initially under the WMD Defeat Technology IDIQ Contract DTRA01-03-D-0014, Task Order 0015 and subsequently under Task Order 0025. The period of performance was three years in length.

The health effects or biological response from inhaled chemical and biological hazards depends on where in the respiratory tract the particles are deposited. Figure 2.1 illustrates the fraction of particles in the ambient air that will be deposited in the three main regions of the respiratory system for nasal breathing according to Snipes (1994). The complex shapes of the curves represent interplay between the main processes involved in respiratory mechanics: impaction, diffusion and gravitational settling. Particles with diameters above about 50 microns have only a 50% chance of entering the nostrils during inspiration, but those that do will be deposited entirely in the ET region by impaction and settling. In the 10 to 20 micron diameter range, ambient particles have a 70 or 80% of entering the nostrils with most being deposited in the ET region, a few percent reaching the TB region, and essentially none reaching the pulmonary (P) region. Below 10 micron diameter, impaction and settling rates lessen and particles begin to reach the P region. Between about 2 and 5 microns in diameter, ambient air particles have nearly 100% chance of entering the nostrils during inspiration, with about 15 to 20% reaching the P region and depositing there. A few percent will deposit in the TB region during transit to and from the P region and 40 to 70% will deposit in the ET region, partly during inspiration and partly during expiration. In this 2 to 5 micron range, 10 to 20% of particles entering the nostrils will not be deposited at all, but are exhaled. Interestingly, in the 0.3 to 0.5 micron range, nearly 80% of inhaled particles avoid deposition and are exhaled. Contrary to intuition, particles below 0.01 microns in diameter (the nanoparticle range) tend not to reach the pulmonary region. For these small particles, diffusion rates increase dramatically so that nearly all particles diffuse to the walls of the ET and TB airways and are deposited before reaching the pulmonary region. Note that besides the peak in pulmonary deposition between 2 and 5 microns, there is another, larger peak in pulmonary deposition between 0.01 and 0.1 microns. This range is not of significance for bacterial organisms, which are larger than 0.1 microns, but could be important for viral agents, depending on methods of preparation and dissemination.

Historically, computational models of biological agent aerosol hazards typically ignored large particles (greater than five, sometimes ten microns) because large particles were not considered "respirable" (*i.e.* they had low probability of reaching the pulmonary region of the lung). However, as shown by Figure 2.1, larger particles will deposit in the extrathoracic area where they may cause upper respiratory infections that for some agents may be as significant as pneumonic infections. The new DARRT model improves casualty assessment for these hazards, especially in urban environments, in which many people near a release may be exposed to particles larger than five microns and where larger particles may remain suspended in the air for longer times due to turbulent effects. Accounting for particle size effects will provide better estimates of both the magnitude and nature of the patient stream and, therefore, will improve medical planning.

The development process for DARRT included leveraging existing models of the human respiratory tract coupled with the particle size distribution (PSD) of atmospheric aerosol hazards to estimate the rate and location of agent deposition in the body as a function of particle size. We investigated several existing models and chose the Multiple Path Particle Dosimetry (MPPD) model. Section 3 describes the different models and our analysis of them. The section also includes a detailed analysis of MPPD.
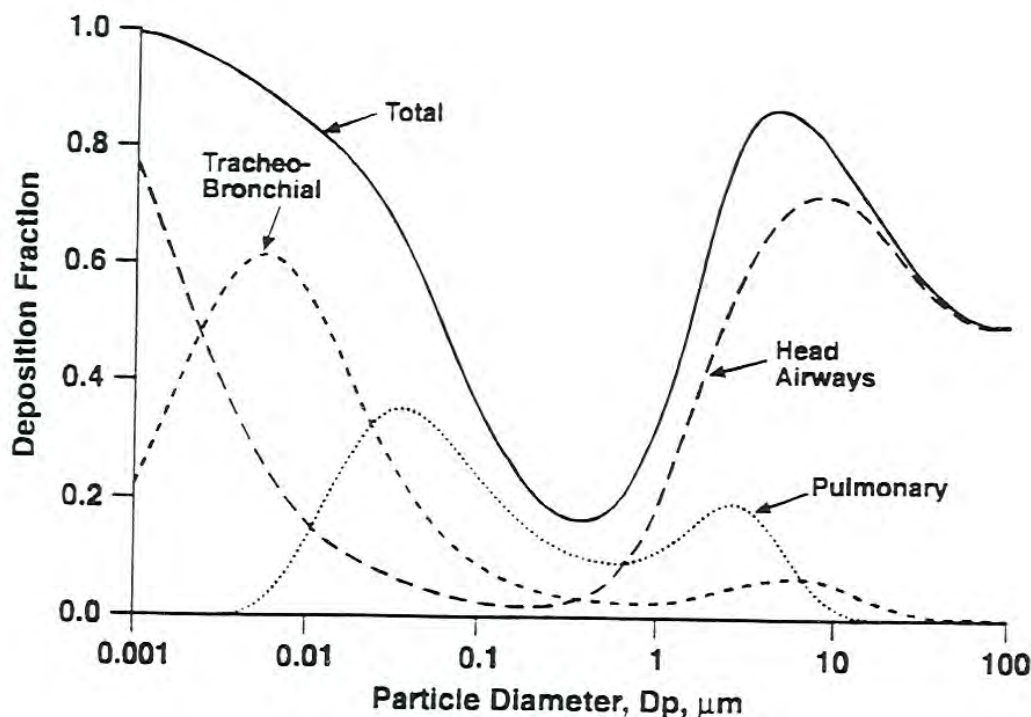
Figure 2.1. Particle deposition in the respiratory tract as a function of particle arerodynamic diameter (Snipes, 1994). "Head airways" refers to the ET region.

We also developed medical models to quantify the dependence of agent health effects on deposition site and on aerosol particle characteristics. Our study is focused on applying data taken from rare human inhalation experiments and animal studies to the development of mathematical models that predict the effect of particle size on the course of development of an intoxication or infectious process. These models can then be used to improve the fidelity of existing models for estimation of casualties resulting from chemical and biological warfare incidents. We developed biological response models for *F. tularensis* (which causes tularemia) and ricin and we implemented the models with the respiratory deposition model for the dry particulate form of these two biological agents and integrated these models into the Hazard Prediction and Assessment Capability (HPAC). The previous biological agent dry particulate models in HPAC did not account for size and assumed all the particles were five microns in diameter and cause pulmonary infection. The biological agent material files used in incident modules like CB Weapon only included a single particle size bin with bounds of 4.9-5.1 micron. Although CB Weapon would allow the user to define a particle size distribution, in fact all particles were artificially transported as 5 micron particles. Since our health effects model will account for particle size distributions, the tularemia and ricin material files have been modified to allow the particle size distribution the user defines in CB Weapon to be accurately "flown". In other words, our new model not only improves the calculation of the biological response to the agent, we have also improved the actual transport and dispersion of the agent by allowing for an accurate representation of the particle size distribution specified by the user.

2.1. Dry Tularemia

The dry particulate tularemia model accounts for the regional deposition of particulate in the respiratory tract. The model calculates the dose deposited in the extrathoracic (ET) region, tracheobronchial (TB) region and the pulmonary (P) region. Based on the presented dose and the particle size, the model converts the dose to the number of particles and, based on the agent concentration (organisms per unit mass), calculates how many of the particles are agent containing particles (ACP). The probability of ET or upper respiratory infection is calculated based on the number of ACP deposited in the ET region and the probability of P or pulmonary infection is based on the number of ACP deposited in the P region. Output contour plots are available to indicate the total probability of infection (upper respiratory and pulmonary). Also, the casualty table individually identifies the population with upper respiratory infection, pulmonary infection and the total infected population. Those predicted to acquire both upper respiratory and pulmonary infections are listed in the pulmonary category and not in the upper respiratory category because the pulmonary infection usually develops first.

For 5 micron particle size, the DARRT model casualty estimates for tularemia are similar to previous estimates as expected. However, there are substantial differences for other particle sizes. Figure 2.2 and Figure 2.3 show hazard areas and casualty tables for 5 micron particles and for 80 micron particles, respectively, using the previous model for tularemia and the current material files in HPAC. Note that the plumes appear the same and the casualty table data is identical. Figure 2.4 and Figure 2.5 show hazard areas and casualty tables for the same two particle sizes, using the DARRT model and material files with improved size bins. The results are significantly different for the larger particles, creating a much smaller hazard area and fewer casualties.

Section 4 provides a detailed analysis of the tularemia model.
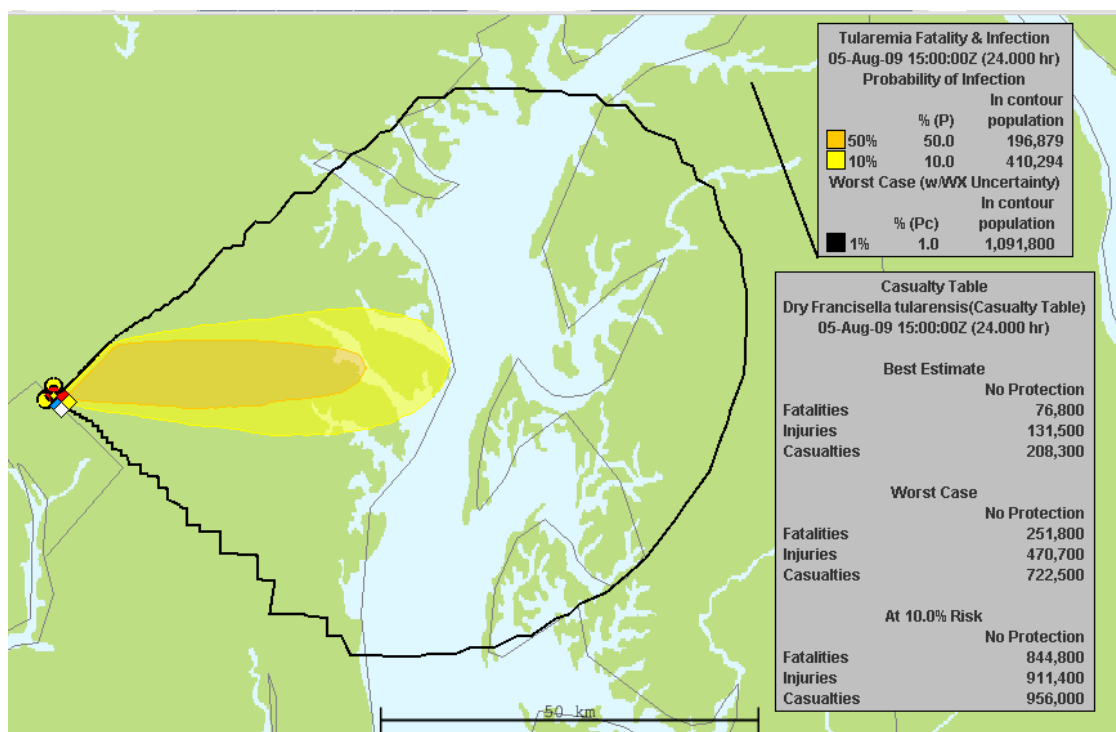
Figure 2.2. Previous model for tularemia: 5 micron particles using the old dry-agent material file (one size bin at 5 microns).
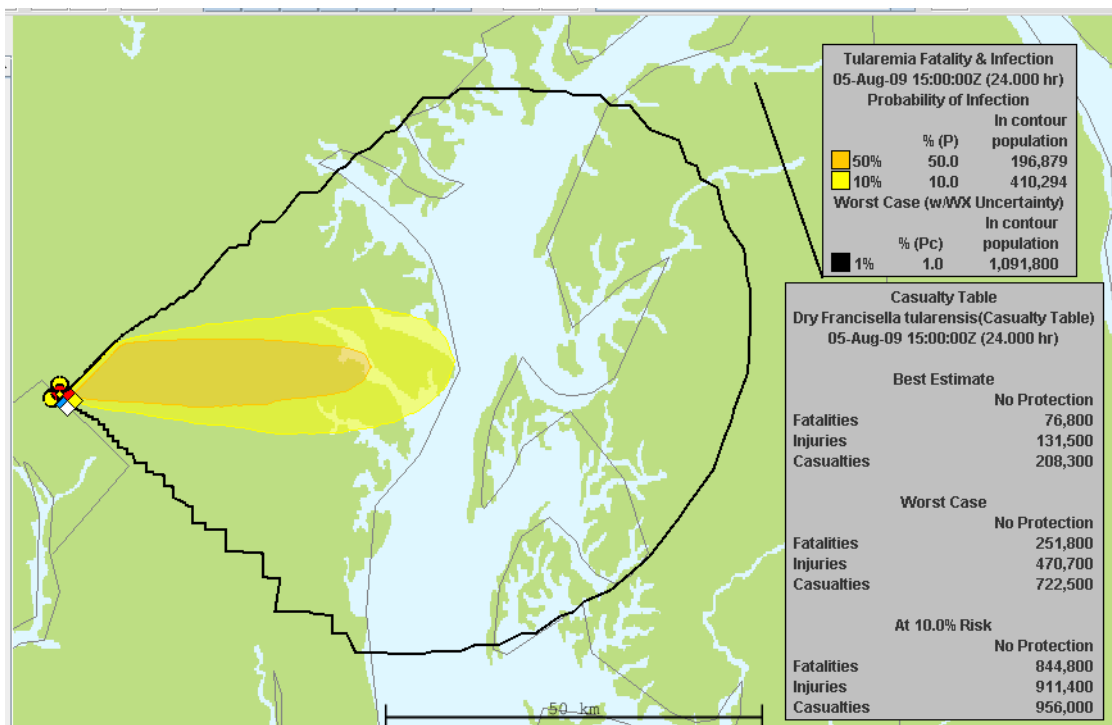
Figure 2.3. Previous model for tularemia: 80 micron particles using the old dry-agent material file (one size bin at 5 microns). Note that the results are the same as in Figure 2.2.
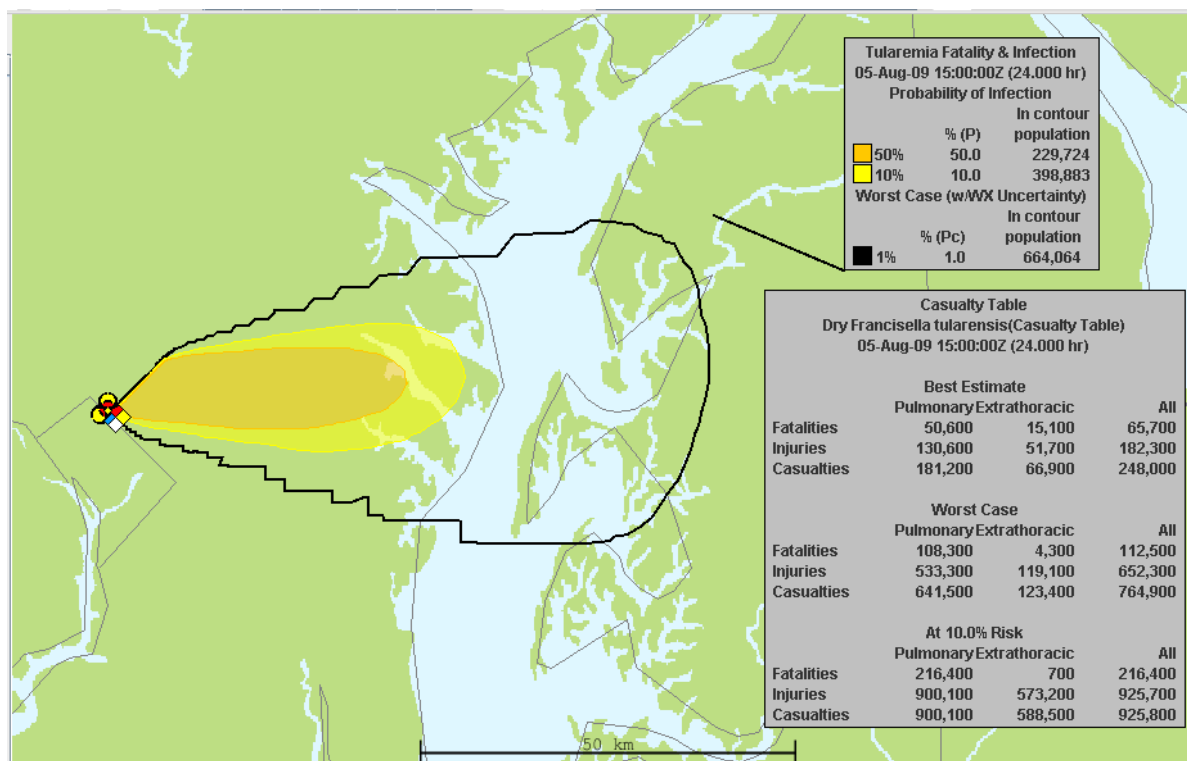
Figure 2.4. DARRT model for tularemia: 5 micron particles using the new dry-agent material file.
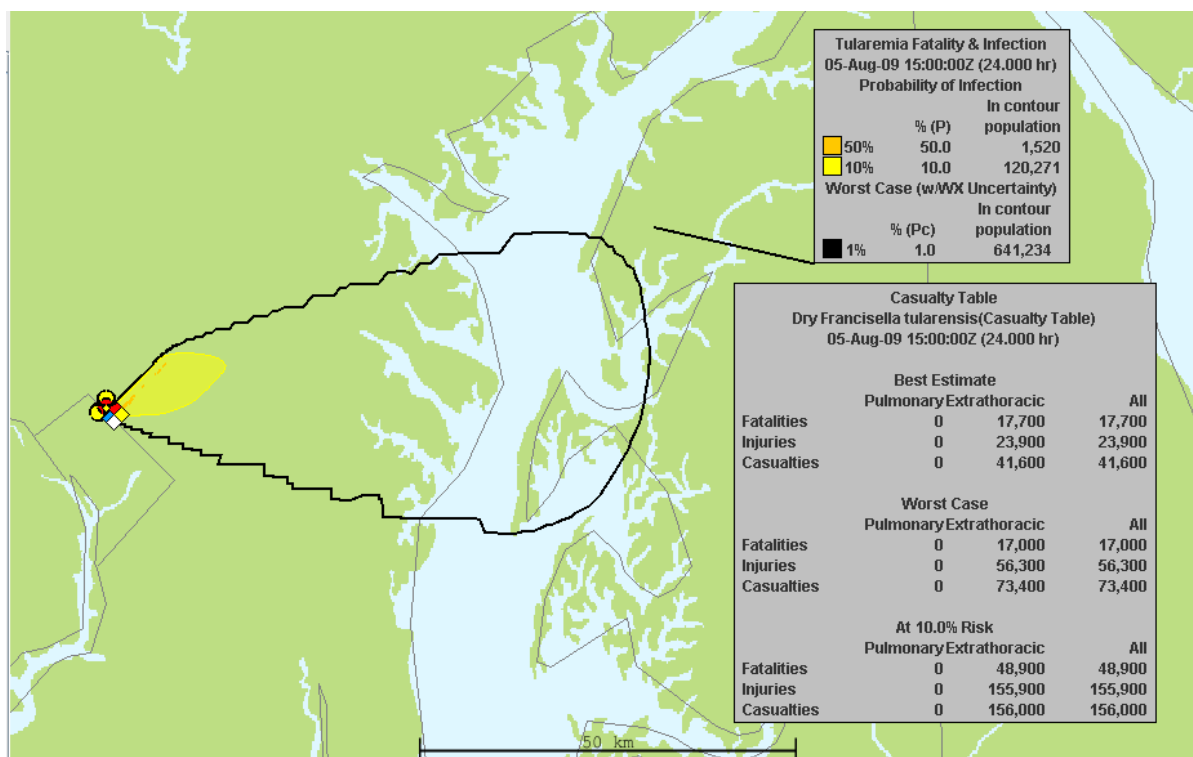
Figure 2.5. DARRT model for tularemia: 80 micron particles using the new dry-agent material file. Unlike Figure 2.3, these results are significantly different that those of Figure 2.2 (or Figure 2.4).

2.2. Ricin

Like the dry tularemia material file, the previous ricin material file only included five micron particles. In addition, there was no detailed injury or mortality models; the human response calculation only provided LCt 10, 20, 50 and 90 values based solely on presented dosage in mg-min/m^3. As a result, much like the tularemia calculations, the LCt values for large particles were grossly overestimated. The new dry particulate ricin model accounts for particle size distribution and the regional deposition of particulate in the respiratory tract. Based on our analysis of the literature, the probability of mortality calculation is a function of the mass of ricin that deposits in the pulmonary region; deposition in the ET and TB regions from aerosolized ricin do not typically result in mortality. Since ricin is a toxin, the mass of the animal is also a factor, so the probability of mortality is based on the mass of ricin deposited in the pulmonary region divided by the mass of the animal (in the case of a human (standard man), 70 kg) in units of μg/kg.

The ricin model does not include a probability of injury model, a task that was outside the scope of our effort. An injury model would perhaps include ET effects, as well as pulmonary effects since both deposition locations can result in transfer of the toxin to the bloodstream. The new ricin model includes plotting options for the probability of mortality and a casualty table to calculate the population affected. A comparison of Figure 2.6 and Figure 2.7 shows the differences between 5 micron and 10 micron particle sizes on the probability of mortality. Since the probability of mortality depends on the amount of material that reaches and deposits in the lung, large particles do not pose a significant mortality threat. Particles larger than 10 to 15 microns display no probability of mortality. Section 5.1 presents a detailed analysis of the ricin model.
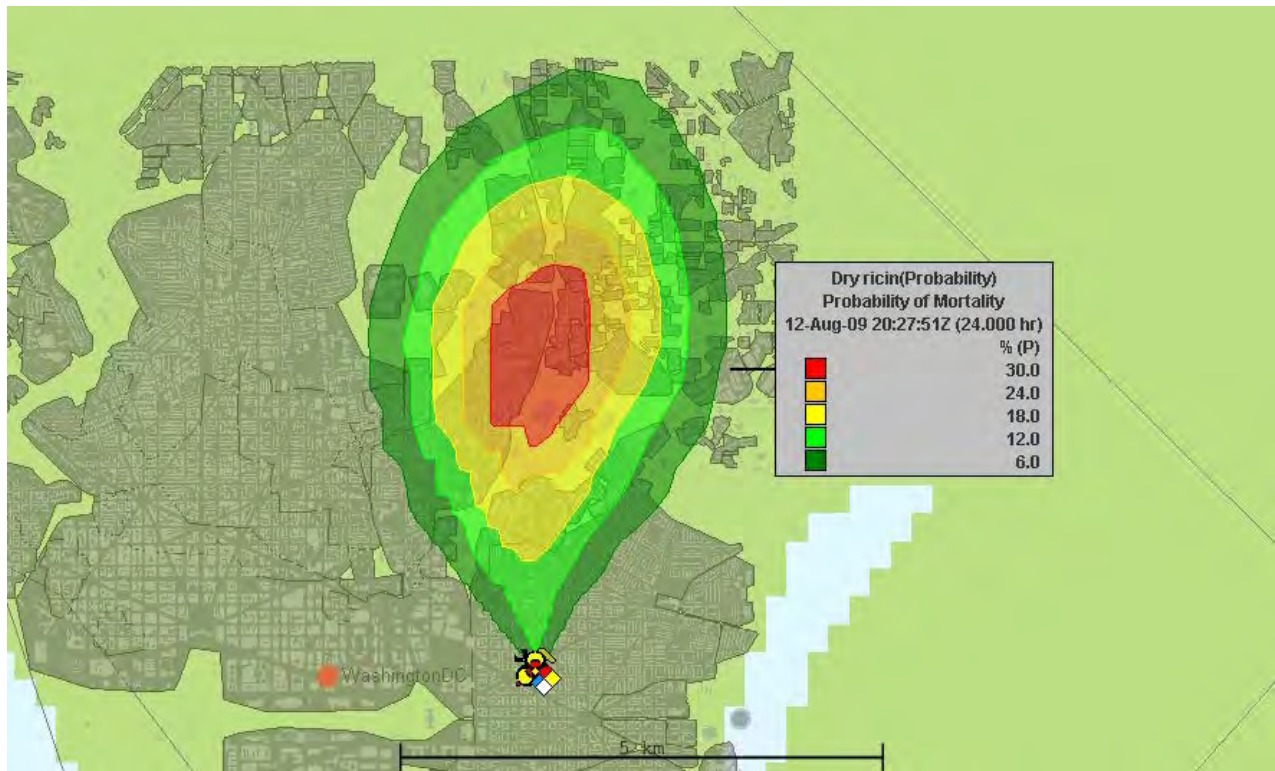
Figure 2.6. 5 micron particles using the new dry ricin material file and DARRT model.
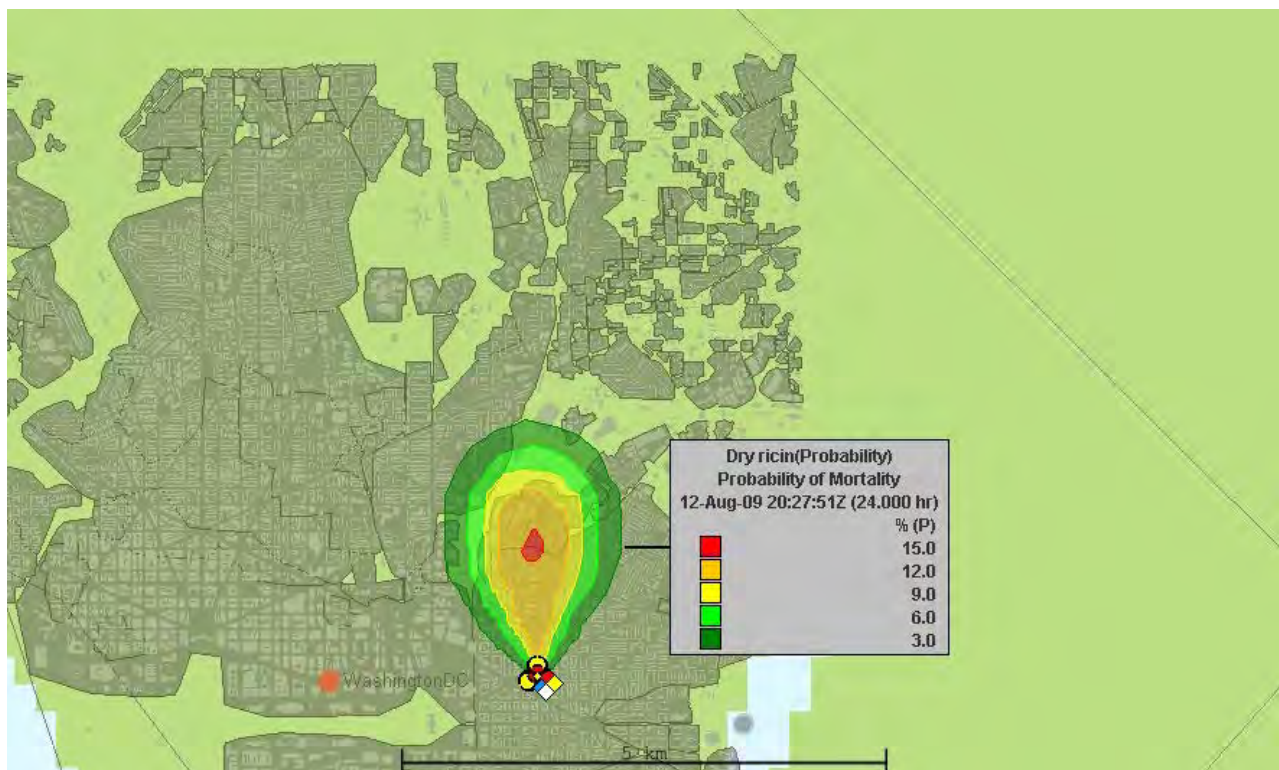
Figure 2.7. 10 micron particles using the new dry ricin material file and DARRT model.

2.3.　　　Liquid Chemical Agents

ARA also developed a mathematical process to include liquid droplet inhalation effects for volatile, aerosolized chemical agents. The mathematics is in place and documented in this report; however, integration of this chemical agent model with HPAC and JEM was not possible at the time of this report due to constraints associated with the information provided by SCIPUFF. Specifically, DARRT needs to capture dosage by droplet size; currently, data regarding the dosage by size can be provided by SCIPUFF to outside models for dry particulate materials, but not for liquid droplets or wet particulates.

In order to test the DARRT model for liquid chemical agents, ARA developed a prototype capability for calculating the effect of inhaled liquid droplets by post-processing a sampler file output from HPAC. The sampler file can provide the required dosage by droplet size bin even though this information is not yet available to DARRT during HPAC execution. Figure 2.8 shows a CBWPN incident; the release is an aerial spray at 50 meters. The droplet size distribution is modeled as a lognormal distribution with the CBWPN default parameter, that is, a mass median diameter of 200 microns and a sigma of 2.0. A sampler is located as indicated in Figure 2.8. Figure 2.9 shows the vapor dosage contours 11 minutes after the release; similarly, Figure 2.10 shows the liquid dosage contours at 11 minutes.
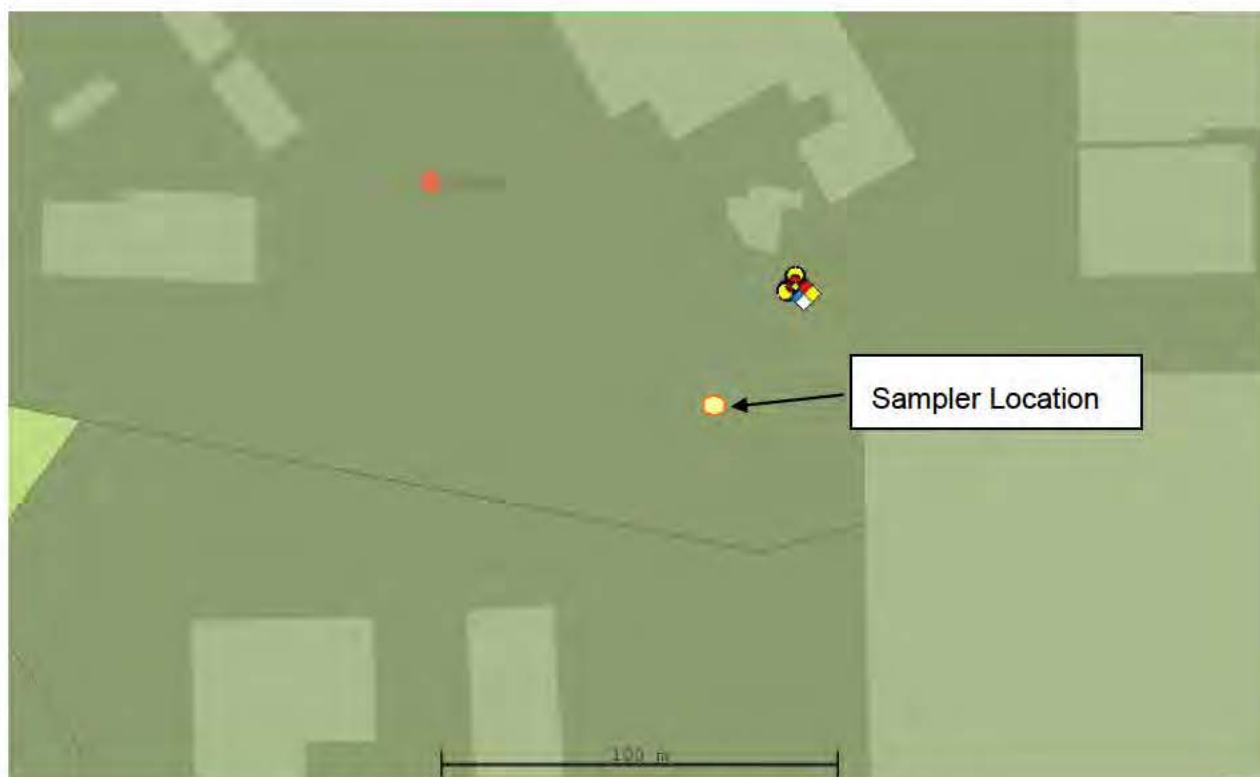
Figure 2.8. Layout of HD release and sampler.
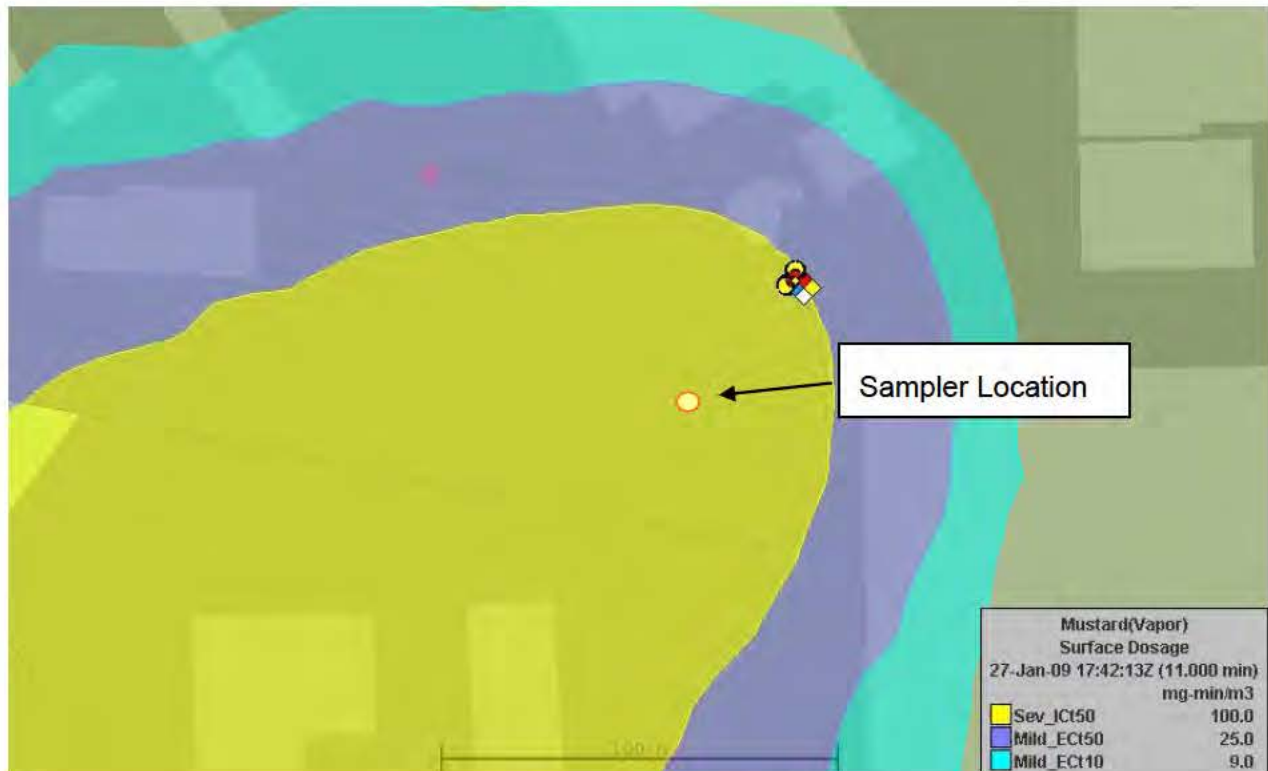
Figure 2.9. Vapor dosage contours at 11 minutes.
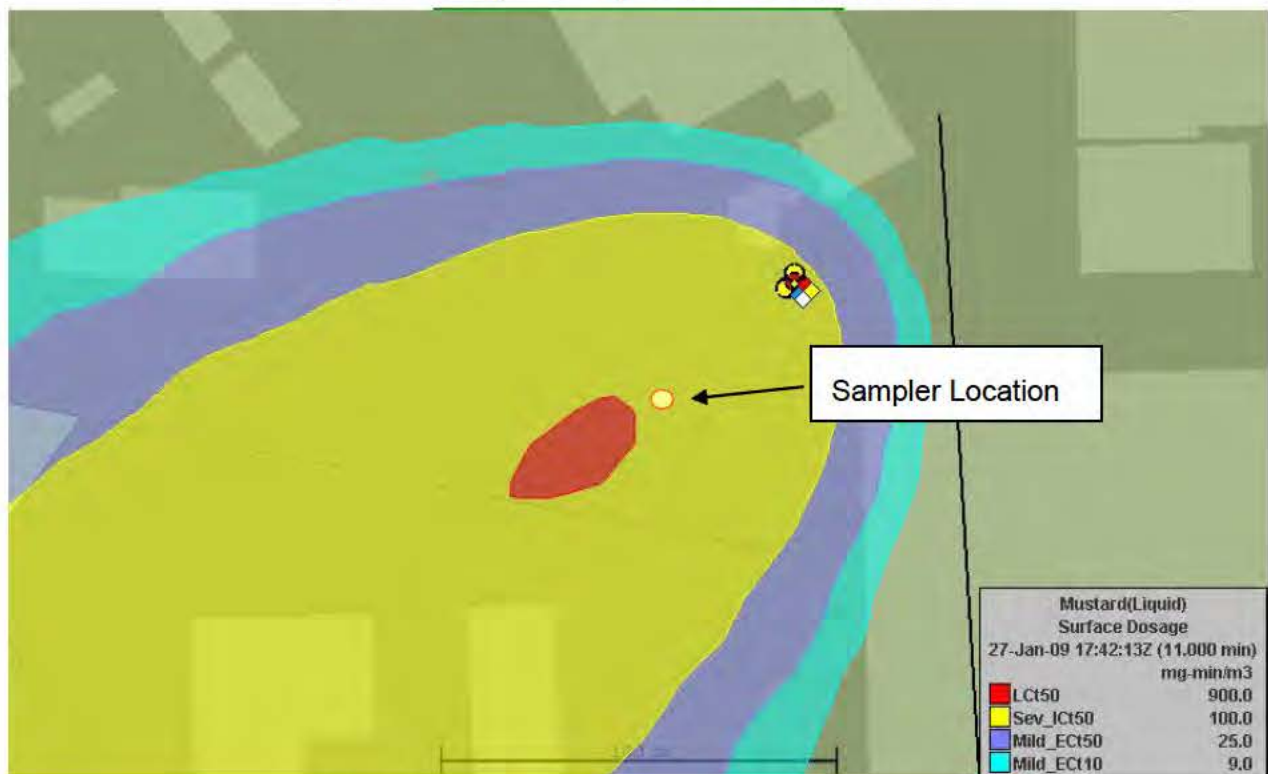
Figure 2.10. Liquid dosage contours at 11 minutes.

We used the sampler output from this calculation in the DARRT inhalation model. We ran one case with only the vapor component included and a second case with the inhalation of liquid droplets included. Keep in mind, the *Ct* values shown in the HPAC contour plots (Figure 2.9 and Figure 2.10) include effects from inhalation, ocular and cutaneous exposures. The results from the DARRT model only address the effects due to inhalation. Figure 2.11 and Figure 2.12 show the results for the vapor only DARRT calculation and Figure 2.13 and Figure 2.14 include the effects of both vapor and liquid droplet inhalation. The wind speed was set at 4 m/s for these calculations. When liquid droplet inhalation is included, the probability of injury (incorrectly labeled as infection in the figure) increases by about 10% and the probability of mortality increases 30-40%.

Although the impact of liquid droplet inhalation will vary with environmental conditions and exposure duration, this example demonstrates that liquid droplets should not be ignored in all cases.
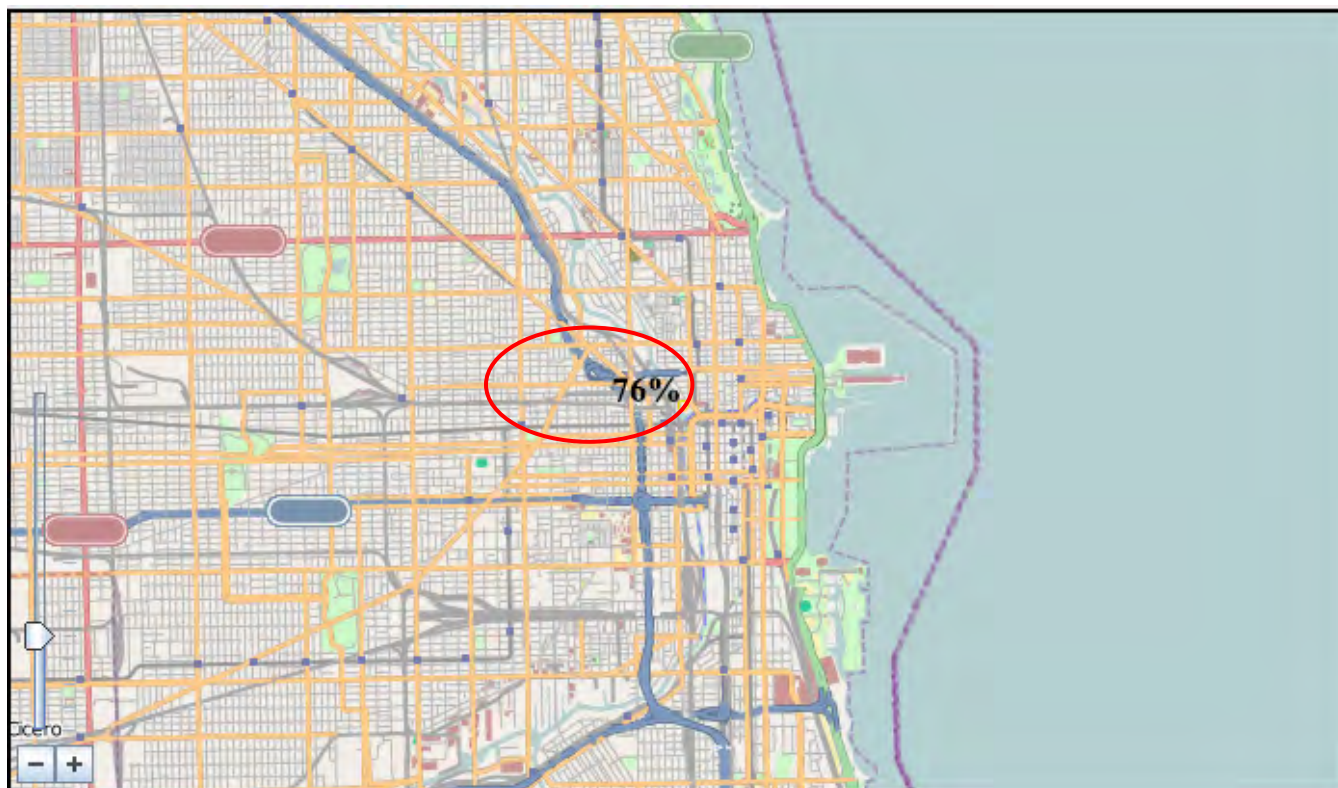
Figure 2.11. HD injury calculations from vapor inhalation alone (DARRT postprocessor).
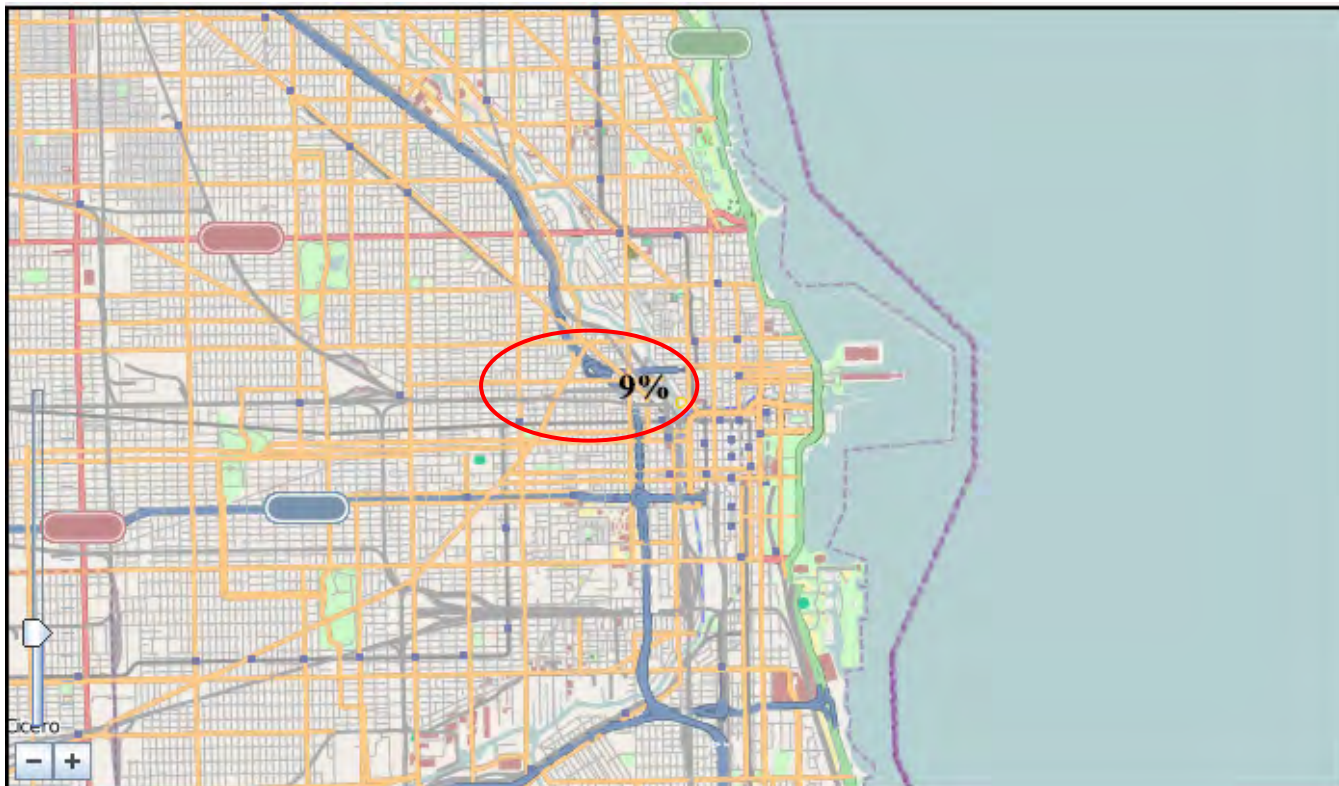
Figure 2.12. HD mortality calculations from vapor inhalation alone (DARRT postprocessor).
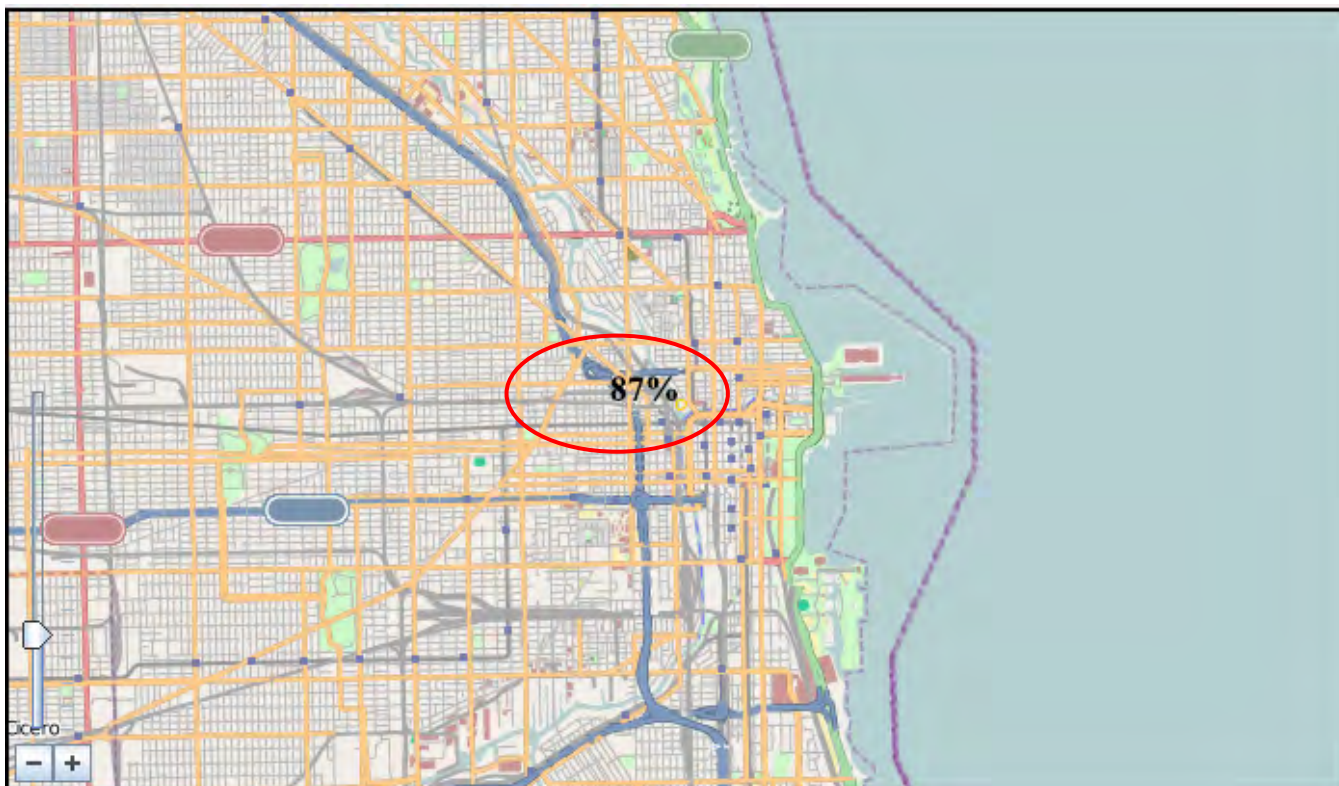
Figure 2.13. HD injury calculation from combined vapor and liquid droplet inhalation (DARRT postprocessor).
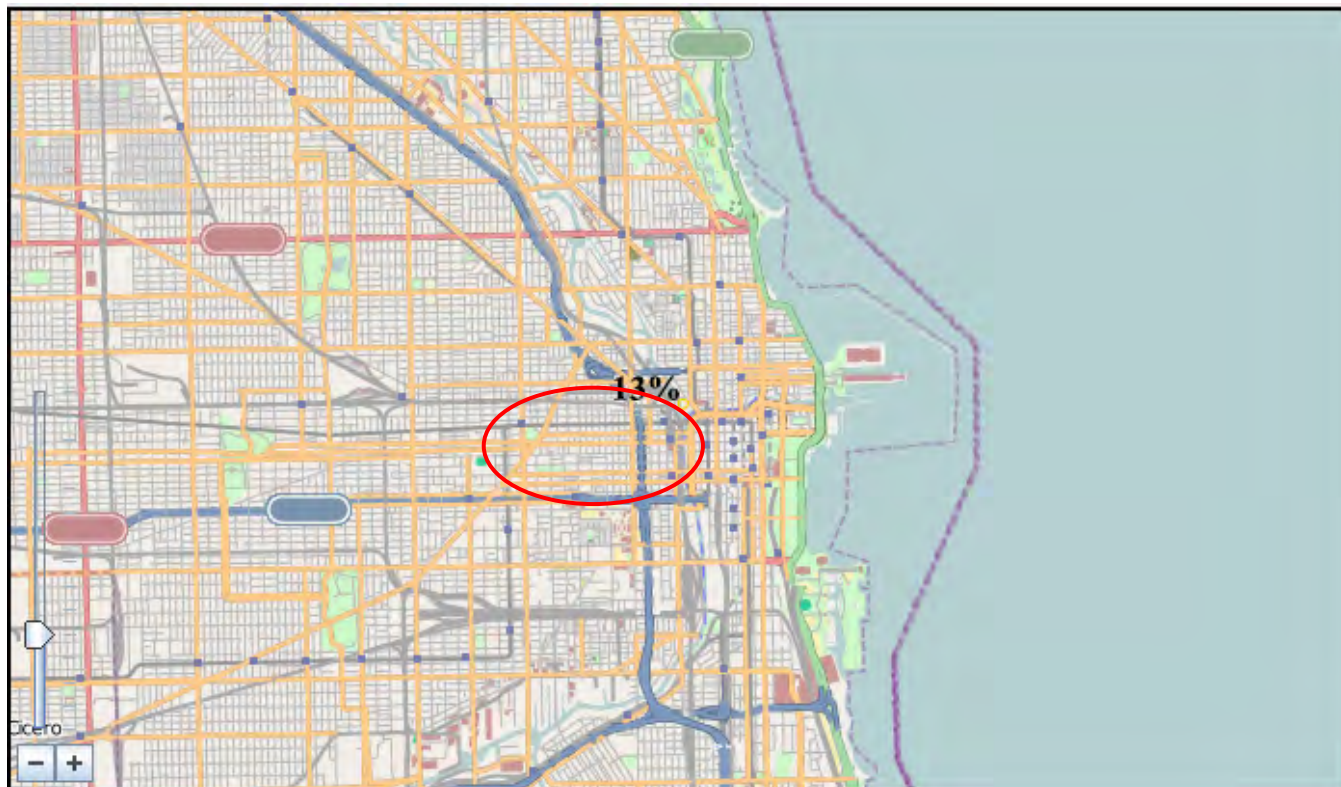
Figure 2.14. HD mortality calculations from combined vapor and liquid droplet inhalation (DARRT postprocessor).

3. Implementation of a Particle Deposition Model for the Respiratory Tract

Mathematical modeling of the inhalation, deposition and retention of chemical and biological aerosols forms the foundation for estimating the resultant effects on the human body. This section describes the technical basis for recommending implementation of the Multiple-Path Particle Dosimetry (MPPD) model for the development of the medical model of inhalation hazards.

3.1. Selection of a Model of Inhalation Mechanics

The objective of this project was to develop models for the influence of aerosol particle size on the health effects of inhaled chemical and biological hazards. In accordance with the first deliverable of the project, initial work focused on examining existing models that describe the particle size-dependent nature of the inhalation and deposition of particulates in the human respiratory tract and selecting an model of inhalation mechanics for further use. This subsection reviews our findings.

3.1.1. Background

The radiological community has extensively studied the biological effect of inhaled radioactive particles and has developed extensive models to describe the dose delivered to the body as a result of inhaling radioactive material of various particle sizes. The first international guidelines for particle size dependent radiological inhalation hazards was published in 1959 by the International Commission on Radiological Protection (ICRP, 1959). The ICRP has continued to improve the models and some aspects of their models are still considered to be state-of-the-art.

The chemical and biological community has more recently begun to develop models of inhalation hazards of toxic substances and microorganisms, but the nature of the modeling is widely varied in both purpose and scope. Much of the work in this area is focused on animal experiments rather than mathematical modeling, particularly in the area of vapor inhalation of toxic industrial chemicals (TICs) and toxic industrial materials (TIMs). These studies often do not address particle size dependence, a factor that is critically important in determination of the deposition pattern in the respiratory track (Benson *et al.*, 2001, Benson *et al.,* 2003). Modeling and experiments are also being performed to understand the deposition of fibers, which poses unique deposition hazards (Su and Cheng, 2005), and extensive inhalation and retention work is being performed to predict the particle deposition sites to assess the delivery of therapeutic drugs via inhalers (Sweeney and Brain, 1991). Extensive epidemiological modeling work is related, but not explicitly applicable to this project, particularly with regards to environmental and pollution hazards (Georgopolous *et al.*, 2005).

3.1.2. Investigative Discussions

We visited several research centers involved in inhalation research to investigate existing respiratory mechanics models. Each center has their specific areas of expertise and although there were some overlapping research efforts, the general area of research was much broader than the scope of this project. Although by no means an exhaustive survey, the following centers were visited and their input was solicited to determine who was currently involved in mathematical modeling of inhalation.

1. The Hamner Institutes for Health Sciences (The Hamner, formerly CIIT, the Chemical Industry Institute of Toxicology), Research Triangle Park, NC. CIIT has been a leader in developing mathematical and animal models to describe particulate inhalation (Asgharian *et al.*, 1999 and 2001). Researchers at CIIT have developed highly complex computational fluid dynamics

(CFD) models to simulate inhalation flow patterns as well as simpler, fast-running models to describe inhalation patterns, such as the MPPD software.

2. Environmental Occupational Health and Safety Institute (EOHSI), Rutgers University. EOHSI is involved in a variety of source-dispersion-dose modeling, as well as detailed systems biology effects modeling. EOSHI indicated that they use the MPPD model in some of their research.

3. Lovelace Respiratory Research Institute (LRRI), Albuquerque, NM. The LRRI is a leader in animal studies and does research using human lung casts to experimentally investigate deposition patterns. They do not have an active mathematical modeling program. They confirmed the usefulness and positive inhalation community view of MPPD.

The ICRP Publication 66 (ICRP, 1994) has developed mathematical models of inhalation and deposition that is focused on radiological protection. It would obviously be time consuming to develop a new software implementation of these models; however, a few commercial software programs already exist:

LUDEP$^{©}$ (LUng Dose Evaluation Program). LUDEP Version 1.0 (1993) was published by the National Radiation Protection Board (NRPB) of the United Kingdom of Great Britain (the UK) to implement a late draft of the proposed lung model; Version 1.1 (1994) incorporated all of the recommendations of ICRP Publication 66 and Version 2.0 (1996) included a "bioassay" module, and the facility to evaluate ingrowth of progeny radionuclides in a radioactive series (ACJ and Associates, 2006). NRPB is now the Radiation Protection Division of the UK Health Protection Agency.

Dose and Risk Calculation (DCAL) Software. DCAL is a comprehensive software system for the calculation of tissue dose and subsequent health risk from intakes of radionuclides or exposure to radionuclides present in environmental media (U.S. EPA, 2007).

While generally applicable, the focus of these codes is on radioactive material and the resultant internal energy deposition; extracting the inhalation and deposition portions of the code from the remainder would likely prove difficult. In addition, although many aspects of the ICRP 66 inhalation model are widely used, the foundation of the model is solely based on a semi-empirical relationship between deposition and particle size. The use of the ICRP model is justified within the range of the measurements used to build the model. However, use of the model which requires extrapolation beyond the use conditions may produce unreliable results.

The MPPD model (Asgharian *et al.*, 2006a and 2006b; Asgharian and Price, 2006) is a widely used, fast-running, GUI-driven, Java-based set of algorithms that can calculate the deposition and retention of both mono-dispersed and poly-dispersed particulates and aerosol droplets in rat and human respiratory tracts. Version 1.0 of MPPD code was first introduced in 2002 and version 2.0 was released in 2006; The human respiratory model includes both single-path, symmetrical calculations as well as several multi-path variations of limited-asymmetric, asymmetric and stochastic models. The limited asymmetric model uses a 5-lobed model with subsequent symmetric airways. An age-dependent set of lung morphologies is also available. The model can calculate deposition in three regions, extrathoracic (ET), tracheobroncial (TB) and pulmonary (P), or by specific airway generation. Figure 3.1 illustrates the anatomy and functionality of these three regions. Deposition according to these three regions will likely be adequate to correlate with the human response data currently available.

3.1.3. *Recommendation to Use MPPD*

Based on our review of the state-of-the-art in modeling inhalation mechanics and dosimetry, the positive recommendations regarding MPPD given by EOSHI and LRRI, and the willingness of the Hamner Institutes to provide source code through a subcontract to ARA, we decided to proceed with the MPPD as the foundation of this project. A subcontract was issued and executed, providing ARA

with a functional version of MPPD adapted for the goals of this project. Subsequently, The Hamner made a business decision to reduce its involvement in modeling respiratory mechanics and released its MPPD copyright to Dr. Bahman Asgharian, who then joined ARA (Asgharian, 2006). The next section of this report provides more details on respiratory mechanics and the MPPD dosimetry model.

Head (or extra-thoracic, ET) airways
- Nose and mouth to the larnyx
- Nasal airways and the oral cavity

Tracheobronchial (TB) region
- Larynx to the terminal bronchioles
- Ciliated epithelium, mucous-secreting

Pulmonary (P) region
- Respiratory bronchioles to the terminal alveoli
- Gas-exchange epithelium, non-ciliated
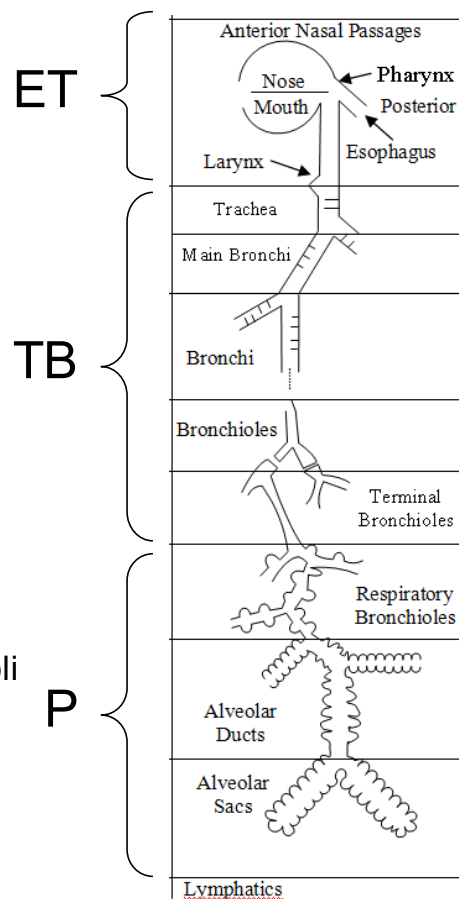
Figure 3.1. The respiratory tract may be divided into three anatomical-functional regions. (Asgharian et al., 2006a)

3.2. Dosimetry Assessment of Inhaled Materials in the Lungs: Multiple-Path Particle Dosimetry (MPPD) Modeling

Particles suspended in the atmosphere whether generated naturally or for commercial use or even for malicious intent (such as biological or chemical warfare) may create adverse health effects when inhaled. Once the materials enter the respiratory tract, they may deposit on the airway surfaces depending on their physical and chemical properties. In addition to inflicting injury at the site of deposition (for hazardous materials), deposited particles may be translocated throughout the lung and removed from airway surfaces by various clearance mechanisms that are operative at different locations in the respiratory tract. The retained portion (dose) in the lung may pose short and long term health effects. Therefore, estimations of the initial and retained dose throughout the lung are needed to correlate biological response from exposure to airborne agents.

Two different approaches are adopted in calculating deposition and retention of particles in the respiratory tract depending on available information on airway geometry and the desired level of details for the dose. The first approach is site-specific modeling for which the precise airway geometry for the region of interest as well as information on airflow and compound transport through the region at inlets and outlets are known. This approach is most useful at the entry port to the respiratory tract (*i.e.*, nasal and oral airways) for which airway passages are reconstructed from scanned images of airway cross sections and combined with breathing information to form anatomically and physiologically realistic models. Since the complete form of the transport equations with the full account of dominant physical mechanisms are solved, detailed information regarding the airflow and compound losses to the airway walls is obtained, but at the expense of a heavy computational toll.

The second approach is whole-lung modeling in which airways are described dimensionally, but precise geometric features (such as curvature and smoothness of airway walls) are neglected. The entire respiratory tract geometry can be constructed from information on airway length, diameter, and orientation and gravity angles. Averaged transport equations that include dominant mechanisms for the flow and particle transport and deposition, when applied to idealized lung geometries, will greatly reduce computations. However, deposition predictions may only be made per airway or region of the lung. In this modeling approach, higher order effects such as local variation in airflow and fluctuations in particle trajectory due to non-smooth geometry can be neglected in favor of higher order assessment of particle losses in the lung. Approximations in predictions are justified considering uncertainties in lung and breathing parameters and inter-subject variability in lung geometry across a population. The whole-lung modeling approach is ideal for regional calculations of deposition in the entire lung whereas site-specific modeling is handicapped by the enormity of the lung airways and lack of knowledge on airflow mechanics in the lung. By making simplifying assumptions, computations can be carried out in a relatively short time when detailed, site-specific deposition information is either unavailable or unreliable.

3.2.1.   *Whole lung modeling/regional and total dosimetry calculations*

Lung airway dimensions span multiple scales, ranging from centimeters to micrometers . Currently, the resolution of imaged scans is at the millimeter level; therefore, reconstruction of the entire respiratory tract based on imaged scans is not feasible with today's technology. Lung reconstruction from scanned images can be made only for the first few airway generations of the lung conducting tree. Even if the entire geometry of the respiratory tract were available from scanned images, limited information on airflow mechanics in the lung and particularly deep lung would hamper a thorough investigation of the airflow field and particle deposition. Detailed fluid mechanics computations of the airflow in the lung would require information on airway expansion and contraction and exit boundary conditions of most distal airways. Outlet boundary conditions that encompass lung elastic properties (compliance), must be constructed based on pressure information in the pleural cavity. Pressure in the pleural cavity is gravity dependent and varies vertically. As a result, lung expansion is nonlinear, or simply each lobe of the lung expands at a different rate. In addition, pleural pressure varies with the time into the breathing cycle and breathing frequency thus adding further challenges to detailed computations of lung ventilation. Hence, fluid dynamics analysis (site-specific modeling) in the deep lung is severely limited by the lack of detailed information on lung geometry and time- and volume-dependent, pleural pressure.

A whole-lung deposition model contains three major components. First, a complete lung geometry extending from nasal and oral airways to most distal alveolar airways (sacs) must be constructed. Second, the airflow through this geometry must be determined. Inhaled air will preferentially carry the suspended particles to various airways of the lung depending on the mechanics of breathing. Finally, a mathematical description of particle transport and deposition is needed based on the mass balance on

the inhaled material. Typically, a modified version of the convective-diffusion equation is employed for particle deposition calculations.

To facilitate computations of losses to the lung from inhaling airborne materials, simplifications regarding lung geometry and airflow mechanics are needed. The lung geometry is assumed to be a collection of cylindrically-shaped tubes arranged as a dichotomous branching network. Airway dimensions and orientations are found from morphometric measurements. Additional volumes are added to respiratory bronchial airways in the acinar region to account for the alveolar space.

The most popular lung geometry for humans is the typical-path lung structure obtained from available airway measurements in the lung (Weibel, 1963). The lung geometry is assumed to consist of 23 airway generations, of which the first 16 generations comprise the tracheobronchial region (conducting airways), and the last 7 generations form the alveolar region. Using measurements of Raabe *et al.*, (1976), Yeh and Schum (1980) constructed a similar typical path, but additionally developed a 5-lobe lung model with each lobe being symmetric but different in dimensions. Koblinger and Hofmann (1985) further expanded the human geometric model by using measurements of Raabe *et al.*, (1976) to create stochastic lung geometries that were asymmetric and closely resembled the anatomical structure of the lung. However, airway shapes were still cylindrical and deviated from reality. In rats, Anjilvel and Asgharian (1995) created an asymmetric lung geometry based on measurements of Raabe *et al.* (1976).

To compute lung ventilation, lung expansion and contraction are assumed uniform. Consequently, airflow rate at a location in the lung is proportional to the distal volume to that location. In addition, the airflow velocity profile in an airway is assumed uniform with a magnitude equal to the average parabolic velocity. Using the above geometries and airflow distribution model, mathematical models of particle transport in the model geometry were developed and solved to calculate head and lung losses (Anjilvel and Asgharian, 1995; Asgharian *et al.,* 2001).

A number of deposition models are available in the literature for the calculations of particle deposition. Early deposition models were compartmental and limited in predictive capability. More realistic deposition models assumed the lung to expand and contract uniformly and resembled a trumpet in shape when symmetric lung geometry was assumed (Schere *et al.,* 1972; Yu, 1978). These models have been confirmed for regional and lobar fractions. The human lung has an asymmetric branching structure that affects both airflow and particle deposition. Asgharian *et al.,* (2001) used the multiple-path analogy in 10 stochastically generated lungs of human adults to calculate site-specific and regional deposition of particles. The stochastic lungs were based on morphometric measurements of Raabe *et al.* (1976) and developed by Koblinger and Hofmann (1985). Significant dose variations among the lung structures were found, which indicated intersubject variability in the population to some extent.

Deposition models based on asymmetric lung geometries (Asgharian *et al.,* 2001) offer an advantage over previous models in that lung physiology and morphometric variability within each generation are accounted for. These two parameters are shown to be most critical in accurate microdosimetry predictions of particles in the lung (Asgharian *et al.,* 2001; Subramaniam, *et al.,* 2003; Asgharian *et al.,* 2004). To make the deposition model available to the public and to allow other investigators in related fields such as toxicology and risk assessment to use the model, a software package with a graphical-user-interface was developed based on the models to calculate particle deposition and retention in human adults and children and rats (Asgharian *et al.,* 1999). The software was used to reduce the uncertainty factor due to dosimetric adjustment in animal-to-human dose extrapolation. It was also used by the U.S. Environmental Protection Agency (EPA) in the toxicology assessment (U.S. EPA, 2004) of particulate material (PM).

3.2.2. MPPD Software development

In collaboration with scientists from the Dutch Ministry of Health, Dr. Asgharian and colleagues at CIIT developed a software package Multi-Path Particle Deposition (MPPDep) based on the deposition models to aid computations and simulations required by toxicologists, risk assessors, and the drug delivery community (Asgharian *et al.,* 1999; Cassee *et al.,* 1999; Subramaniam *et al.,* 2003). The computer algorithms in the software calculated the deposition of aerosols in the respiratory tract of rats and humans for particles ranging from ultrafine (0.01 micrometers) to coarse (20 micrometers) sizes. The graphical user interface (GUI) feature of the software enabled easy and quick calculations of deposition. The MPPDep software allowed various inputs such as selection of lung geometry, lung parameters such as functional residual capacity, particle characteristics (including size distribution), and breathing types (oral, nasal, oronasal, tracheal) and parameters (tidal volume, breathing frequency). A set of default values for the above parameters are used if the parameters were not specified. The software provided graphical and textual outputs. Simulation results were provided for total, regional and lobar deposition, and as a function of airway generation number. The option of bar plots of total, regional (head, TB, P) and lobar deposition was provided. Also included with the software was an extensive Help Menu that described model details, software features and operation procedure. Several tutorials and a quick start guide helped the user to get launched quickly. An upgraded version of the software (MPPD) was released to the public in 2002. It included additional asymmetric lung geometries for humans that enabled more realistic calculations of deposition as well as models of particle clearance in various regions of the lung. The software also included predictions of particle deposition in children (Winter-Sorkina and Cassee, 2002). Recently, a new version of MPPD has been made available through the ARA web site (http://www.ara.com/products/mppd.htm). New features in this version include a deposition model specifically for nanoparticles, nonuniform lung ventilation to include the effect of body orientation (posture) on deposition, and availability of 30 stochastic lung geometry for more realistic assessment of variation of dose in the population. In addition, various improvements were made to the input and output of MPPD. Sample screenshots of MPPD are shown in Figure 3.2.
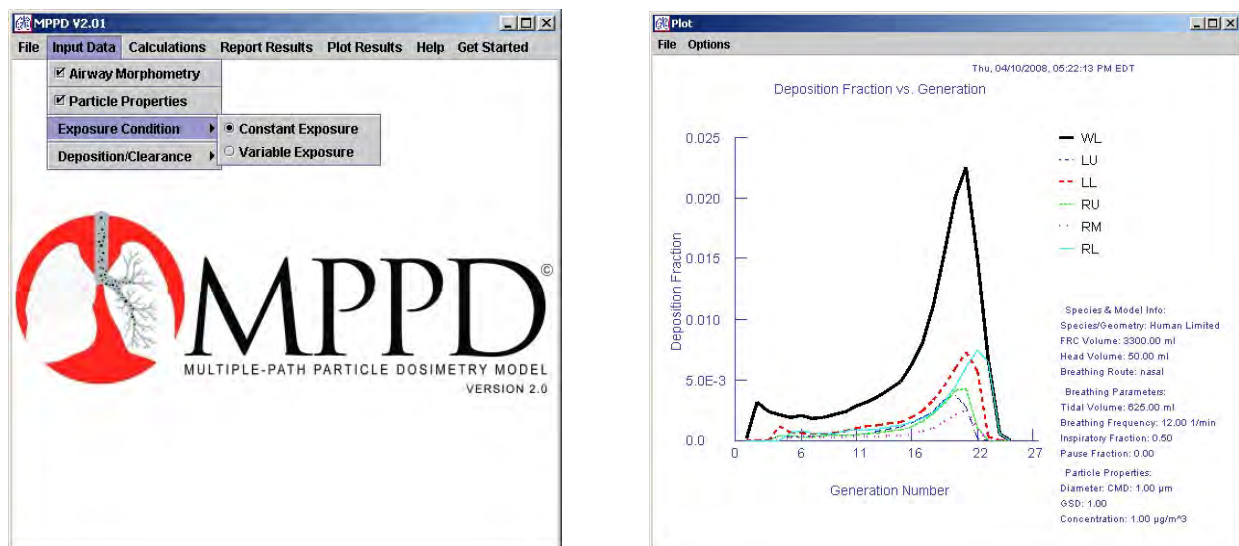
Figure 3.2. MPPD screen shots.

3.2.3.   *Users of the MPPD Software*

Scientists in government agencies, research laboratories, private industry, and colleges have used the software in their studies. A list of registered users who downloaded the software from The Hamner website is given in Appendix 1. The software has been widely used by toxicologists to interpret inhalation studies of particles and risk assessors to assess human exposure limits. The software was used by the EPA in its risk assessment of particulate matter (U.S. EPA, 2004). The software was the basis of proposed revisions to update the inhalation reference concentration (RfC) methods of the EPA. The software was also used by scientists at the National Institute of Occupational Safety and Health (NIOSH) to study the retention of insoluble particles in the lungs of rats.

3.3.   Inhalability

One important parameter we investigated is the inhalability factor. Inhalability is a measure of the fractional concentration of material that is inhaled, *i.e.*, enters the head, relative to the concentration in the ambient air. Deposition takes place after inhalation. Some inhaled material does not interact with the respiratory system and is simply exhaled, but that effect is not considered in inhalability. Inhalability refers strictly to the intake process is defined as a function of particle size:

$$I(d_{ae}) = \frac{C_{Inspired}(d_{ae})}{C_{Ambient}(d_{ae})} \quad , \tag{3.1}$$

where $C_{Inspired}(d_{ae})$ is the concentration of particles of a given size that is present in inhaled air and $C_{Ambient}(d_{ae})$ is the concentration of particles of the same size in the ambient breathing zone. The particle size d_{ae} is the aerodynamic diameter.

We reviewed the literature, examined the data from inhalability measurements, and investigated current mathematical models of inhalability. Based on this review, we developed a mathematical model that provides the best description of the data across a variety of conditions, while minimizing mathematical inconsistencies. An article (Millage *et al.*, 2009) describing this work has been accepted for publication in the peer-reviewed journal, *Inhalation Toxicology*. Attachment 1 contains a copy of the article as it will appear in the journal and Figure 3.3 shows a family of inhalability curves for various ambient wind speeds. Note that the value of 50% for 100 micron particles at a wind speed of 4 m/s corresponds to the value assumed by Snipes (1994) for the curves show in Figure 2.1.

3.4.   MPPD as Implemented in the DARRT Model

The MPPD code has several different lung models and many parameter settings to modify the lung performance. The code has a symmetric model which is commonly used because of its simplicity and speed, but the human respiratory system is not symmetric. The code also includes a 5-lobed asymmetric model which is a better representation, having two lobes in the left lung and three lobes in the right. Finally, because lobe structure varies from person to person, the code includes ten stochastically developed lung models as well. The airway branching angles, the length and diameter of segments differ, and even the number of generations can differ slightly from person to person. Attachment 2 presents a comparison of the stochastic models with the symmetric and 5-lobe asymmetric models. We decided to represent the average human respiratory system for present purposes by calculating the deposition fractions with each of the ten stochastic models and averaging the results for each particle size. We also report the standard deviation for each deposition value.
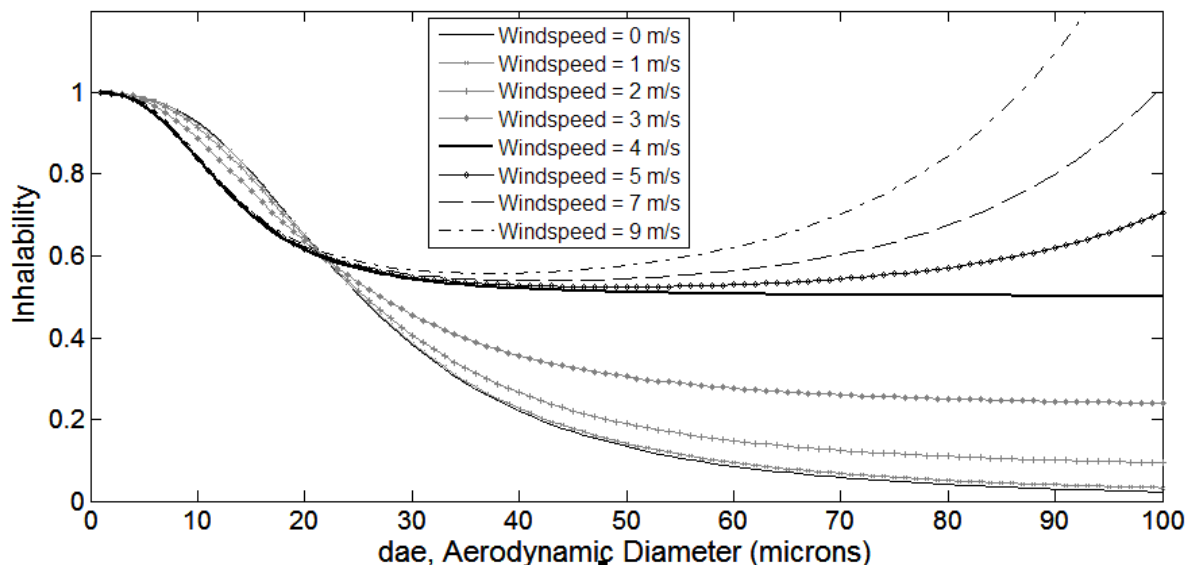
Figure 3.3. Recommended set of inhalability curves for a normal augmenter at a low breathing rate (Millage et al., 2009).

Another input parameter that changes the regional deposition is the breathing rate. The human response models that are implemented in HPAC allow the user to specify breathing rate with suggested values ranging from 15 liters per minute (*lpm*) to 75 *lpm*. Clearly the airflow rates are significantly different over this breathing rate range. In addition, with a normal augmenter (a person who normally breaths through their nose until the breathing rate increases to the point that they need to augment with oral breathing), the transition from 100% nasal breathing to a combination of oral and nasal breathing occurs around 35 *lpm* (Niinimaa *et al.*, 1981). The nose is a very good particulate filter; so much of the material that would be trapped in the ET region at low breathing rates (100% nasal breathing regime) may actually reach deeper into the respiratory tract at higher breathing rates because airflow is being supplemented with mouth breathing, bypassing the nasal filter.

We decided to implement MPPD in the DARRT model using the stochastic lung models, but we wanted to avoid running multiple cases and averaging the results in an operational code. Therefore, we built a look-up table of regional deposition for the desired range of parameters and implemented a linear interpolation scheme for breathing rate and particle size. We used the 10 stochastic lung models, including the largest and smallest models available for our analysis. We ran each lung model at 8 different breathing rates, ranging from 15 to 75 *lpm* and for 22 particle sizes. We based the particle sizes on the bin midpoints that we expect to use for the dry particulate materials; however, this choice does not constrain future choice of bin sizes. We collected the regional deposition fraction for the ET, TB and P regions. For each breathing rate and particle size, we calculated the average deposition and associated standard deviation in each respiratory tract region for tabulation.

Figure 3.4 shows the average fractional deposition and standard deviations as a function of particle size for a breathing rate of 15 *lpm* and Figure 3.5 shows the same for a breathing rate of 40 *lpm*. Note that there are no standard deviations associated with the ET region. The stochastic portion of the MPPD model is associated only with the TB and P regions, therefore there is no variability incorporated in the ET deposition. These curves may be compared with the older work of Snipes (1994) shown in Figure 2.1. One difference is that the curves of Snipes include inhalability, leading to the apparent 50% deposition fraction for 100 micron particles. In DARRT, we separate the calculation of inhalability from the deposition calculation and do not include it curves plotted in Figure 3.4 or Figure 3.5. These figures show correctly that 100% of inhaled 100 micron particles are deposited by impaction and settling.
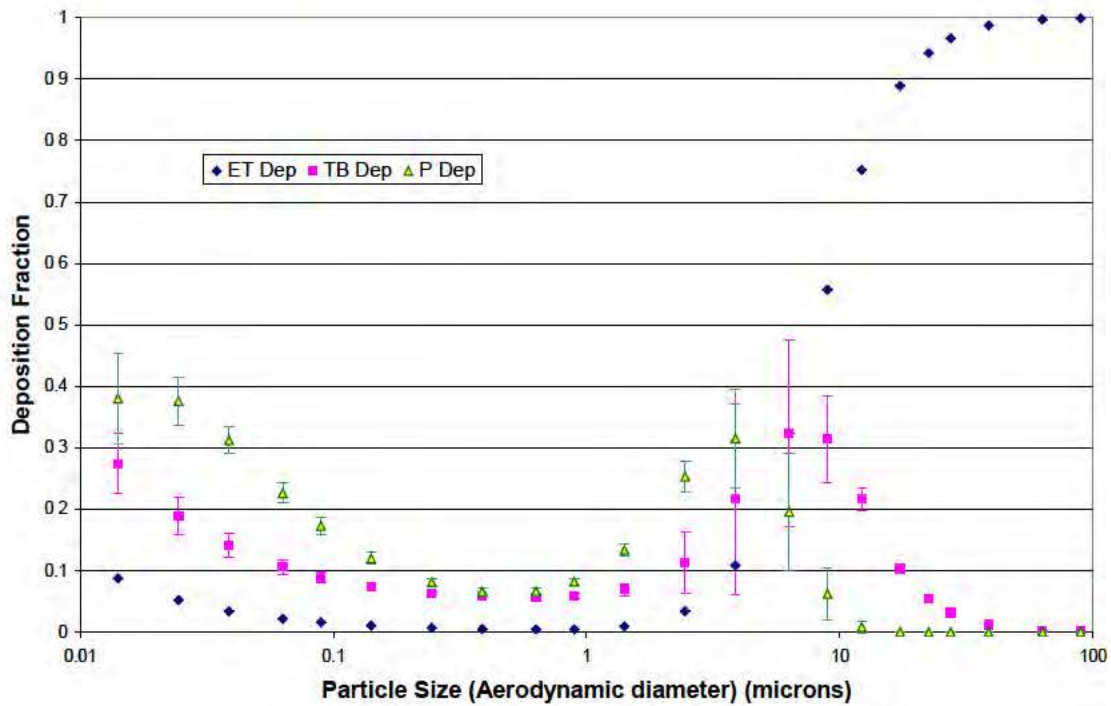
Figure 3.4. Fractional deposition and standard deviations of inhaled particles for 15 lpm breathing rate.
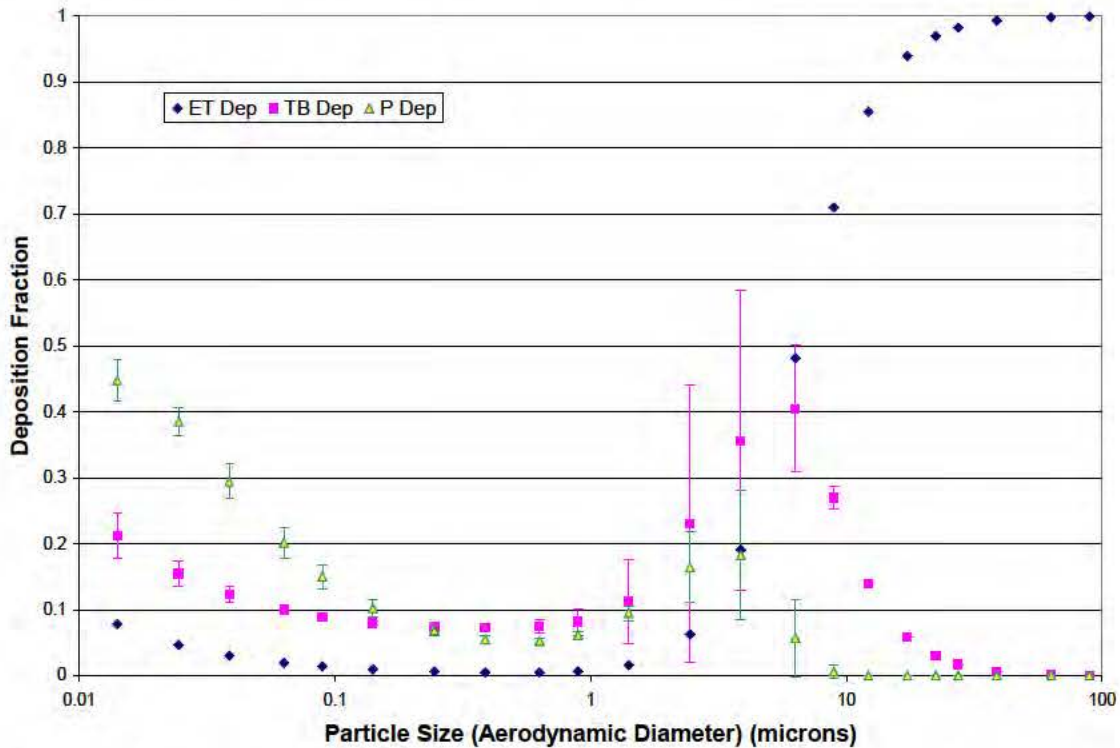
Figure 3.5. Fractional deposition and standard deviations of inhaled particles for 40 lpm breathing rate.

Another notable feature at both breathing rates is the large standard deviation (variability) associated with TB and pulmonary deposition in the 1 to 5 micron particle size range. In this size range, impaction is a primary mechanism for deposition. The variability in deposition is due to changes in the number and size of pathways in the TB region for the 10 stochastic models and how that affects impaction. With fewer and smaller pathways through the TB region, air flow speed and, hence, impaction is increased, causing increased deposition in the TB region. In this case, the filtering effect of increased deposition in the TB region reduces deposition in the P region. More and larger pathways through the TB region reduce deposition there and increase it in the P region, so variability in deposition for the two regions is negatively correlated. We believe this variability fairly represents the person-to-person variability of the human population. Research is being conducted in the toxicology community on how this variability influences the interpretation of data from animal models of asthma and the susceptibility to and treatment of asthma in humans (Moss and Oldham, 2006; Moss, 2010). For present purposes, we note that the pulmonary retained dose for different persons exposed to the same 5 micron aerosol environment is expected to vary by at least a factor of three.

A complete table of the average and standard deviation data is contained in Appendix 2.

The data used to develop these look-up tables does not include the inhalability factor. The inhalability factor is calculated and applied to the ambient concentration independently.

By implementing the MPPD stochastic models as a look-up table, we utilize the best estimate of the regional deposition for the average human respiratory system. We are also able to determine the standard deviation associated with the deposition fraction. Further development of the inhalation model should include the deposition uncertainty with the dosage uncertainty to improve the uncertainty of overall probability of effect calculations.

3.5. Agent Containing Particle Calculation

The physiological response to biological agents depends on a number of factors; as we demonstrate, the particle size and resultant deposition location is one factor. For some agents, probability of infection correlates best with the number of agent containing particles (ACP) deposited in a given region of the respiratory tract. Adding more organisms to a given particle does not significantly increase its probability of causing infection. In other words, how many organisms are deposited is less important than the total number of agent-containing particles deposited. For other agents, the probability of infection is a function of both the size (deposition location) and the total number of organisms deposited. The data indicate that *F. tularensis* is of the former type (Day and Berendt, 1972) and spores of *B. anthracis* are of the latter type (Druett *et al*., 1953). Bacteria are fairly large, on the order of a micron or more, so small particles prepared from a medium of both carrier and organisms may not in fact contain an organism. Recall that releases are usually defined by a particle size distribution, typically a log-normal distribution, so the aerosol can contain small particles that may only be composed of carrier. We developed a means of predicting the probability that a particle of a given size was actually an ACP. We use a Poisson distribution and the bulk material property of concentration, the number of organisms per unit mass (or volume). This subsection briefly describes the calculation and how it is used in the DARRT model.

3.5.1. *Discussion*

Experimental aerobiology studies use various methods to determine the number of organisms in a particle, including simple optical scanning and counting. More often, data on the number of organisms in an aerosol is simply reported as the bulk concentration, either in organisms per unit mass or volume. For a large particle, the bulk concentration value times the particle volume gives a reasonable approximation of the number of organisms in the particle. However, as the particle size decreases we

approach the situation in which only one organism is expected. At this point, whether or not the particle contains an organism becomes a random process. Since particles can only contain integer numbers of viable organisms, we may use Poisson statistics to estimate whether a particle contains one or more organisms.

To test this approach, we first compared the average number of organisms per unit volume as a bulk property compared with experimental data on organism count per particle. Reports of *F. tularensis* aerobiology studies performed in the early 1970's included data regarding the average number of organisms per particle for particles of given sizes (Day and Berendt, 1972). They also provided a bulk concentration of 4×10^{10} cells (organisms) per milliliter (*ml*). If we assume a spherical particle shape, we can calculate the expected (average) number of organisms per particle. Figure 3.6 shows the measured average number of cells for a given particle size associated with four different particle size distributions used in the study. For comparison, the dot-dash line shows the prediction based on the simple volumetric calculation. As can be seen in the graph, simply scaling the bulk cell concentration value by the particle volume gives a reasonable approximation of the number of cells per particle.
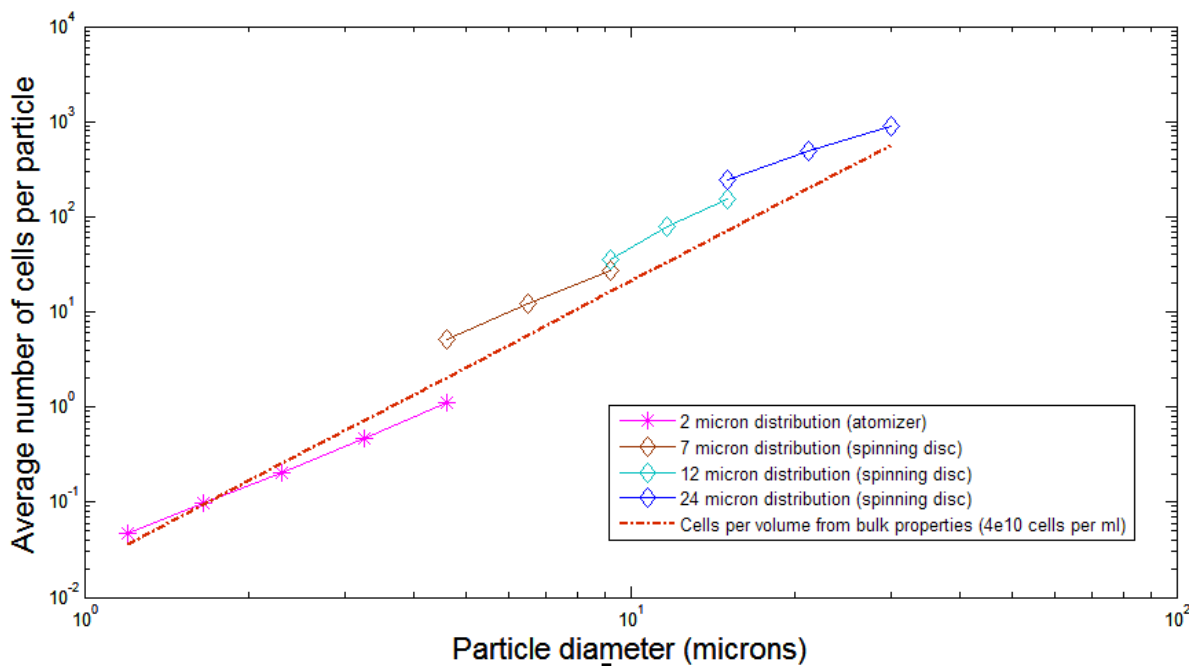
Figure 3.6. Experimentally measured (Day and Berendt, 1972) average number of cells per particle compares well with the estimate (dot-dash line) based on bulk concentration.

As noted above, particles can have only integer numbers of cells, but one can see from Figure 3.6 that small particles may have, on average, much less than one cell per particle. At this point, we must develop a method for calculating the probability that a particle of a given size does, or does not, contain at least one cell.

We assume the number of cells per particle follows a Poisson distribution and that the bulk material concentration provides a reasonable estimate of the average number of cells per unit particle volume. For a Poisson distribution, the probability that a particle of diameter d_{ae} contains no agent cells (*i.e.*, is not an agent containing particle) is:

$$P(0, d_{ae}) = e^{-\overline{C}(d_{ae})} \tag{3.2}$$

where $\overline{C}$ is the average (expected) number of cells in a given particle size d_{ae} based on the volume of the particle and the bulk concentration of the medium. Conversely, the probability that a particle of diameter d_{ae} contains at least one cell (is an agent containing particle) is:

$$P(\geq 1, d_{ae}) = 1 - P(0, d_{ae}) \tag{3.3}$$

We include this relationship in the DARRT model as part of the overall estimation of the number of agent containing particles, of a given size, that are deposited in a region of the respiratory tract. This relationship also provides a parameter to judge the potential biological effectiveness that one might attribute to a given biological threat. For example, the *F. tularensis* slurry mixture used in the experiments described above contained a cell concentration of 4×10^{10} cells per ml. The material used to generate the aerosol for the White Coat studies had a cell concentration of 3×10^{11} cells per ml (Saslow, 1961). For a given size particle, the probability of being an ACP increases with bulk concentration. Figure 3.7 shows an example using the two concentrations just described.
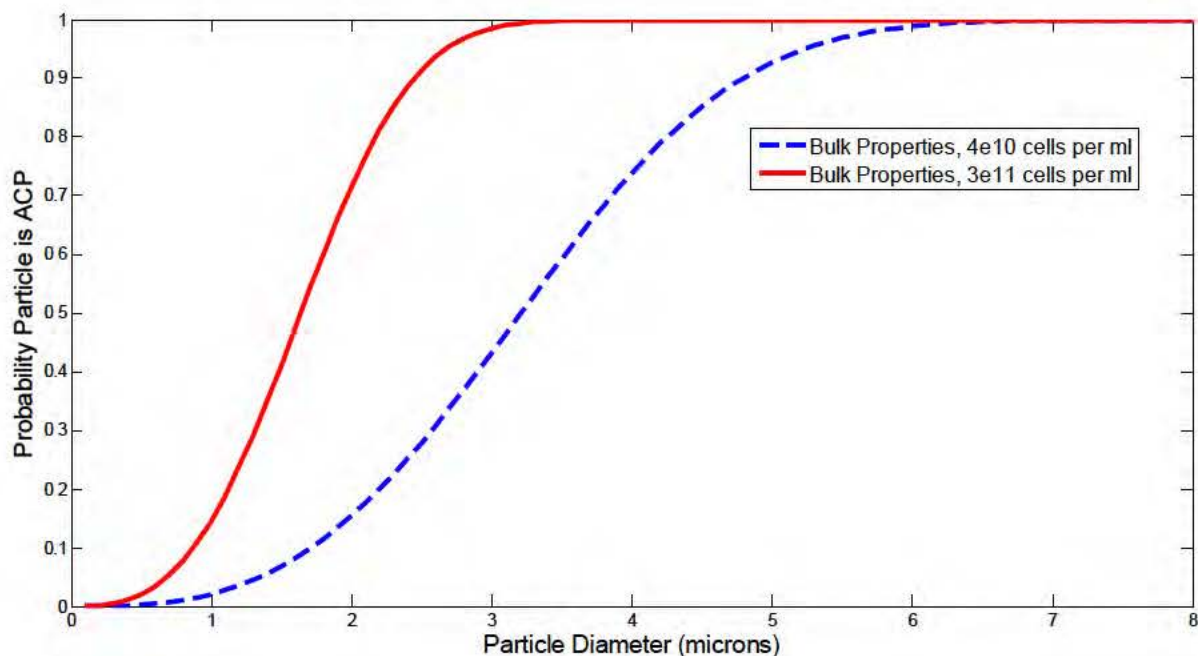
Figure 3.7. Effect of cell concentration of ACP particle size.

As seen in Figure 3.7, for the higher concentration material, a particle of 3 microns in diameter has nearly a 100% probability of containing a cell. However, at the lower concentration, the same size particle has less than a 50% probability of containing a cell. This calculation is performed as part of the estimate of the number of ACPs deposited in a specific region of the respiratory tract and should always be factored in when evaluating potential threats.

3.5.2. Summary

The bulk material property of concentration of infectious organisms (cells) is used to estimate the average number of organisms in a given volume. The parameter is an accurate estimate for relatively large volumes, but as the volume of interest gets smaller, the bulk property is less useful. In particular, as the volume associated with a particle gets small, the bulk property characteristic must be replaced with the expected number of cells per particle. For small particles, we need to calculate the probability that a particle of a given size does or does not contain an agent cell. We assume Poisson statistics and use the bulk cell concentration to estimate the probability that a particle of a given size contains a cell, *i.e.,* is an agent containing particle (ACP).

4. Development of a Human Response Model Accounting for Aerosol Size – Prototype Agent *Francisella tularensis*

4.1.   Literature review

An extensive literature review was conducted to extract experimental data from the available literature concerning the relationship between development of respiratory illness and particle size of inhaled aerosols. Many of the studies reviewed were concerned with respiratory illness caused by *Francisella tularensis,* listed by the Centers for Disease Control and Prevention (CDC) as a Class A Biowarfare (BW) agent. It has been observed that the nature of illness caused by *F. tularensis* is related to the organism's port of entry into the body. Our review included open and classified literature. An unclassified technical report was drafted to summarize the data and since the report was written as a stand-alone document, it is shown in Attachment 3.

The effects of aerosol exposure to *F. tularensis* were extensively studied in the US offensive biological warfare program before the program was dismantled in 1969. "Operation Whitecoat" was the name given to a series of experiments involving human volunteer test subjects that took place during the period from 1954-1973. Most of the 2300 volunteers were conscientious objectors who agreed to be exposed to live agent aerosol clouds in chamber tests and in field tests simulating battlefield deployment of biological agents as an alternative to combat duty. During the program's height, a 1-million-liter aerosol test chamber was constructed at Fort Detrick MD to study agent characteristics under controlled conditions. The 40-foot-high, gas-tight globe was nicknamed the "Eight Ball". Enclosed in a 60-by-60-foot laboratory building, the structure had control panels and exposure chambers at the base of the test sphere, as well as catwalks that allowed scientists to observe exploding biological weapons and collect samples from portals. Both animal and human test subjects were exposed to biological aerosols generated in the chamber. Human subjects ascended to equator level to be exposed at specially designed exposure cubicles. Animals were exposed at other portals. (Perretta 1999, AMEDD 2000, Jemiski 1961) This unique set of experimental data provided a valuable resource from which mathematical models could be constructed to aid in understanding the impact of particle size on the disease development process. Availability of both human and animal data facilitated the modeling process.

4.2.   Development of the Human Response Model

Particles from an aerosol hazard that can be inhaled and deposited in different parts of the respiratory tract can cause location-specific disease manifestations. For example, biological particles containing *Fransicella tularensis* that deposit in the pulmonary region can cause a pulmonary infection resulting in pneumonitis or, once the infection has manifested, can transfer to the bloodstream and cause a subsequent systemic infection. Likewise, biological particles that deposit in the extrathoracic region can cause localized infections in the cervical lymph nodes. As such, it is important to estimate the probability of infection initiating in a given location as a function of the deposition in that region. The probability of infection can be either a function of the number of agent containing particles (ACP) deposited or a function of the number of organisms, whichever function is indicated by the data.

Naturally occurring disease, accidents, and experimental studies with aerosol challenge from *Fransicella tularensis* indicates at least three possible initial infection sites, the pulmonary (P), extrathoracic (ET), and ocular regions (Day and Berendt, 1972). Since this study is focused on the respiratory tract, only the P and ET regions will be considered. The infection probability functions utilize data from human exposures wherever possible. When necessary, the human exposure information will be supplemented with animal data.

Prior to the current study, probability of infection calculations were based on the inhaled dose; that is, the estimated number of particles (or organisms) that were breathed during the exposure. *F. tularensis* was used in sets of controlled exposure studies (the Whitecoat studies) to estimate infection rates and vaccine efficacy using volunteer human subjects (Anno *et al.*, 1997). The data from these studies serves as the foundation of the probability of pulmonary infection. Based on the estimated particle size of the aerosol, the inhaled dose data is modified to account for the likely fraction that will deposit in the pulmonary region. Further, the concentration of organisms per unit volume is used to estimate the number of particles that include one or more organisms (are ACPs). Data indicate that the probability of infection is not a function of the number of organisms deposited, but rather the number of ACPs that are deposited. In other words, it doesn't matter if a particle contains one or more than one organism, but rather only if the particle contains at least one organism. Note that throughout this paper the terms "organism" and "cell" are used interchangeably.

Tularemia is a highly infectious disease that apparently can be caused by very few organisms within the respiratory tract. In the Whitecoat studies, 28 human volunteers received doses of less than 52 organisms of Type A tularemia challenge, but most were still infected (22/28). The data associated with these 28 subjects are used to estimate the probability of pulmonary infection. References indicate that the aerosol challenge to these individuals was less than 1 micron in diameter (Saslaw, 1969).

4.2.1. ET Infection Calculation

Day and Berendt (1972) conducted a tularemia infection study in the early 1970's using rhesus monkeys. Four different size distributions were used with median diameters of approximately 2, 7, 12 and 24 microns. Table 4.1 summarizes results of the Day and Berendt experiments, grouping the data for the two smaller and two larger size particles.

Table 4.1. Results for macaca mulatta *(rhesus) monkeys exposed to* Pasteurella tularensis *(Day and Berendt, 1972).*

Particle size:	2.1 and 7.5 μm	12.5 and 24.0 μm
# of animals exposed	48	45
% Infected	100%	84%
Primary infection site	Lower respiratory system, pneumonitis	Upper respiratory tract, nasal pharyngeal area, cervical and mandibular lymph nodes; eyes, also (15%)
Onset of illness	2-3 days	6-10 days
% fatal (of those ill)	69%	63%
Time to death	4-8 days	8-21 days
LD$_{50}$ (organisms)	14 and 378	872 and 4,447
LD$_{50}$ (agent-containing particles - ACPs)	14 and 28	11 and 8

The smaller particle sizes, 2 and 7 microns, resulted in 100% pulmonary infection with 69% mortality and a time-to-death of 4-8 days. The larger particle sizes, 12 and 24 microns, resulted in 84% infected animals with significant levels of infection of the cervical lymph nodes and the nasal pharyngeal area and onset times ranging from 6-10 days; the initial infection site appeared to be the extrathoracic (ET) area. Of the infected animals, 63% died with a time to death of 8-21 days. The next to last row of Table 4.1 shows the median lethal dose (LD$_{50}$) values reported by the authors for the four particle sizes, ranging from 14 for the smallest particles to 4,447 for the largest, a variation of more than two orders of magnitude. The last row of the table shows the LD$_{50}$ values expressed in terms of ACPs. Here, the variation is only about a factor of three, showing that probability of infection correlates better with number of ACPs inhaled rather than number of organisms.

The data from this study can be used to provide an estimate of probability of infection for particles deposited in the ET region. Table 4.2, reproduced from the Day and Berendt paper summarizes the raw data for the exposures.

Table 4.2. Rhesus monkey infection and death data (Day and Berendt, 1972).

ONMD[a] (µm)	Calculated inhaled dose (cells)	Animals dying at designated day postexposure											Monkey response[b]	
		4	5	6	7	8	9	10	11	12	13	14 to 21	D/T	I/T
2.1	5					1							1/6	6/6
	11			1	1	1							3/6	6/6
	32	1	1	1	1								4/6	6/6
	65	2	2	2									6/6	6/6
7.5	240			1	1	1							3/6	6/6
	720		2	1	1								4/6	6/6
	2,208		3	1	1	1							6/6	6/6
	4,416	1	1	2	1	1							6/6	6/6
12.5	556				1	1	1						3/6	5/6
	1,141					2	1	1	1				5/6	6/6
	2,745[c]					2		1	1	1	1		6/7	7/7
	29,863					1	1	1					3/3	3/3
24.0	146												0/6	2/6
	873											1	1/6	4/6
	2,315							1				1	2/6	6/6
	11,616[c]				1		2					1	4/5	5/5

^{a} ONMD, organism number median diameter. See text for a full explantation.
^{b} D/T, dead/total exposed; I/T, infected/total exposed.
^{c} One animal died at each dose due to the effects of anesthesia.

Note that for nearly all particle sizes and doses, the infection response was essentially 100%. Only the lower doses associated with the largest particles, 24 microns, showed any animals with no infection. The working hypothesis is that the probability of an infection depends on the number of particles deposited in a given region that contain one or more organisms regardless of the size of the particle. In other words, the total number of *organisms* deposited is of secondary importance compared to how many *ACP* are deposited in the region. Therefore, the 24 micron particle size data provides a range of doses and incidence of infection that can be used to estimate a probability function.

The characteristics of the 24 micron particle size distribution are shown as "Aerosol 3" in Table 4.3. The distribution is described by three size bins, with the center bin (17.6-24.9 micron) accounting for 83.6% of all the particles in the distribution; in other words, a nearly mono-dispersed aerosol. Since the distribution is assumed to be represented by a log-normal distribution, the geometric mean is the best approximation of the bin mid-points. The data also include the average number of cells in each particle. These data allow for the conversion from total dose in organisms to the number of particles. Note that given the average number of cells per particle, all particles can be assumed to have one or more cells.

Table 4.3. Aerosol characteristics (Day and Berendt, 1972).

Particle size range (μm)	Particle frequency (%)	Organ-ism frequency (%)	Avg no. of cells/ particle	ONMD[b] (μm)	SD[c] (σ_g)
Aerosol 1				7.5	1.24
3.8–5.4	4.8	0.2	5.1		
5.4–7.6	85.4	79.4	12.2		
7.6–10.8	9.8	20.4	26.7		
Aerosol 2				12.5	1.22
7.6–10.8	7.2	3.1	35.6		
10.8–12.5	83.8	82.1	78.4		
12.5–17.6	9.0	14.8	151.3		
Aerosol 3				24.0	1.33
12.5–17.6	3.6	1.6	241.5		
17.6–24.9	83.6	76.9	490.0		
24.9–35.0	12.8	21.5	895.0[d]		

[a] Spray concentrations were 4×10^8 (aerosol 1), 4×10^9 (aerosol 2), and 4×10^{10} (aerosol 3) cells per ml.
[b] ONMD, organism number median diameter. See text for a full explanation.
[c] SD, geometrical standard deviation.
[d] Cell count was obtained by extrapolation.

The final input for determining the probability of infection is estimating the fraction of particles of a given size deposited in a specific respiratory region, which is calculated using the MPPD model. MPPD does not specifically model rhesus monkey respiratory system, but the rhesus is a reasonable animal suggogate model for human respiratory mechanics (Hislop *et al.*, 1984). MPPD accounts for a number of variables that can influence the inhalation and deposition of particles. For example, the model includes a calculation of a particle's inhalability, breathing rate, and the breathing mode (nasal or oral). In the example of the rhesus monkey study the inhalability fraction was set to 1.0. The animals were anesthetized, so it was assumed they were prone and masked, and this environment would probably allow for all the particles in the breathing zone to be inhaled. Further, since the animals were anesthetized, the breathing rate was equivalent to a sleeping breathing rate of 7.5 l/min. MPPD results of the deposition fractions for the ET region, using these parameters, is shown in Table 4.4. A detailed discussion of the respiratory mechanics model is presented in the previous section.

Table 4.4. ET deposition fraction

Particle Size (microns)	ET
14.83	0.9891
20.93	0.9974
29.52	0.9994

The data set for estimating the probability of ET infection can now be created as shown in Equation 4.1.

$$D^{ET} = D \sum_{i=1}^{3} \frac{f_i d_i^{ET}}{\overline{C}_i}$$

(4.1)

Where:

D^{ET} = Number of particles deposited in the ET region

D = Total dose delivered as number of organisms

$f_{i=}$ = Fraction of particles in a specific size bins

d_i^{ET} = Fractional deposition in the ET region for a particle in a specific size bin

$\overline{C}_i$ = Average number of cells per particle for a specific size bin

i = Each of three size bins

The results of using Equation 4.1 on the dose levels associated with the 24 micron particle size data from Table 4.2 results in the D_{ET} shown in Table 4.5.

Table 4.5. ET deposition

Inhaled Dose	Deposited Particles, ET	Infected / Total
146	0.2908	2 / 6
873	1.7391	4 / 6
2315	4.6116	5 / 5
11616	23.1398	6 / 6

Note that the lowest inhaled dose resulted in an expected ET deposition of less than 1 particle. Obviously fractional particle deposition is not physical, so this value shows the stochastic nature of the probability of infection. The I/T data from Table 4.2 can be fit to a cumulative log-normal distribution using a non-linear least squares fit. This was performed using the Curve Fit Routine in MATLAB®. Results of the probability of ET infection equation are shown in Equation 4.2 and shown graphically in Figure 4.1.

$$P^{ET}(D^{ET}) = 0.5 * \left[1 + erf \frac{\left(\ln(D^{ET}) - \mu\right)}{\sigma\sqrt{2}} \right]$$

(4.2)

where:

$\mu = -0.7187$

$\sigma = 1.527$

The statistical analysis of the curve-fit includes a Sum of the Squares due to Error (SSE) = 0.01651, an R-square = 0.946 and a Root Mean Squared Error (RMSE) = 0.09085.
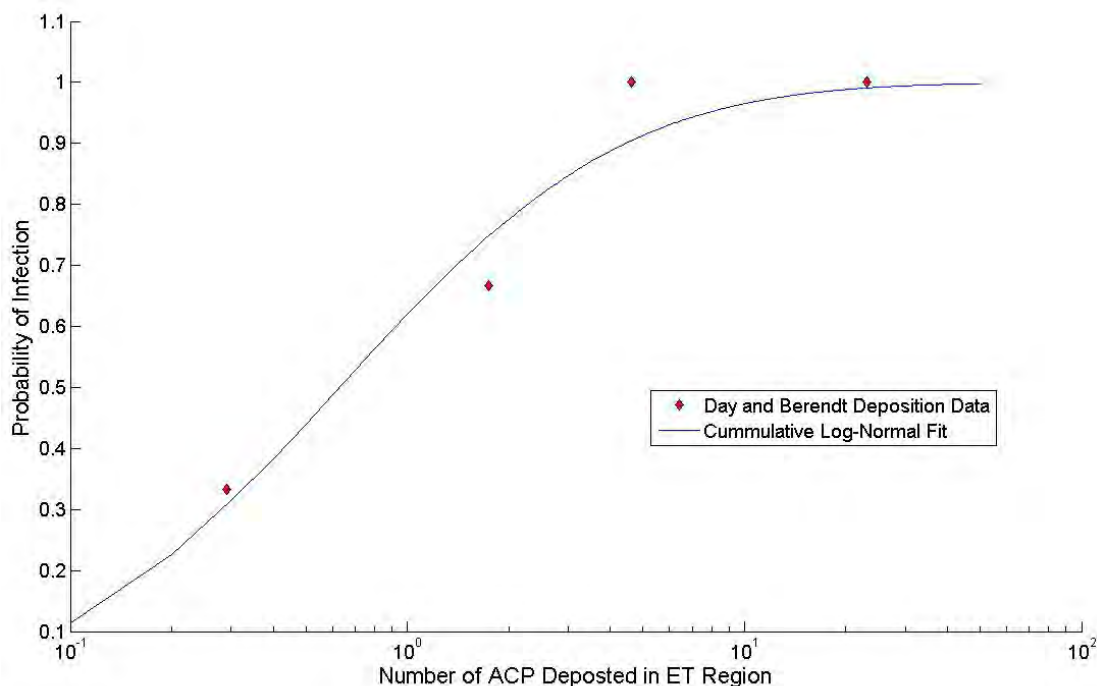
Figure 4.1. Probability of ET infection

The ID_{50} for this probability of infection curve is 0.49 particles deposited in the ET region and the ID_{90} is 3.5 particles deposited in the ET region.

4.2.2. Pulmonary Infection Calculation

The probability of infection has been calculated using the Whitecoat data (Anno, Deverill, 1997) based on the inhaled dose. The probability curve for infection can be correlated to the number of particles deposited in the pulmonary region by estimating the fraction of the inhaled dose that will result in deposition of agent containing particles in the pulmonary region.

According to the Saslaw paper, the particle size used in the set of experiments resulting in inhaled doses of 52 organisms or less was 0.7 microns in diameter. This small particle size is not very efficiently retained in the pulmonary region; MPPD estimates a deposition fraction of only 0.067 at a breathing rate of 15 liters/minute. The probability of infection based on the cumulative log-normal distribution developed by Anno and Deverill has a μ^{AD} of 2.2803 and a σ^{AD} of 1.1939. The geometric

standard deviation, σ^P for the scaled distribution will be the same as σ^{AD}, but the median value (μ^P) will change as shown in Equation 4.3.

$$\mu^P = \ln\left(0.067 \cdot e^{\mu^{AD}}\right) = -0.4228 \qquad (4.3)$$

As an alternative, the same non-linear least square curve-fit routine used for the ET calculations was used to fit the scaled deposition data. This new fit compares very well with the scaled Anno and Deverill fit as shown in Figure 4.2.
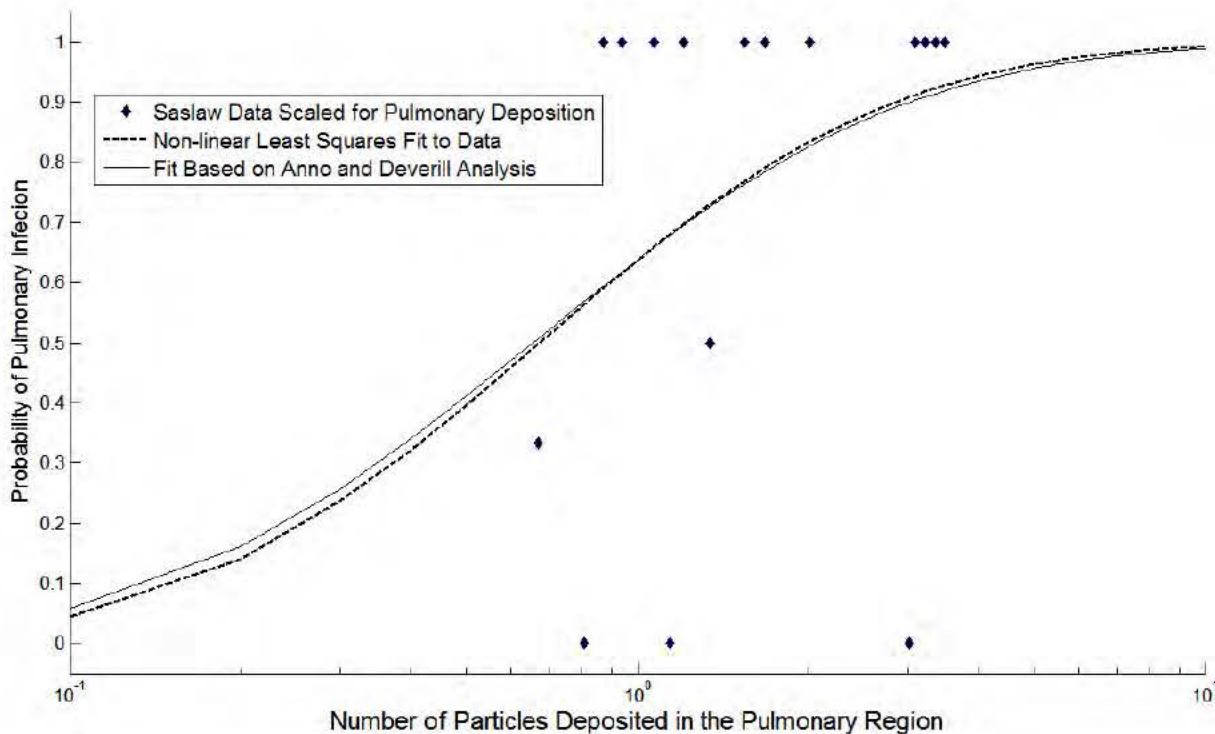
Figure 4.2. Probability of pulmonary infection

4.3.   Summary

Estimates of the probability of pulmonary or ET infection can be calculated from available data. The Whitecoat studies were used to calculate a probability of infection and the original function can be scaled to estimate the probability of pulmonary infection. The resultant probability function is shown in Equation 4.4.

$$P^P(D^P) = 0.5 * \left[1 + erf\frac{\left(\ln(D^P) - \mu^P\right)}{\sigma^P\sqrt{2}}\right] \qquad (4.4)$$

where:

$\mu^P = -0.4228$

$\sigma^P = 1.1939$

The probability of ET infection can be estimated from rhesus monkey studies conducted by Day and Berendt. Equation 4.5 shows the ET probability function.

$$P^{ET}(D^{ET}) = 0.5 * \left[1 + erf \frac{\left(\ln(D^{ET}) - \mu^{ET} \right)}{\sigma^{ET} \sqrt{2}} \right]$$

(4.5)

where:

$\mu^{ET} = -0.7187$

$\sigma^{ET} = 1.528$

5. Development of Additional Models for Particle Size-Dependent Health Effects

In addition to the prototype biological agent for tularemia, we developed a biological toxin model for inhaled dry ricin. We also have developed a model for predicting the effects of inhaled liquid droplets of volatile chemical agents. However, due to software constraints, primarily associated with current input/output capabilities of SCIPUFF, we were unable to integrate the chemical agent model with JEM. We have developed the mathematics of the model and have a prototype that can run stand-alone based on sampler file output. The ricin model and the mathematics of the prototype chemical agent models are described below.

5.1.   Ricin

The purpose of this section is to describe the calculations involved in estimating a probability of mortality function for inhaled ricin. Toxic effects of ricin vary according to the route of administration, but the clinical symptoms frequently are related to a severe inflammatory response and multiorgan failure. Numerous studies, including Roy's study with Balb/C mice (Roy *et al.*, 2002), have shown inhaled ricin appears to cause significant damage only if it reaches the pulmonary region. Therefore, a reasonable working assumption is that the probability of mortality by the inhalation route is based on the inhaled dose delivered to the lung. Since ricin is a toxin, the dose should be scaled to the body mass and the resultant dose is calculated as (mass of deposited toxin)/(body mass) expressed in μg/kg.

5.1.1.   Background

Roy showed in his study that 1 μm aerosolized ricin particles caused mortality in Balb/C mice, while 5 or 12 μm particles did not. Few of the larger particles can reach the pulmonary region of the mouse, but the toxin showed up in other organs due to extrathoracic deposition and clearance. Further, pathology of rodents and non-human primates show aerosolized ricin resulting in significant lesions and edema in the alveolar and terminal bronchial region (Griffiths *et al.*, 1993, Leffel, *et al.*, 2007). Therefore, one can hypothesize that after an inhalation exposure the probability of significant effect or mortality is a function of the mass of ricin that is deposited in the pulmonary (P) region of the respiratory tract.

Griffiths performed a series of exposures to rats using a ricin aerosol with a particle size distribution (PSD) of 0.9 μm mass-median aerodynamic diameter (MMAD) and a σ of 1.6; a fairly narrow distribution. Griffiths used six groups of six rats each (one group had only 5) and used dosages ranging from 1.51-119.3 mg-min/m^3. Table 5.1 provides a summary of Griffiths' data.

Table 5.1. Griffiths' data summary (Griffiths et al., 1993)

Exposure (minutes)	Aerosol Concentration (μg/l)	Ct (mg-min/m^3)	Estimated Inhaled Dose (μg/kg)	N	N (Mortality)	Autopsy Day
40	2.98	119.3	85.77	5	5	1
4	2.98	11.93	7.47	6	6	1,2,3
2	2.98	5.96	3.83	6	4	5
3	1.48	4.54	3.55	6	1	14, 21
2	1.48	3.01	2.02	6	0	5, 7, 2
2	1.31	1.51	1.05	6	0	5, 7, 1

Our goal is to make a meaningful estimate of the lung dosimetry associated with Griffiths' study; in other words, use the data available, and make additional assumptions as necessary to estimate the mass of ricin deposited in the lung and correlate it with the mortality rates from the experiment. We need to make some assumptions regarding his data and we use the Multiple Path Particle Dosimetry (MPPD) Rat model to calculate the lung dosimetry associated with the study.

Griffiths notes that the calculation of inhaled dose is an estimate based on the integrated concentration (Ct). Unfortunately, he does not provide guidance on data he used to calculate the dose, i.e. the ventilation rate (VR) and body mass of the animals (BM). At its simplest, the inhaled dose calculation, D_I, is:

$$D_I\left(\mu g / kg\right) = \frac{Ct \cdot VR}{BM}$$
(5.1)

We use MPPD to calculate the fraction of the inhaled dosage that is deposited in the rat lung. MPPD uses data from Mauderly for the rat respiratory dynamics data and sets the default values of 102 bpm for breathing rate and 2.1 ml for tidal volume (Mauderly *et al.*, 1979). Based on the PSD parameters noted above, and using the default ventilation rate parameters MPPD calculates a pulmonary lung deposition fraction of 0.070.

5.1.2. Calculations

We can now calculate a non-linear, least square fit to a cumulative log-normal distribution of the mortality rate as a function of the presented dosage provided by Griffiths. The fit was calculated using the MATLAB CurveFit Toolkit. Based on the fit, shown in the upper half of Figure 5.1, the ICt_{50} is 5.5 mg-min/m^3, which corresponds to a μ of 1.707, and has a σ of 0.1946.

Next, we convert the presented dosage to deposited lung dose, D_L. The calculation is based on:

$$D_L\left(\mu g / kg\right) = \frac{Ct \cdot VR}{BM} \cdot f_P$$
(5.2)

In other words, we will simply calculate the fraction of the inhaled dose that is deposited in the lung. Just as we show above, we fit a cumulative log-normal to the mortality rate as a function of lung dose. The fit results in an LD_{50} of 0.265 $\mu g/kg$, which corresponds to a μ of -1.34 and a σ_g of 0.0543. The curve is shown in the lower half of Figure 5.1.
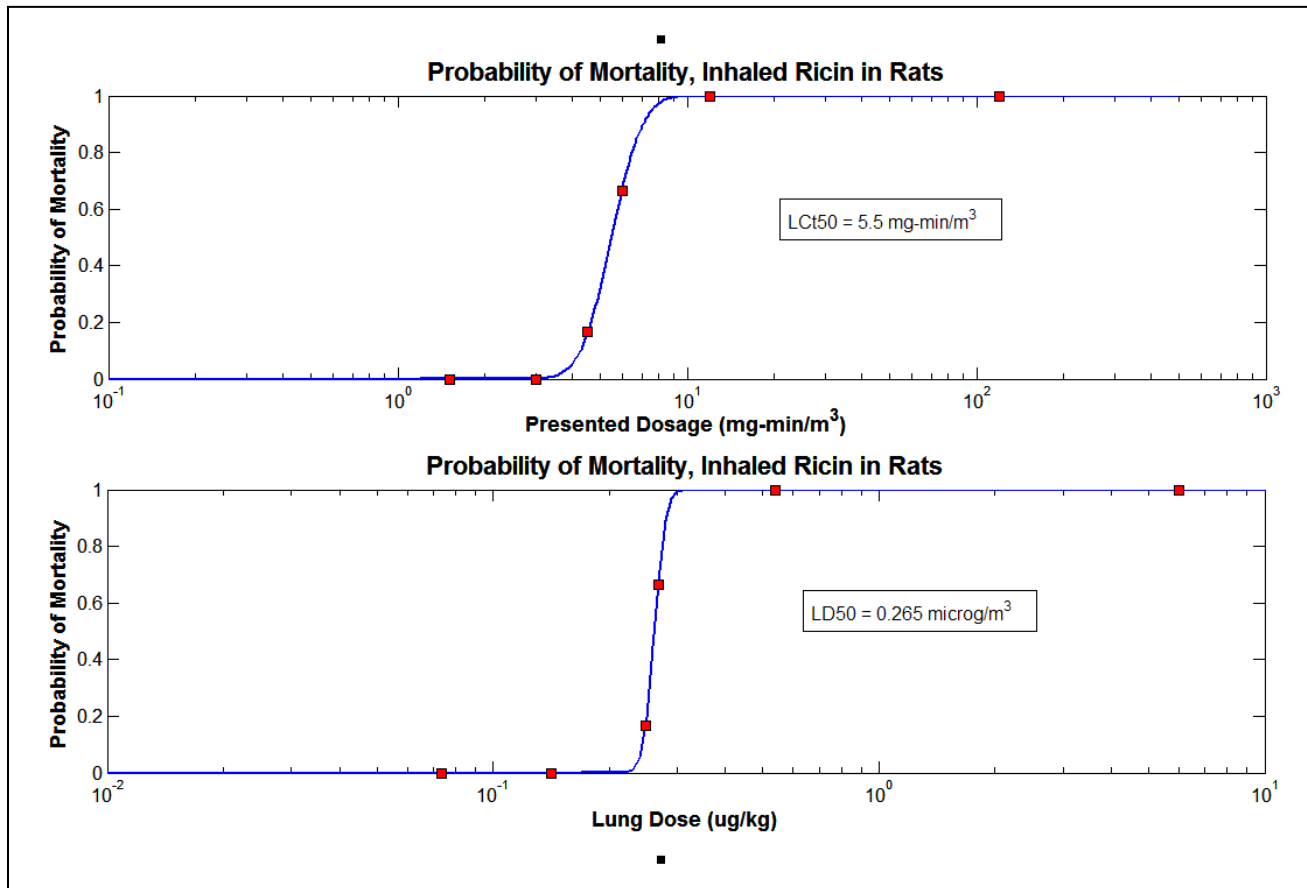
Figure 5.1. Curve Fits to Dosage and Lung Dose Based on Griffiths' Rat Study.

Note the steepness of the curve as compared to the fit to presented dosage. As we look at the data from Table 5.1, the two highest dosages (and dose) result in 100% mortality, while the two lowest results in no mortality. So, the two intermediate data points are key drivers in the shape of the curve. For the dosage calculation, the 1/6 mortality data point is associated with a dosage of 4.54 mg-min/m^3, while the 4/6 mortality is associated with 5.96 mg-min/m^3, a difference of nearly 25%. However, the inhaled dose values associated with those data points have only a difference of about 7%. In other words, as compared to dosage, a much smaller increase in dose will result in a significantly higher mortality rate. This result is consistent with laboratory studies which have shown that in mice and dogs there is a narrow range between the highest ricin dose at which all animals survive and the lowest dose at which all animals die. (Fodstad *et al.*, 1979).

How does our calculated LD$_{50}$ lung dose in the rat compare to human estimates? Multiple sources indicate an LCt$_{50}$ of 30 mg-min/m^3 (Franke 1977, Whaley 1990, SIPRI 1971). We can use MPPD to provide lung dosimetry for a comparison if we make some assumptions. Unfortunately, none of the references for the 30 mg-min/m^3 have PSD data, so we just assume the same particle size as was used in the rat study; 0.9 μm MMAD and a σ of 1.6. We also assume a ventilation rate of 0.015 m^3/min and a body mass of 70 kg (Standard Man). MPPD estimates a pulmonary deposition fraction of 0.104 therefore, our calculated human LD$_{50}$ lung dose is 0.665 μg/kg or about 2.5 times higher than what was calculated for the rat model using Griffiths' data. Given the uncertainty associated with the PSD of the

human data and the fact that the calculations were performed using completely different starting points and different species, the comparison is adequate.

5.1.3. Summary

Multiple studies have indicated that aerosolized ricin toxicity is of primary concern when the aerosol is deposited in the pulmonary region. Deposition in the extrathoracic or tracheobronchial regions does not appear to result in significant mortality risk. As a result, it is reasonable to postulate that the best parameter to model the probability of mortality from aerosolized ricin is the mass of ricin deposited in the pulmonary region of the lung. One must also take the animal's body mass into account, so we are left with a parameter of deposited pulmonary dose measured in mass of ricin deposited in the lung per unit mass of animal, typically μg/kg. We can use MPPD to provide a dosimetry model to translate experimental dosage and inhaled dose data into lung deposition.

Based on the experimental data from Griffiths and modeling from MPPD, we calculate an LD_{50} lung dose of 0.265 μg/kg. We can also use MPPD to translate the currently used 30 mg-min/m^3 LCt_{50} value for humans that is shown in the literature to a lung dose. The translation results in an LD_{50} lung dose of 0.665, a factor of 2.5 higher than from the rat model. Therefore, we recommend using a lung dose value of 0.264 μg/kg as a basis for calculating the probability of mortality from aerosolized ricin.

5.2. Mustard (HD) and other volatile liquid chemical agents

Mustard and other volatile liquid chemical agents present both technical and software implementation challenges for estimating the biological impact of liquid droplets. The current human response model used in HPAC and JEM for HD takes into account dermal deposition of liquid, ocular and dermal effects of vapor, and inhalation of vapor. The component that is lacking is the inhalation of liquid (aersol) droplets. HD is a volatile chemical, so liquid droplet inhalation may not be significant hazard for large downwind range or for an initial release of fine droplets especially for warmer temperatures. However, we have been questioned about potential situations where people may be near a crude device that would release large droplets, for which the potential for liquid droplet inhalation may exist.

For this project, we reviewed the medical effects of the inhalation of HD. Attachment 5 provides an overview of the available literature, which focuses primarily on vapor inhalation. The human response associated with the inhalation of a liquid droplet is technically challenging. A complete analysis would include the potential localized effect that could be caused by the liquid drop depositing on a given surface within the respiratory tract. The surface deposition could also be transferred through the membrane barrier and potentially cause systemic effects as it reached the blood stream. In addition, the liquid will continue to evaporate at a rate consistent with an environment of effectively 100% humidity and a temperature of 98.6° F. The resultant vapor from this evaporation will add to the vapor inhalation that is already being calculated. To fully address the multiple types of effects would require an analysis beyond the scope of our current effort. It would require capturing time-dependent effects to account for the evaporation rate and membrane migration and a physiologically based pharmacokinetic model (PBPK) of the chemical movement throughout the body. While this would be an interesting and challenging analysis, it was beyond the scope of our effort.

We believe we have developed a conservative approximation of the human response. Chemical agents, like mustard, will rapidly volatilize in the environmental conditions that exist within the respiratory tract. Therefore, we calculate the accumulated dosage from inhaled liquid droplets and combine it with the inhaled vapor dosage. We then pass the total inhaled dosage to human response model as a vapor dosage term. In other words, any liquid mass that is inhaled will be added to the inhaled vapor mass and the combined total will be used to estimate the human response as if it were vapor. This approach is conservative in that it does not assume that the droplet needs to deposit in the

respiratory tract to contribute to the vapor dose; we assume the volatility is rapid enough that the droplet is effectively instantaneously volatilized and therefore contributes to the inhaled vapor dosage.

We can use HPAC/JEM sampler files to capture dosage, by droplet size, so we initially developed this methodology to work with sampler file output, with the intent of integrating the calculation directly with SCIPUFF later. This allowed us to focus on performing the calculations correctly before we addressed application program interface (API) issues with SCIPUFF. SCIPUFF performs the calculations of the transport and dispersion of liquid droplets downwind and takes into account evaporation. Unlike dry particulates, liquid drops can evaporate and droplet sizes are calculated in a continuous fashion. The droplet can completely volatilize during transport (and often does for chemical agents), *i.e.* the droplet size goes to "0". Since SCIPUFF calculates the droplet size in a continuous fashion, the sizes are not constrained to fixed size bins like the dry aerosol is. As a result, the mathematical mechanisms of calculating the dosage by size is different than for dry particulate and, we eventually discovered, the data is not currently kept in a form that can be readily passed into FXCODA.

We have developed a stand-alone module that will work with mustard sampler files. The module will read in the material file and capture the data it needs. You can then find the sampler file output that contains the dosage by size data that is of interest and read in the data. The module will calculate the inhalability of each droplet size and use that value to predict fraction of droplets of a given size that are inhaled. The module then calculates the total mass associated with all the inhaled droplets and adds the mass total to the vapor mass total. The resultant vapor total is passed to FXCODA to calculate the probability of mortality and morbidity. The following sequence shows screen captures from the module. Figure 5.2 is a screen capture of the opening splash screen with the "File" pull-down showing the option of loading a material file (only used for the dry particulate aerosols and will not be discussed further) or a sampler file.
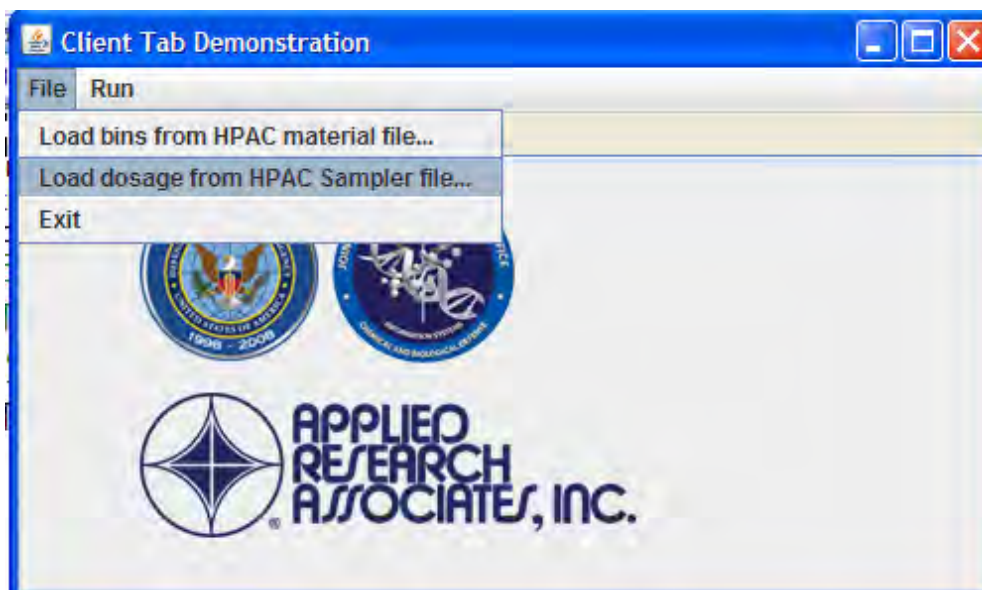
Figure 5.2. Opening screen with File pull-down menu exposed.

Once you have chosen a sampler file output (note both the .smp and the .sam file must be present), the screen shown in Figure 5.3 is displayed. The bin structure and dosage is on the left hand side; inhalation parameters and other variables are listed on the right.

Figure 5.3. Example shot of the DARRT HD post-processor properties screen.

Once the input and variables have been set, the user chooses the Run Sampler file pulldown and will see an output similar to what is shown in Figure 5.4.
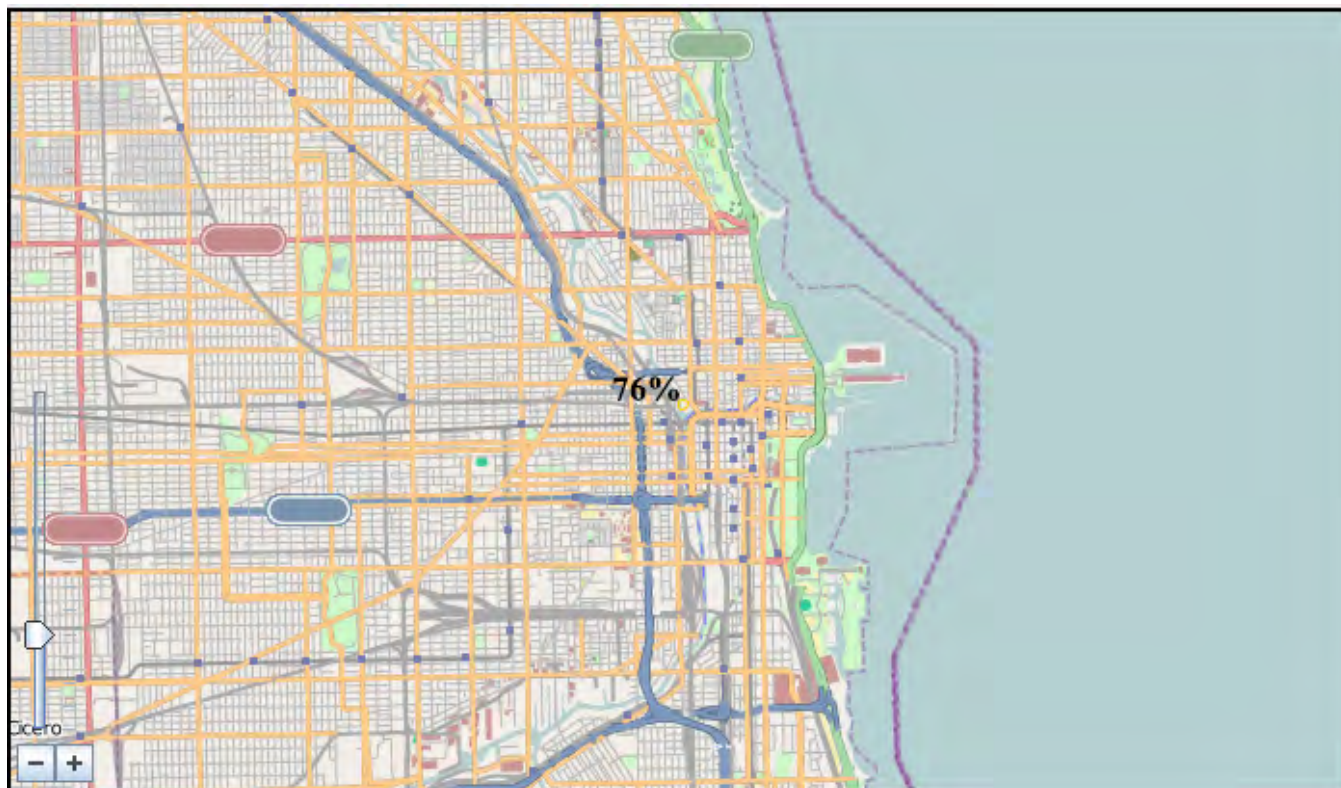
Figure 5.4. Example output from a loaded HD sampler file in a typical city.

As has been described, many of the parameters in the model are hard-coded due to limitations in data transfer with SCIPUFF. When fully integrated with HPAC or JEM, these parameters will be handled consistent with existing models within FXCODA.

6. Software Implementation

The DARRT model is coded in a modified version of the FXCODA module that is presently used in HPAC and JEM. FXCODA includes all the chemical and biological human effects models, including the performance decrement models that are used for some agents. For most agents, FXCODA will calculate probability of effect (infection, injury or mortality) for a given dosage or concentration and pass the information back so it can be overlaid with the affected population to calculate the number of people affected. So typically, one can plot either contours of probability of effect, or casualty tables with the actual number of people affected. FXCODA has stand-alone documentation which will be updated to include the new DARRT model.

6.1.   Structure

The programmatic structure of FXCODA is documented in "HPAC Effects Module FXCODA: Chemical-Biological Operational Degradation Analysis (CODA) Human Effects" that was originally drafted for DTRA under contract DTRA01-03-D-0016. A summary of the changes made to FXCODA to implement the DARRT model is contained in Attachment 4. The FXCODA report will also be updated to reflect the changes included for the DARRT model.

6.2.   Application Program Interface (API)

Appendix 3 contains a summary of the FXCODA API changes. Complete documentation for the modifications to the FXCODA API will be submitted with the software.

6.3.   Coordination with JSTO and JPM IS and Model Transition

A modified version of FXCODA that includes the DARRT inhalation model for dry particulate tularemia and ricin is ready for transition to JEM. Software Problem/Change Request (SPCR) 5492 was submitted to request the change be made to JEM. As noted in this report, this initial version of DARRT includes a hard-coded wind speed of 4 m/s. SPCR 5494 was submitted to request SCIPUFF be modified to allow the wind speed information to be transferred to FXCODA. Finally, SPCR 5493 was submitted to request that the dosage by size information be transferred to FXCODA; this would enable us to implement the liquid droplet inhalation model for chemical agents, as well as the wet particle biological agents.

7. Parameters for the Inhalation Mechanics of Aerosol Hazards

In this section we define several parameters that are relevant to modeling particle size effects for aerosol inhalation hazards. This set of definitions and relationships between the quantities of interest grew out work done for the Joint Effects Model (JEM) Data Certification Panel, which first met 18-19 May 2006 at the Naval Postgraduate School, Monterey, California. The panel was split into three subpanels to consider data related nuclear, chemical and biological weapons, respectively. The Biological Subpanel was led by Dr. Louise Pitt, USAMRIID, with two additional members, Mr. Tim Bauer of the Naval Surface Warfare Center (NSWC) Dahlgren, and Dr. Gene McClellan of ARA. The Biological Subpanel met twice more during the summer of 2006 to complete its recommendations on bioagent data to the JEM Data Certification Panel.

During its meetings, the Subpanel was faced with reviewing several decades of work by many authors, who were not always careful and consistent regarding terminology and definitions. The Subpanel participants agreed on the following working definitions of quantities needed to simulate biological agent aerosols, whether disseminated from wet or dry preparation. These definitions provide a context for current and future work for both biological and chemical agents.

7.1.　　　　Parameter Definitions

Generally, the following parameter definitions focus on the agent fill of the dissemination device, whether sophisticated or improvised, and are aimed at supporting calculations of the disseminated aerosol downwind of the device. In a hazard prediction code, some of the properties may be specified or derived from data in a material properties file and others should be under direct user control via the graphical user interface (GUI) of the hazard source model.

- $V \equiv$ Volume of agent filling a container (m^3)

  The container may be for storage or transport or it may be the payload of a weapon system. If the container is only partially filled, then V refers only to the portion of the container that actually contains agent.

- $M_W \equiv$ Wet bulk mass (kg)

  M_W refers to the total mass of wet agent loaded into some container, where the agent may be an emulsion, solution, suspension or slurry.

- $M_D \equiv$ Dry bulk mass (kg)

  M_D refers to the total mass of dry agent loaded into some container. This parameter is also applicable to the mass of agent remaining when a wet agent dries out after being fully disseminated as an aerosol.

- $M_x \equiv$ Active mass (kg)

  M_x refers to the mass of that portion of the agent which is biologically active in producing the intended effect of the agent. For biological agents, the active mass is generally assumed to be part of the dry bulk mass rather than part of the volatile component of the wet bulk mass.

- $N \equiv$ Number of viable infectious organisms in V

  N must be referenced to a specific time, usually just before dissemination of agent. Note that viability may have decreased during storage and transport in the weapon system, and viability may decrease further during dissemination and transport in the atmosphere.

- $P \equiv$ Purity (a dimensionless ratio)

Purity is the mass fraction of agent that is biologically active in producing the intended effect of the agent.

- $C \equiv$ Concentration (number per unit mass)

    Concentration is the number of viable infectious organisms per unit mass of agent.

- $\rho_W \equiv$ Wet bulk density (kg/m^3)

    Wet bulk density, generally near the density of water, is equal to M_w / V.

- $\rho_D \equiv$ Dry bulk density (kg/m^3)

    Dry bulk density is equal to M_D / V. For particulate matter, the dry bulk density is generally less than the density of individual particles. This definition applies only when V is the fill volume for the dry agent.

- $P_W \equiv$ Wet bulk purity (dimensionless ratio)

    Wet bulk purity is defined as the ratio M_x / M_W.

- $P_D \equiv$ Dry bulk purity (dimensionless ratio)

    Dry bulk purity is defined as the ratio M_x / M_D.

- $C_W \equiv$ Wet bulk concentration (#/kg)

    Wet bulk concentration is defined as the ratio N / M_W.

- $C_D \equiv$ Dry bulk concentration (#/kg)

    Dry bulk concentration is defined as the ratio N / M_D.

7.2. Definitions Applied to Dissemination of Dry Preparations

Figure 7.1 illustrates relationships among M_x, M_D, and N for dry preparations of biological agents, which may be either infective organisms or toxins. If the agent is a biological toxin, then the active mass should be measured in mass units. If the agent is a infective organism, then the quantity may be further specified according to the number of organisms by dividing the active mass M_x by the mass of a single organism.

$$Purity \equiv \frac{M_x}{M_D}$$
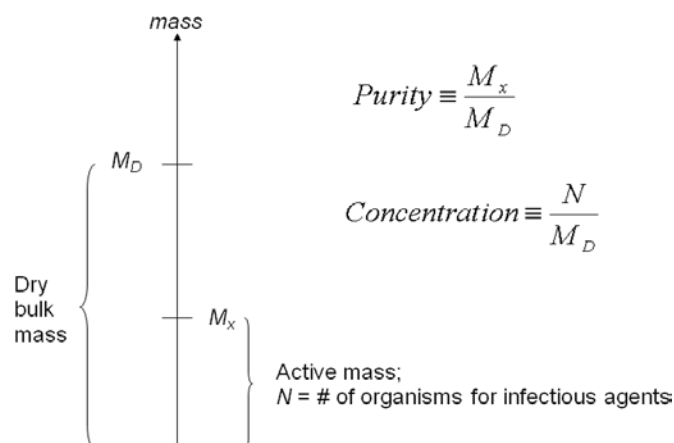
$$Concentration \equiv \frac{N}{M_D}$$

Figure 7.1. Purity and concentration for dry biological agents.

7.3. Definitions Applied to Dissemination of Wet Preparations

Figure 7.2. illustrates the relationships among M_x, M_W, and N for wet preparations of biological agents, which might also be either toxins or infective organisms.

$$Purity \equiv \frac{M_x}{M_W}$$

$$Concentration \equiv \frac{N}{M_W}$$

Active mass;
N = # of organisms for infectious agents
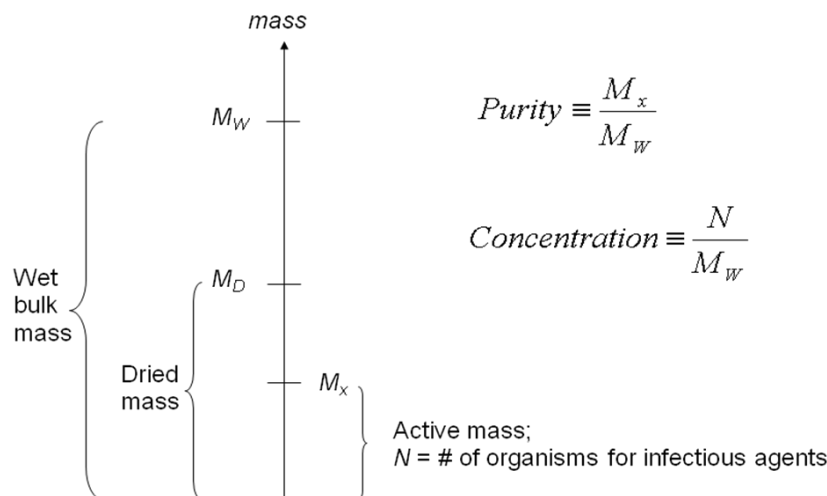
Figure 7.2. Purity and concentration for wet agents.

From these definitions, we see that

$$P_W = (C_W / C_D) P_D$$

In practice, it is unusual for all four of these quantities to be reported for the same agent batch, so the relationship is only approximate when the quantities are taken from different reports. Moreover, concentration for wet agents is frequently reported in number of viable organisms per unit volume, so the density of the wet agent must be known or assumed to derive the concentration in terms of unit mass.

7.4. Applications to Inhalation Modeling

The calculations of primary concern regarding the inhalation model are inhalability, hygroscopicity, and the amount of active agent per particle.

7.4.1. Inhalability

The inhalation model first calculates inhalability for aerosol hazards. This calculation requires:

1. the aerodynamic diameter distribution of the ambient aerosol particles at the location of the head and

2. the ambient wind speed.

These two requirements are the same for either wet or dry bioagents and likewise apply to either dry or liquid chemical agents. The diameter required is the actual physical diameter at the time of inspiration,

regardless of the composition of the particle at that time. That is, the diameter must include both carrier material and non-viable agent in addition to viable agent.

7.4.2. Hygroscopicity

Aerosol particles may either gain or lose water content by condensation or evaporation, respectively, depending on the ambient water vapor concentration (determined by temperature and humidity) and the hygroscopicity of the material making up the particle. Condensation and evaporation are strongly affected by particle size because of the influence of surface tension, which is in turn influenced by curvature of the particle surface. For hygroscopic particles, there is an equilibrium size that depends on ambient humidity. The equilibration time is fast enough that the size of particles entering the respiratory tract will essentially follow the local humidity during inspiration. Furthermore, the air entering the respiratory tract rapidly reaches body temperature and 100% humidity as it passes through the ET region and into the TB region. Therefore, the relevant size for calculation of deposition in the TB and ET regions, especially, is this new equilibrium diameter accounting for humidity as opposed to the diameter in the ambient atmosphere. Thus, this diameter depends on whether the aerosol particles are hygroscopic.

These processes, as well as possible evaporation of liquid chemical agents, would ideally be modeled at the same level of fidelity in the respiratory tract as they are modeled during transport in the atmosphere and vice versa. Therefore, hazard simulation codes should make available to the inhalation model the required parametric data for these calculations.

7.4.3. Active agent

The inhalation model requires sufficient data from the atmospheric transport model to calculate the amount (mass) of active agent in each inhaled particle, whether the active agent is a solid or liquid chemical agent, an infective organism, or a toxin of biological origin. If the agent is an infective organism, it is necessary that the inhalation model be able to calculate the expected number of viable organisms corresponding to the mass of active agent in each particle.

In the context of infective agents, we equate "active" with "viable", *i.e.*, able to cause infection. The loss of viability during atmospheric transport should be calculated by the atmospheric transport code but the particle size must still include the non-viable toxin or organisms.

For some infectious agents, such as anthrax spores, the infective organisms in each deposited particle tend to disperse on deposition so that each organism contributes equally to the probability of infection. For other agents, such as *F. tularensis*, the probability of infection correlates strongly with the number of agent-containing particles deposited, as if the organisms in a single particle stay together and suffer a common fate as they encounter the immune system.

8. Recommendations

SPCR 5492 has been submitted to JEM and we expect to complete integration of the dry tularemia and ricin models into JEM 2.0. Additional SPCRs have been implemented to allow for integration of the liquid droplet model. Some of the work necessary to implement the models will require support from other developers, such as the SCIPUFF developers and possibly the source model developers. Further development of the inhalation model should also include the deposition uncertainty with the dosage uncertainty from SCIPUFF to improve the uncertainty of the overall calculation. As noted in Section 3.4, the pulmonary retained dose for different persons exposed to the same 5 micron aerosol environment is expected to vary by at least a factor of three.

During the completion of this study, we identified several additional areas of science and technology work that will further improve our ability to model the effects of chemical and biological hazards. Much of the data used in our modeling comes from animal experiments; for obvious reasons, high quality data for human exposures from studies like the Operation Whitecoat studies for tularemia are the exception, not the rule. As a result, the data analysis will greatly benefit from further development of animal modeling and extrapolation from animals to humans. Developing models of both respiratory mechanics, as well as biological response mechanisms for animals will greatly improve our understanding of how the animal experiments translate to human effects.

Additional work should be done to understand the impact of inhalation hazards on specific subpopulations such as children and the elderly, as well as to understand differences between sexes. Not only will this improve our ability to model effects on general population, a significant concern for current trends in military support for civilian response, but also to understand the effects on the current make-up of today's military. The military currently does not consist entirely of healthy adult males; nearly 16% of today's military is female.

During the development of the DARRT model, we discovered data that could be used to model the effect of particle size on inhalation effects of several other agents that may be of interest, including *Coxiella burnetti* (Q fever) *and Yersinia pestis* (plague)*. The fidelity of existing casualty prediction models could be significantly improved utilizing these data.

One other area of interest is in extreme particle size ranges, ultra-large and ultra-small. Little data is available for inhalation of ultra-large (>100 micron) particles, and viral agents and other nano-scale particles that pose a special threat due to their extremely small particle size. The impact of various carriers and other components of the final aerosolized agent mixture need to be systematically addressed as well. Additional work is warranted to investigate non-traditional, fourth generation and dusty agents. These highly specialized agents could pose unique threats not captured in normal models.

9. References

ACJ and Associates (2006). Website: http://www.acj-associates.com/Products/LUDEP%20Products/LUDEP.htm

Anjilvel, S., and Asgharian, B. (1995). A multiple-path model of particle deposition in the rat lung, *Fund. Appl. Toxicol.* 28:41-50.

Anno, GH *et al.* (1997). Consequence Analytic Tools for NBC Operations Vol 1- Biological Agent Effects and Degraded Personnel Performance for Tularemia, Staphylococcal Enterotoxin B (SEB) and Q-Fever, DSWA-TR-97-61-VI, Defense Special Weapons Agency, Alexandria, VA.

Asgharian B (2006). Private communication, October 9, 2006.

Asgharian, B., W. Hofmann, and F. J. Miller, (2006a). Dosimetry of particles in humans: from children to adults. In Gardner, D.E., *Toxicology of the Lung*, 4th ed. Boca Raton: CRC Press, ,pp. 151-194.

Asgharian, B., Price, O.T., and W. Hofmann, W. (2006b). Prediction of Particle Deposition in the Human Lung Using Realistic Models of Lung Ventilation, *Journal of Aerosol Science* 37:1209-1221.

Asgharian, B., and Price, O.T. (2006). Airflow Distribution in the Human Lung and its Influence on Particle Deposition, *Inhalation Toxicology* 18:795-801.

Asgharian, B., M. G. Ménache, and F. J. Miller (2004). Modeling Age-Related Particle Deposition in Humans. *Journal of Aerosol Medicine* 17:213-224.

Asgharian. B.*,* Hofmann, W., and Bergmann, R. (2001). Particle deposition in a multiple-path model of the human lung, *Aerosol Sci. Technol.* 34:332-339.

Asgharian, B., Miller, F.J., and Subramaniam, R.P. (1999). Dosimetry software to predict particle deposition in humans and rats, *CIIT Activities* 19(3):1-6.

Benson JM, *et al.,* (2001). Uptake, Tissue Distribution, and Fate of Inhaled Carbon Tetrachloride: Comparison of Rat, Mouse, and Hamster. Inhalation Toxicology. 13:207-217

Benson JM, Tibbetts BM and Barr EB (2003). The Uptake, Distribution, Metabolism, and Excretion of Methyl Teriary-Butyl Ether Inhaled Alone and in Combination with Gasoline Vapor, Journal of Toxicology and Environmental Health, Part A. 66:1029-1052.

Cassee, F.R., Freijer, J.I., Subramaniam, R., Asgharian, B., Miller, F.J., Van Bree, L., Rombout, P.J.A. (1999). Development of a model for human and rat airway particle deposition: implications for crisk assessment, Bilthoven, The Netherlands: National Institute of Public Health and the Envirnoment (RIVM). Report no. 650010018.

Day, W.C., and Berendt, R.F. (1972). Experimental tularemia in Macaca mulatta: relationship of aerosol particle size to the infectivity of airborne Pasteurella tularensis. Infection and Immunity. 77-82.

Druett, H.A., Henderson, D.W., Packman, I., and Peacock, S. (1953). "Studeis on Respiratory Infection I. The Influence of Particulate Size on Respiratory Infection With Anthrax Spores," Journal of Hygeine, 1953, 31:359-371.

Fodstad O., Johannessen J. V., Schjerven L., Pihl A., (1979). Toxicity of abrin and ricin in mice and dogs. J Toxicol Environ Health 5 : 1073-1084

Franke, S. (1977). Textbook of Military Chemistry, Volume 1, Berlin: Military Publisher of the German Democratic Republic 711p

Georgopolous, PG, *et al.,* (2005). A Source-to-Dose Assessment of Population Exposures to fine PM and ozone in Philadelphia, PA, During a Summer 1999 Episode, Journal of Exposure Analysis and Environmental Epidemiology.15:439-457.

Griffiths, G.D., Lindsay, C.D., Rice, P. and Upshall, D.G., (1993). The Toxicology of Ricin and Abrin Toxins – Studies on Immunisation Against Abrin Toxicity, Protceedings of the Medical Defense Bioscience Review, pp.: 1407 – 1416.

Hislop A, *et al.,* (1984). Morphometric studies on the structural development of the lung in *Macaca fascicularis* during fetal and postnatal life, J. Anat.(1984), 138, 1:95-112.

ICRP (1959). Recommendations of the International Commission on Radiological Protection Report of Committee II on Permissible Dose for Internal Radiation (1959) ICRP Publication 2

ICRP (1994). Human respiratory tract model for radiological protection. ICRP Publ 66. *Annals of ICRP*. 24: 23.

Jemski, JV. (1961). Respiratory Virulence of *Pasturella tularensis*, SCHU-S4 Strain, for Man. TE-1462.

Koblinger, L., and Hofmann, W. (1985). Analysis of human lung morphometric data for stochastic aerosol deposition calculations. *Phys. Med. Biol.* 30:541-556.

Leffel, E.K., Hartings, J.M., Pitt, M.L.M, and Stevens, E. (2007). Comparison of Deposition Patterns for Small and Large Particle Aerosolized Toxins and Resulting Disease in Guinea Pigs and African Green Monkeys, *In Defence Against the Effects of Chemical Hazards: Toxicology Diagnosis and Medical Countermeasures,* Meeting Proceedings RTO-MP-HFM-149, pp. 11-1 – 11-12.

Mauderly J.L., Tesarek J.E., Sifford L.J., and Sifford L.J. (1979). Respiratory measurements of unsedated small laboratory mammals using nonrebreathing valves. *Lab. Anim. Sci.* 29: 323-29.

Millage, K.K. *et al.* (2009). A Review of Inhalability Fraction Models: Discussion and Recommendations, Inhalation Toxicology 2009, 1–9, iFirst.

Moss, O. R., and Oldham, M. J. (2006) Dosimetry counts: Molecular hypersensitivity may not drive pulmonary hyperresponsiveness., J. Aerosol Medicine 19(4):555-564.

Moss, O.R. (2010) Chapter 8, Particle Dosimetry in the Nose and Upper Airways of Humans, in "Toxicology of the Nose and Upper Airways" [Series: Target Organ Toxicology, Volume 30], John B. Morris , Dennis J. Shusterman Editors, Informa Healthcare, New York, NY pp 480, ISBN: 9781420081879, 142008187X

Niinimaa, V. Cole, P., Mintz, S., and Shephard, R.J. (1981). Oronasal Distribution of Respiratory Airflow, *Respiration Physiology*, 43:69-75

Perretta, B. (1999). "Historic Structure Stands as Reminder of Biological Warfare" Capital News Service, Maryland NEWSNET newsnet.umd.edu/history/warstructure04.htm

Raabe, O.G., Yeh, H.-C., Schum, G.M., and Phalen, R.F. (1976). *Tracheobronchial geometry: human, dog, rat, hamster, LF-53* Lovelace Foundation, Albuquerque, New Mexico.

Roy, C.J., Hale, M., Hartings, J.M., and Pitt, L., (2002). Impact of Inhalation Exposure Modality and Particle Size on the Respiratory Deposition of Ricin in BALB/c Mice, *Inhalation Toxicology*, 15:619-638.

Saslaw, S, *et al.* (1961). Tularemia Vaccine Study: II – Respiratory Challenge, Arch Ind Med 107:134-146.

Scherer, P.W., Shendalman, L.H., and Greene, N.M. (1972). Simultaneous diffusion and convection in single breath lung washout. *Bull. Math. Biophy*. 34:393-412.

SIPRI (1971). The Problem of Chemical and Biological Warfare Volume 1: The Rise of CB Weapons Stockholm International Peace Research Institute (SIPRI) 1971

Snipes, M. B. (1994). Kinetics of inhaled radionuclides. In *Internal Radiation Dosimetry, Health Physics Society Summer School 1994* (O.G. Raabe, ed.), Medical Physics Publishing, Madison, WI.

Su WC and Cheng YS (2005). Deposition of Fiber in the Human Nasal Airway Aerosol Science and Technology, 39:888-901.

Subramaniam, R. P., Asgharian, B., Freijer, J. I., Miller, F. J., and Anjilvel, S. (2003). Analysis of lobar differences in particle deposition in the human lung. *Inhalation Toxicology,* 15:1–21.

Sweeney TD and Brain JD (1991). Pulmonary Deposition: Determinants and Meausurement Techniques, Toxicology Pathology 19, No.4:384-397.

AMEDD (2000). *Cutting Edge: A History of Fort Detrick, Maryland*, Chapter 7 "Opening the Gates", U.S. Army Medical Department (AMEDD), October 2000. www.detrick.army.mil/cutting_edge/chapter07.cfm

U.S. EPA (2004). Dosimetry of Particulate Matter (Chapter 6). *Air Quality Criteria for Particulate Matter. Volume II of II.* Office of Research and Development, U.S. Environmental Protection Agency, Washington, DC.   EPA 600P-99/002bF.

U.S. EPA (2007). Website: http://www.epa.gov/radiation/assessment/dcal.html

Weibel, E.R. (1963). *Morphometry of the Human Lung*, Springer Verlag, Berlin.

Whalley, C. E. (1990). Toxins of Biological Origin, CRDEC-SP-021 June 1990 pp. 38-40

Winter-Sorkina, R. de and Cassess, F.R. (2002). From concentration to dose: factors influencing airborne particulate matter deposition in humans and rats, Bilthoven, The Netherlands: National Institute of Public Health and the Envirnoment (RIVM). Report no. 650010031.

Yeh, H.C., and Schum, G.M. (1980). Models of human lung airways and their application to inhaled particle deposition, *Bull. Math. Biol.* 42:461-480.

Yu, C.P. (1978). Exact analysis of aerosol deposition during steady state breathing. *Powder Technol.* 21:55-62.

10. Acronym and Abbreviation List

ACP – Agent Containing Particle

API – Application Program Interface

BM – Body Mass of an animal

BW – Biowarfare

CB – Chemical and Biological

CFD – Computational Fluid Dynamics

CIIT – Chemical Industry Institute of Toxicology

CODA – Chemical-Biological Operational Degradation Analysis

Ct – Time-integrated Concentration

DARRT – Deposition and Response in the Respiratory Tract

DCAL – Dose and Risk Calculation

DTRA – Defense Threat Reduction Agency

EOHSI – Environmental Occupational Health and Safety Institute

EPA – Environmental Protection Agency

ET – Extra Thoracic

GUI – Graphical User Interface

HD – Mustard

HPAC – Hazard Prediction and Assessment Capability

ICRP – International Commission on Radiological Protection

lpm – liters per minute

LRRI – Lovelace Respiratory Research Institute

μm – Micron

MMAD – Mass-Median Aerodynamic Diameter

MPPD – Multiple Path Particle Dosimetry

NIOSH – National Institute of Occupational Safety and Health

NRPB – National Radiation Protection Board (now the Radiation Protection Division of the UK Health Protection Agency)

nm – nanometer

P – Pulmonary

PM – Particulate Material

PBPK – Physiologically Based PharmacoKinetic model

PSD – Particle Size Distribution

RfC – inhalation Reference Concentration

RMSE – Root Mean Squared Error

SCIPUFF – Second Order Closure Integrated PUFF

SPCR – Software Problem/Change Request

SSE – Squares due to Error

TB – Tracheobronchial

TICs – Toxic Industrial Chemicals

TIMs – Toxic Industrial Materials

UK – United Kingdom of Great Britain

VR – Ventilation Rate

11. Appendix 1 - List of Registered Users of MPPD Software

Government Agencies

Air Force Research Laboratory, Dayton, OH

California Environmental Protection Agency, Sacramento, CA

CDC Jiangsu Province, Nanjing, China

CONTARP, Rome, Italy

Danish Working Environment Authority, Copenhagen, Denmark

Defense R & D Canada, Medicine Hat, Canada

Defense Science and Technology Laboratory, Salisbury, UK

Edgewood Chemical and Biological Center, Aberdeen Proving Ground, MD

Environment Canada, Toronto, Canada

European Commission – Joint Research Centre, Ispra, Italy

Federal Institute for Occupational Safety and Health, Dortmund, Germany

Federal Office for Radiation Protection, Oberschleiheim, Germany

Idaho National Laboratory, Idaho Falls, ID

Hamilton County Environmental Services, Cincinnati, OH

Health Canada, BGTD, Ottawa, Ontario, Canada

Health and Safety Laboratory, Buxton, Derbyshire, United Kingdom

Indian Institute of Technology, Mumbai, India

Institute for Defense Analyses, Alexandria, VA

Institute of Energy and Environmental Technology, Duisburg, Germany

Institut National de la Recherche Scientifique, Nancy, France

INERIS, Verneuil en Halatte, France

INSERM U-618, TOURS, France

Michigan DEQ, Lansing, MI

Ministry of the Environment, Toronto, Ontario

National Center for Toxicological Research, FDA, Jefferson, AR

Naval Health Research Center/Environmental Health Effects Lab, WPAFB, OH

Naval Surface Warfare Center, Dahlgren, VA

Oak Ridge National Laboratory, Oak Ridge, TN

Ontario Ministry of the Environment, Toronto, Canada

RIDEM, Providence, RI

Swedish Chemicals Agency, Sundbyberg, Sweden

Swiss Federal Institute of Technology, Zurich, Switzerland

Texas Commission on Environmental Quality, Austin, TX

U.S. Army Center for Health Promotion and Preventive Medicine, Perryville, MD

US Consumer Product Safety Commission, Bethesda, MD

U.S. Department of Labor, Occupational Safety & Health Administration, Washington DC

U.S. Department of Energy, Washington DC

U.S. Environmental Protection Agency, Washington DC and Research Triangle Park, NC

WorkSafeBC, Policy & Research Division, Vancouver, Canada

National Institute of Public Health and the Environment, Bilthoven, the Netherlands

National Institute for Environmental Studies, Tsukuba, Japan

National Institute for Industrial Environment and Risk (INERIS), Verneuil en Halatte, France

National Institute of Advanced Industrial Science and Technology, Tsukuba, Japan

National Research Center for Environment and Health (GSF), Munich, Germany

National Institute of Occupational Health, Copenhagen, Denmark

National Institute of Occupational Safety and Health, Cincinnati, OH

National Research Centre for the Working Environment, Copenhagen, Denmark

Research Laboratories

Applied Research Associates, Arlington, VA

Battelle Memorial Institute, Cincinnati, OH

Center for Environmental Science and Engineering, Bombay, India

Dept. of Medical Physics and BioEng., Southampton General Hospital, Southampton UK

Desert Research Institute, Las Vegas, NV

Eurometaux, Brussels, Belgium

FoBiG, Freiburg, Germany

Fraunhofer-ITEM, Hannover, Germany

German Research Center for Environmental Health, Oberschleissheim, Germany

Healthcare Applications R & D, Tonawanda, NY

Huntingdon Life Sciences, Huntingdon, UK

IIT Research Institute Chicago, IL

Industrial Technology Research Institute, Hsin-Chu, Taiwan

Institute for Defense Analyses, Alexandria, VA

Institute of Occupational Medicine, Edinburgh, UK

Lovelace Respiratory Research Institute, Albuquerque, NM

Pacific Northwest National Laboratory (PNNL), Richland, WA

Research Center for Chemical Risk Management, Tsukuba, Japan

Research Triangle Institute, Durham, NC

Schering-Plough Research Institute, Kenilworth, NJ

Syngenta Central Toxicology Laboratory, Macclesfield, United Kingdom

TERA, Cincinnati, OH

VITO, Mol, Belgium

White Eagle Laboratories, Doylestown, PA

Private Sector, Industry and Consulting

3M, St. Paul, MN

Aerogen, Galway, Ireland

Aerovance, Inc., Berkeley, CA

AirLiquide, Les Loges en Josas, France

Akzo Nobel Chemicals, Dobbs Ferry, NY

Allist, Shanghai, China

Amgen, Thousand Oaks, CA

Amphastar, San Gabriel, CA

Anoixis Corporation, Natick, MA

ANSYS Inc, Evanston, IL

Aradigm Corp., Hayward, CA

Astrazeneca RED, Lund, Sweden

Atlantic Health, Morristown, NJ

Australian Broadcasting Corporation, Sydney, Australia

Aventis Pharma Ltd., Cheshire, United Kingdom

BASF, Ludwigshafen, Germany

Bayer CropScience, Research Triangle Park, NC

Bayer HealthCare, Wuppertal, Germany

Bespak Europe Ltd, Milton Keynes, UK

Boehringer Ingelheim Pharam GmbH, Biberach, Germany

British American Tobacco, Millbrook, UK

Bruce Allen Consulting, Chapel Hill, NC

Janusz Byczkowski, Fairborn, OH

Caterpillar, Peoria, IL

Chadbourne & Parke LLP, New York, NY

ChemRisk, Pittsburgh, PA

Chrysalis Technologies, Richmond, VA

Cincinnati Drug and Poison Information Center, Cincinnati, OH

Clariant, Sulzbach, Germany

Constella Group, Durham, NC

DA Nonclinical Safety Ltd, Godmanchester, UK

Eastman Chemical Company, Kingsport, TN

Kemic Bioresearch, Kentsville, Canada

Kennedy/Jenks Consultants, Portland, OR

LAB International Research, Szabasagpuszta, Hungary

L'Oreal, Clark, NJ

L'OREAL, Clichy, France

Lorillard Tobacco Company, Greensboro, NC

Maine Pulp and Paper Industry (AMEC), Portland, Maine

MannKind BioPharmaceuticals, Danbury, CT

Reed McConnell, Austin, TX

Merck & Co., Inc, Whitehouse Station, NJ

Merck Frosst, Kirkland, Canada

Merckle/ratiopharm GmbH, Ulm, BW, Germany

Therthala Murali, Madison, WI

Mystic Pharmaceuticals, Inc., Cedar Park, TX

Nalco Company, Naperville, IL

*Nektar Therapeutics, San Carlos, CA

Novartis, Horsham, UK

Novo Nordisk, Hillerød, Denmark

Parion Sciences, Durham, NC

Pfizer, Groton, CT

Philip Morris USA, Richmond, VA

Praxair Inc, Tonawanda, NY

Procter & Gamble, Cincinnati, OH

ReckittBenckiser Healthcare Ltd, Hull, UK

Respironics, Inc., Pittsburgh, PA

RJ Reynolds, Winston Salem, NC

SKS Consulting Services, Siler City, NC

Southampton General Hospital, Southampton, UK

Sumitomo Chemical, Osaka, Japan

Sybilla Ltd, Athens, Greece

Syracuse Research Corporation, Cicero, NY

The Dow Chemical Company, Midland, MI

Eastman Kodak, Rochester, NY

EBRC Consulting GmbH, Hannover, Germany

Eli Lilly and Company, Indianapolis, IN

Environ International Corporation, Houston, TX

Euphoric Pharmaceuticals, Ahmedabad, India

ExxonMobil Biomedical Sciences, Inc., Annandale, NJ

Fred J. Miller & Associates LLC, Cary, NC

GE, Fairfield, CT

General Motor Global R&D Operations, Warren, MI

GlaxoSmithKline, London, UK

Gobbell Hayes Partners, Inc., San Antonio, TX

Gradient Corporation, Cambridge, MA

Hospital del Sur, Bogotá, Colombia

ICaRuS Japan Limited, Tokyo, Japan

ICF Consulting, Fairfax, VA

IFC Research Corporation, Huntsville, AL

International Flavors & Fragrances, Shrewsbury, NJ

Erin Kaiser, Salt Lake City, UT

Karolinska Institutet, Stockholm, Sweden

Wayne Ting Consultant, Belle Mead, NJ

Toxicology Excellence for Risk Assessment (*TERA*), Cincinnati, OH

Toyota Central Research and Development Laboratories, Nagakute, Japan

Unilever Safety and Environmental Assurance Centre, Sharnbrook, UK

Vectura, Chippenham, United Kingdom

Allen Vinegar, Hebron, KY

WIL Research, Ashland, OH

Yorkshire Biomedical Consultants Association, Harrogate, UK

Colleges and Universities

Air Pollution Health Effects Laboratories (APHEL), University of California at Irvine

California Institute of Technology, Pasadena, CA

China Agricultural University, Beijing, China

Department of Environmental Sciences, the State University of New Jersey

Department of Mechanical Engineering, Clarkson University, Potsdam, NY

Department of Medicine, University of Rochester

Department of Nuclear Engineering, North Carolina State University

Duke University, Durham, NC

Georgetown University Medical Center, Washington, DC

Harvard School of Public Health, Cambridge, MA

Hokkaido University, Sapporo, Japan

IIT Research Institute, Chicago, IL

Indian Institute of Technology, Mumbai, India

Industrial University of Isfahan, Isfahan, Iran

Jinan University, Tripoli, Lebanon

Johns Hopkins Bloomberg School of Public Health, Baltimore, MD

Karolinska Institutet, Stockholm, Sweden

Kurume University School of Medicine, Fukuoka, Japan

Louisiana State University, Baton Rouge, LA

Lund University, Lund, Sweden

Medical College of Virginia, VCU, Richmond, VA

Michigan State University, East Lansing, MI

McMaster University, Hamilton, Ontario, Canada

National Taiwan University, Taipei, Taiwan

North Carolina State University, Raleigh, NC

NYU School of Medicine, Tuxedo, NY

Politecnico di Torino, Torino, Italy

Texas A&M University, College Station, TX

Universidade Tecnológica Federal do Paraná, Paraná, Brazil

Universitt Dusseldorf, Dusseldorf, Germany

University of North Carolina, Chapel Hill, NC

University of Occupational and Environmental Health, Fukuoka, Japan

University of Oklahoma College of Public Health, Oklahoma City, OK

University of Pittsburgh, Pittsburgh, PA

University of Rochester Medical Center, Rochester, NY

University of Salzburg, Salzburg, Austria

University of Southern California, Los Angeles, CA

University of Texas Health Science Center, Houston, TX

University of Texas Medical Branch, Galveston, TX

University of Utah, Department of Anesthesiology, Salt Lake City, UT

University of Waterloo, Waterloo, Canada

University of Washington, Seattle, WA

University of Alberta, Edmonton, Alberta, Canada

University of Amsterdam, Amsterdam, the Netherlands

University of Bern, Bern, Switzerland

University of Brighton, Brighton, UK

University of California at Los Angeles, Los Angeles, CA

University of Edinburgh, Edinburgh, UK

University of Florida, Gainesville, FL

University of Georgia, Athens, GA

University of Iowa, Iowa City, IA

University of Leicester, Leicester, United Kingdom

University of Medicine and Dentistry of New Jersey, Newark, NJ

University of Minnesota, School of Public health, Minneapolis, MN

University of Montreal, Montreal, Canada

12. Appendix 2 - Data Tables for Stochastic Lung Models

Average values, Part 1.

BrRate	BinMidPts==>	0.0141	0.0245	0.0387	0.0632	0.0894	0.141	0.245	0.387	0.632	0.894	1.41
15000	ET	0.087953	0.052422	0.034094	0.021713	0.01596	0.010859	0.007171	0.005384	0.004569	0.005094	0.009521
16000	ET	0.087278	0.052012	0.033825	0.021541	0.015833	0.010773	0.007117	0.005351	0.004573	0.00516	0.009827
20000	ET	0.084982	0.050618	0.03291	0.020955	0.015401	0.010481	0.006932	0.005243	0.004599	0.005419	0.010985
25000	ET	0.082744	0.049261	0.03202	0.020385	0.014981	0.010197	0.006754	0.005143	0.004646	0.005726	0.012311
35299	ET	0.079394	0.047231	0.030689	0.019533	0.014355	0.009773	0.006493	0.005009	0.004776	0.00634	0.014831
35300	ET	0.079394	0.047231	0.030689	0.019533	0.014355	0.009773	0.006493	0.005009	0.004776	0.00634	0.014831
40000	ET	0.078213	0.046516	0.030221	0.019233	0.014135	0.009624	0.006402	0.004966	0.004838	0.006601	0.015876
60000	ET	0.074495	0.044269	0.028749	0.018293	0.013443	0.00916	0.006127	0.004868	0.005179	0.007797	0.020464
75000	ET	0.072522	0.043078	0.02797	0.017795	0.013078	0.008916	0.005992	0.004851	0.005496	0.008787	0.024127
15000	TB	0.274388	0.189135	0.14075	0.105982	0.089198	0.073942	0.062966	0.058098	0.056708	0.059185	0.069228
16000	TB	0.269544	0.186144	0.138993	0.105168	0.088848	0.074016	0.063369	0.058685	0.057441	0.060022	0.070498
20000	TB	0.253702	0.176653	0.13359	0.102893	0.088081	0.074635	0.065094	0.061047	0.060827	0.063544	0.076097
25000	TB	0.239276	0.16842	0.129215	0.101394	0.087955	0.075809	0.067315	0.063925	0.064502	0.068024	0.084128
35299	TB	0.219273	0.157763	0.124117	0.100307	0.088801	0.078525	0.071603	0.069752	0.071432	0.077382	0.102994
35300	TB	0.219272	0.157762	0.124116	0.100307	0.088801	0.078525	0.071603	0.069753	0.071433	0.077383	0.102995
40000	TB	0.212952	0.154633	0.122845	0.100342	0.089477	0.079833	0.073463	0.072209	0.074517	0.081628	0.112456
60000	TB	0.194195	0.146015	0.119872	0.101324	0.092477	0.084848	0.08044	0.080762	0.086664	0.100227	0.156533
75000	TB	0.185272	0.142363	0.119054	0.102531	0.094759	0.088238	0.085475	0.086619	0.095593	0.115996	0.192957
15000	P	0.380479	0.376113	0.312128	0.226406	0.173021	0.12009	0.081439	0.066054	0.066688	0.082137	0.133892
16000	P	0.386623	0.378395	0.312167	0.225508	0.172029	0.119158	0.08081	0.065395	0.065859	0.080888	0.131643
20000	P	0.406661	0.38514	0.311591	0.221938	0.1683	0.116245	0.078478	0.063263	0.062965	0.076633	0.123705
25000	P	0.424411	0.389737	0.309519	0.217676	0.164287	0.112936	0.076014	0.060966	0.060022	0.072274	0.115431
35299	P	0.442775	0.387573	0.29886	0.20595	0.154088	0.105321	0.070532	0.056178	0.054296	0.064119	0.100093
35300	P	0.442777	0.387572	0.298859	0.205949	0.154088	0.10532	0.070532	0.056177	0.054296	0.064119	0.100092
40000	P	0.447706	0.385474	0.294222	0.201382	0.150371	0.102535	0.068546	0.054441	0.052335	0.061368	0.094802
60000	P	0.443203	0.358757	0.263743	0.176322	0.130304	0.088292	0.058862	0.046382	0.043529	0.049725	0.072875
75000	P	0.426794	0.332267	0.238804	0.157534	0.115816	0.078192	0.052099	0.041037	0.037892	0.042524	0.059298

Average values, Part 2.

BrRate	BinMidPts==>	2.45	3.87	6.32	8.94	12.2	17.3	22.4	27.4	38.7	63.2	89.4
15000	ET	0.034096	0.10891	0.323363	0.557324	0.752084	0.88893	0.942399	0.966511	0.987039	0.996685	0.998741
16000	ET	0.03552	0.113297	0.333265	0.568392	0.760381	0.893298	0.944795	0.967938	0.987603	0.99683	0.998796
20000	ET	0.040851	0.129444	0.368098	0.605543	0.787206	0.907065	0.952273	0.972373	0.989348	0.99728	0.998967
25000	ET	0.046854	0.147121	0.403559	0.640733	0.811252	0.918963	0.958647	0.97613	0.990818	0.997658	0.999111
35299	ET	0.058008	0.178642	0.460737	0.692554	0.844458	0.934746	0.96698	0.981009	0.992717	0.998145	0.999296
35300	ET	0.058009	0.178645	0.460742	0.692558	0.844461	0.934747	0.96698	0.98101	0.992718	0.998145	0.999296
40000	ET	0.062553	0.191018	0.481317	0.709874	0.855015	0.939614	0.969521	0.982491	0.993292	0.998292	0.999352
60000	ET	0.08197	0.241099	0.555579	0.767276	0.88823	0.954481	0.977204	0.986948	0.995014	0.998732	0.999519
75000	ET	0.096935	0.276883	0.601211	0.79905	0.905526	0.961964	0.981026	0.989155	0.995862	0.998949	0.999601
15000	TB	0.113349	0.216578	0.323622	0.314214	0.216373	0.103342	0.054059	0.031479	0.012184	0.003117	0.001184
16000	TB	0.117181	0.223492	0.327501	0.313126	0.211402	0.099665	0.051943	0.0302	0.011678	0.002986	0.001134
20000	TB	0.135097	0.249997	0.344972	0.309319	0.1939	0.087823	0.045257	0.0262	0.010102	0.00258	0.000979
25000	TB	0.1605	0.280448	0.366802	0.30267	0.176362	0.077278	0.039474	0.022785	0.008765	0.002236	0.000848
35299	TB	0.21007	0.334008	0.397535	0.28046	0.148919	0.062804	0.031781	0.018277	0.007009	0.001785	0.000677
35300	TB	0.210074	0.334013	0.397537	0.280457	0.148916	0.062803	0.03178	0.018277	0.007009	0.001785	0.000677
40000	TB	0.230094	0.356368	0.404907	0.269829	0.139568	0.058283	0.029417	0.016899	0.006475	0.001648	0.000625
60000	TB	0.304196	0.443411	0.398737	0.224225	0.10839	0.044143	0.022107	0.012657	0.004836	0.00123	0.000466
75000	TB	0.351464	0.493457	0.372825	0.194614	0.091618	0.036886	0.0184	0.010517	0.004013	0.00102	0.000387
15000	P	0.253435	0.314854	0.195865	0.062563	0.008125	0.00019	2E-06	3.77E-09	0	0	0
16000	P	0.248801	0.30788	0.188479	0.057546	0.007027	0.000149	1.32E-06	8.17E-10	0	0	0
20000	P	0.231631	0.282232	0.159361	0.040231	0.003949	4.97E-05	7.97E-08	0	0	0	0
25000	P	0.212467	0.254015	0.126268	0.025074	0.001862	1.01E-05	0	0	0	0	0
35299	P	0.177019	0.202454	0.073711	0.009353	0.000313	0	0	0	0	0	0
35300	P	0.177016	0.20245	0.073707	0.009353	0.000313	0	0	0	0	0	0
40000	P	0.16452	0.182835	0.057351	0.006045	0.000128	0	0	0	0	0	0
60000	P	0.11597	0.106772	0.017318	0.000675	6.69E-08	0	0	0	0	0	0
75000	P	0.087794	0.065629	0.006548	8.44E-05	0	0	0	0	0	0	0

Standard Deviations, Part 1.

BrRate	BinMidPts==>	0.0141	0.0245	0.0387	0.0632	0.0894	0.141	0.245	0.387	0.632	0.894	1.41
15000	ET	1.08E-25	7.6E-26	0	3.1E-10	2.33E-26	0	1.1E-10	7.76E-11	0	0	6.72E-27
16000	ET	1.32E-25	6.21E-10	4.39E-10	1.9E-26	3.1E-10	9.5E-27	7.76E-11	0	5.49E-11	3.36E-27	0
20000	ET	1.32E-25	0	0	1.9E-26	1.34E-26	2.2E-10	7.76E-11	4.75E-27	3.36E-27	7.76E-11	0
25000	ET	5.38E-26	0	3.8E-26	0	2.2E-10	2.2E-10	4.75E-27	5.49E-11	3.36E-27	7.76E-11	0
35299	ET	8.78E-10	0	2.69E-26	0	1.55E-10	0	8.23E-27	0	5.49E-11	6.72E-27	0
35300	ET	0	0	0	0	9.5E-27	1.1E-10	4.75E-27	5.82E-27	5.49E-11	4.75E-27	2.2E-10
40000	ET	0	0	3.8E-26	0	0	0	4.75E-27	5.49E-11	0	4.75E-27	1.34E-26
60000	ET	7.6E-26	0	0	2.69E-26	1.34E-26	1.1E-10	4.75E-27	0	7.76E-11	9.5E-27	2.33E-26
75000	ET	5.38E-26	3.8E-26	3.8E-26	2.2E-10	9.5E-27	0	7.76E-11	3.36E-27	4.75E-27	6.72E-27	4.39E-10
15000	TB	0.048541	0.030537	0.019494	0.011584	0.007885	0.004584	0.002476	0.002182	0.003173	0.004437	0.010357
16000	TB	0.047729	0.029816	0.018937	0.011214	0.007604	0.004387	0.002409	0.002288	0.003485	0.005013	0.011882
20000	TB	0.044791	0.027309	0.017079	0.009979	0.006669	0.003761	0.002347	0.002845	0.004638	0.00731	0.018639
25000	TB	0.041692	0.024832	0.015305	0.008814	0.005786	0.003255	0.002573	0.003649	0.006109	0.010262	0.028451
35299	TB	0.036468	0.020985	0.01265	0.007074	0.004526	0.002861	0.003452	0.005274	0.00931	0.016696	0.051644
35300	TB	0.036467	0.020984	0.01265	0.007074	0.004526	0.002861	0.003452	0.005274	0.009311	0.016696	0.051646
40000	TB	0.034597	0.019667	0.011762	0.006498	0.004152	0.002894	0.003896	0.00587	0.010855	0.019892	0.063113
60000	TB	0.028001	0.015309	0.008858	0.004714	0.003373	0.003727	0.005913	0.008921	0.017647	0.036682	0.120602
75000	TB	0.024253	0.012944	0.007311	0.003991	0.003507	0.004645	0.00714	0.011436	0.023876	0.053518	0.165953
15000	P	0.074236	0.03839	0.021956	0.016308	0.013369	0.009989	0.00668	0.005122	0.004764	0.005749	0.010046
16000	P	0.071432	0.035822	0.020917	0.016302	0.013609	0.010132	0.006822	0.005151	0.004678	0.005571	0.00958
20000	P	0.061434	0.027793	0.019273	0.017396	0.014651	0.010837	0.007255	0.005453	0.004701	0.005387	0.0091
25000	P	0.051212	0.021994	0.020468	0.019194	0.016186	0.011856	0.007869	0.005775	0.004953	0.005626	0.009708
35299	P	0.036167	0.020159	0.02448	0.021857	0.017854	0.012742	0.008238	0.005976	0.005027	0.005696	0.010625
35300	P	0.036166	0.020159	0.02448	0.021857	0.017854	0.012742	0.008238	0.005976	0.005027	0.005696	0.010625
40000	P	0.031178	0.0214	0.026115	0.022543	0.018295	0.012956	0.008297	0.005963	0.005009	0.005641	0.010962
60000	P	0.020034	0.026434	0.027997	0.022206	0.017274	0.011831	0.007299	0.004981	0.00399	0.004223	0.01105
75000	P	0.018465	0.027698	0.026753	0.020301	0.015473	0.010364	0.006151	0.004082	0.002941	0.002863	0.010953

Standard Deviation, Part 2.

BrRate	BinMidPts==>	2.45	3.87	6.32	8.94	12.2	17.3	22.4	27.4	38.7	63.2	89.4
15000	ET	6.01E-26	1.08E-25	3.51E-09	0	0	1.49E-24	0	1.22E-24	8.6E-25	8.6E-25	1.99E-08
16000	ET	0	7.6E-26	2.15E-25	0	8.6E-25	0	1.99E-08	8.6E-25	8.6E-25	8.6E-25	0
20000	ET	7.6E-10	1.08E-25	3.04E-25	1.22E-08	1.4E-08	0	1.4E-08	0	0	1.99E-08	0
25000	ET	0	0	1.11E-08	4.3E-25	1.99E-08	9.93E-09	1.4E-08	1.99E-08	8.6E-25	8.6E-25	0
35299	ET	0	3.51E-09	0	9.93E-09	8.6E-25	0	2.43E-08	0	1.99E-08	0	0
35300	ET	8.78E-10	0	3.04E-25	0	9.93E-09	9.93E-09	1.4E-08	0	8.6E-25	0	8.6E-25
40000	ET	9.31E-26	2.48E-09	7.02E-09	9.93E-09	0	6.08E-25	8.6E-25	0	1.99E-08	8.6E-25	0
60000	ET	2.15E-09	0	1.22E-08	1.05E-24	0	1.4E-08	1.4E-08	1.4E-08	8.6E-25	1.4E-08	0
75000	ET	0	0	0	9.93E-09	8.6E-25	0	0	0	8.6E-25	0	8.6E-25
15000	TB	0.050808	0.154922	0.1529	0.070334	0.018574	0.001701	0.000309	0.000161	6.22E-05	1.59E-05	6.04E-06
16000	TB	0.058285	0.165478	0.152377	0.068459	0.017066	0.001401	0.000272	0.00015	5.81E-05	1.49E-05	5.64E-06
20000	TB	0.08991	0.19788	0.146011	0.059019	0.011343	0.000655	0.000206	0.000119	4.6E-05	1.17E-05	4.46E-06
25000	TB	0.129176	0.221042	0.135331	0.04577	0.006163	0.000342	0.000164	9.45E-05	3.64E-05	9.28E-06	3.52E-06
35299	TB	0.191321	0.230552	0.109163	0.023276	0.001497	0.000229	0.000116	6.66E-05	2.55E-05	6.5E-06	2.47E-06
35300	TB	0.191325	0.230552	0.10916	0.023274	0.001497	0.000229	0.000116	6.66E-05	2.55E-05	6.5E-06	2.47E-06
40000	TB	0.210782	0.227234	0.09637	0.016376	0.000813	0.000202	0.000102	5.86E-05	2.25E-05	5.72E-06	2.17E-06
60000	TB	0.257239	0.19896	0.047552	0.002784	0.000344	0.00014	7.03E-05	4.02E-05	1.54E-05	3.91E-06	1.48E-06
75000	TB	0.262257	0.172931	0.023113	0.000768	0.000291	0.000117	5.85E-05	3.34E-05	1.28E-05	3.24E-06	1.23E-06
15000	P	0.025737	0.079204	0.095198	0.042225	0.00945	0.00033	3.85E-06	1.06E-08	0	0	0
16000	P	0.026511	0.083722	0.094565	0.04148	0.008821	0.000267	2.55E-06	2.31E-09	0	0	0
20000	P	0.032112	0.097392	0.089816	0.036988	0.006006	9.63E-05	2.26E-07	0	0	0	0
25000	P	0.040967	0.105608	0.083259	0.029277	0.003193	1.95E-05	0	0	0	0	0
35299	P	0.051186	0.102579	0.066832	0.014607	0.000615	0	0	0	0	0	0
35300	P	0.051187	0.102579	0.06683	0.014606	0.000615	0	0	0	0	0	0
40000	P	0.053324	0.098277	0.058636	0.010068	0.000253	0	0	0	0	0	0
60000	P	0.050992	0.073255	0.026202	0.001336	1.89E-07	0	0	0	0	0	0
75000	P	0.043666	0.055224	0.011224	0.000165	0	0	0	0	0	0	0

13. Appendix 3 - CODA Java API Updates for Inhalation Modeling

The existing CODA Java API was modified to include additional parameters in support of inhalation modeling. Only these modifications are described herein. A full copy of the CODA API documentation will be included with the software delivery.

The CODA Java package has 3 basic components, CODAState, CODAManager, and CODAClassBean. CODAClassBean implements the HPAC GUI controls related to the CODA settings. It resides in, and is supported by a number of classes in the mil.dtra.hpac.project.output.effect.coda.swing package. None of these classes needed to be modified to support enhanced inhalation modeling. CODAManager is the primary interface to the CODA Java classes. CODAManager implements the HPACOutputEffectManager interface and uses instances of CODAState to store and maintain values as provided by the user either directly or via the HPAC GUI (CODAClassBean.) CODAManager and CODAState both reside in the mil.dtra.hpac.project.output.effect.coda package. CODAManager and CODAState are delivered in CODAManager.jar. All of the remaining components are delivered in CODA.jar.

In support of the new inhalation model, CODAManager was modified with the addition of a new method, setInhalationModelValues, which reads the model-specific parameters from the material file based on the inhalation model specified as its parameter. The models that are currently supported are ricin and tularemia. This method is called at various times from within CODAManager.

CODAState also needed modification to support the new inhalation model. A number of static declarations were added for use by CODAManager, including CODA_INHALATION_MODEL_DISABLED, CODA_TULAREMIA_INHALATION_MODEL, and CODA_RICIN_INHALATION_MODEL which are used as parameters to the setInhalationModelValues method of CODAManager. Other static declarations are for data access, like PULMONARY_LETHAL_ED50_STRING, PULMONARY_INFECTIVE_ED50_STRING, and EXTRATHORACIC_INFECTIVE_ED50_STRING, which store the expected XML path in a given material file for the respective value.

CODAState stores its data in a series of internal variables. "Getters" and "setters" were added for each of these. These are:

- getInhalationModel and setInhalationModel
- getPulmonaryED50 and setPulmonaryED50
- getPulmonaryProbitSlope and setPulmonaryProbitSlope
- getExtrathoracicED50 and setExtrathoracicED50
- getExtrathoracicProbitSlope and setExtrathoracicProbitSlope
- getParticleSizeBins and setParticleSizeBins

The full documentation for each of these new methods is provided in the appendix. Note that the term "particle size bins" is used throughout the HPAC Material Services component to refer to the boundaries that define the bins into which particle sizes are divided.

CODAState converts its internal variables into an array of floating point values in the method getClassData. This array is passed to the CODA DLL using the Java Native Interface. Modifications to this array include extending its length from 33 values to an arbitrary length. In order, the new values added to the end of the array are the inhalation model, the pulmonary ED50 and pulmonary probit slope, the extrathoracic ED50 and extrathroacic probit slope, and the number of particle size bin boundaries. These are followed by the specified number of bin boundaries as stored in the material file.

The changes to the internal data structures of CODAState necessitated changes to the setState method, which can now take a CODAState object or an array of floating point values of either the old or new length for backward compatibility. Similarly, the readProps method is fully backward compatible with previous ValueProperties objects which do not contain the new inhalation model parameters. In either case however, the new inhalation model will be disabled unless the material is changed or other methods are called to re-enable it and populate the necessary properties.

14. Appendix 4 - Presentations, Posters and Papers

As noted in the following list, we have presented aspects of this project at many different conferences during its development. This list does not include informal discussions, program reviews or other internal presentations.

- Chem-Bio Information Systems, 2007, 10 January 2007, Austin, TX, "Medical Modeling of Particle Size Effects for Inhalation Hazards"

- CBR Consequence Assessment Modeling Conference, 24-26 January 2007, National Ground Intelligence Center (NGIC), Charlottesville, VA, "Medical Modeling of Particle Size Effects for Inhalation Hazards"

- National Academy of Science Committee "Determining a Standard Unit of Measure for Biological Aerosols", 22 March 2007, Washington, DC, "Medical Modeling of Particle Size Effects for Inhalation Hazards"

- Aerobiology in BioDefense II, 10 July 2007, Rocky Gap, MD, "Medical Modeling of Particle Size Effects for Inhalation Hazards"

- 11th Annual Force Health Protection Conference, 13 August 2008, Albuquerque, NM, "Inhalability: A Key Component for Modeling Inhalation Hazards"

- CBW Delivery Methods and Consequence Assessment Modeling Conference, 24 April, 2008, WINPAC, Falls Church, VA, "Medical Modeling of Particle Size Effects for Inhalation Hazards"

- Chemical and Biological Defense Physical Science and Technology Conference, 19 November, 2008, New Orleans, LA, "Medical Modeling of Particle Size Effects for Inhalation Hazards"

- Chemical and Biological Defense Physical Science and Technology Conference, 19 November, 2008, New Orleans, LA, "Inhalability in the Context of Inhalation Hazard Modeling" (Poster)

- Society of Toxicology Annual Meeting, 17 March 2009, Baltimore, MD, "An Improved Model of Human Response to Aerosol Chemical and Biological Agent Hazards"

- Aerobiology in BioDefense III, 15 July 2009, Rocky Gap, MD, "An Improved Model of Human Response to Aerosol Chemical and Biological Agent Hazards"

ATTACHMENT 1

(Next Page)

A Review of Inhalability Fraction Models: Discussion and Recommendations

Kyle K. Millage, Joshua J. Bergman, Bahman Asgharian, and
    Gene E. McClellan

Technical Report

21 July 2009

Prepared by:

Health Effects and Medical Response Group
Applied Research Associates, Inc.
801 N. Quincy St.
Arlington, Virginia 22203

Preface

The research and development work described in this technical report was conducted for Project CB06MSB096 of the Joints Science and Technology Office (JSTO) of the Department of Defense (DoD) Chemical and Biological Defense (CBD) Program. JSTO is also the Chemical/Biological Technologies Directorate (RD-CB) in the Research and Development Enterprise of the Defense Threat Reduction Agency (DTRA). Project CB06MSB096 is titled *Medical Modeling of Particle Size Effects for Inhalation Hazards*.

After clearance from DTRA, this report was submitted to the journal Inhalation Toxicology and accepted for publication. This preprint version is provided as an attachment to the contract final report.

A Review of Inhalability Fraction Models: Discussion and Recommendations

Kyle K. Millage[†], Josh Bergman, Bahman Asgharian, Gene McClellan

Applied Research Associates, Inc., Arlington, VA

[†] Address correspondence to Kyle Millage, Principal Scientist,

Applied Research Associates, Inc.,

801 N. Quincy St., Suite 600

Arlington, VA 22203, U.S.A. Email: Kyle.Millage@ara.com

Telephone: 703.816.8886

Fax: 703.816.8861

Running Title: Review of Inhalability Fraction Models

Abstract

The first step in mathematically modeling the mechanics of respiratory deposition of particles is to estimate the ability of a particle to enter the head, either through the mouth or nose. Models of the biological effects from inhaled particles are commonly, albeit incorrectly, simplified by making an assumption that the only particles of concern are those that can readily penetrate to the pulmonary region of the lung; typically particles less than 5 microns in aerodynamic diameter. Inhalability for particles of this size is effectively 100%, so there is little need to develop a mathematical representation of the phenomenon. However, chemical irritants, biological agents or radioactive material, in the form of large particles or droplets, can cause adverse biological responses by simply being taken into the head and depositing in the extrathoracic area. As a result, it is important to understand the inhalability of both small and large particles. The concept of particle inhalability received little consideration until the 1970's; since then it has been the subject of many experiments with a fairly wide disparity of results, in part due to the variety of dependent variables and the difficulty in adequate measurement methods. This paper describes the currently utilized models of inhalability, recommends specific methods for implementing inhalability into mathematical models of respiratory deposition, and identifies outstanding issues and limitations. In this paper, we describe inhalability as it applies to particulate matter and liquid droplets; modeling the inhalability of fibers is a work in progress and not addressed.

Background

A particle can only pose an inhalation hazard if it can actually enter the body. The ability of a particle to enter the head, either through nasal or oral passages, is described as the *inhalability* of the particle. Inhalability, or inspirability, is defined as the ratio of the inspired particle concentration as a function of particle size (aerodynamic diameter, d_{ae}), to the ambient particle concentration of the same size.

$$I(d_{ae}) = \frac{C_{Inspired}(d_{ae})}{C_{Ambient}(d_{ae})} \qquad (1)$$

Several variables can affect the magnitude of the inhalability term. Obviously, the aerodynamic particle size is the principal variable, but studies have shown additional factors have varying degrees of influence, including ambient wind speed and orientation to the wind, as well as both the mode and rate of inhalation. Several studies have been performed that collectively provide insight into the interrelationships of these variables and have been used to develop guidelines and recommendations for respiratory modeling.

Note that inhalability alone does not necessarily correlate with retention or biological effect; particles can be inhaled and taken into the body, but if they do not impact any structures in the respiratory tract, they may be exhaled without any effect. Conversely, simply because a particle can be inhaled into the head does not mean that it will penetrate into the remainder of the respiratory tract. Nearly all inhaled particles greater than 10-20 microns in diameter will be deposited in the extrathoracic region, but can still pose a hazard. Chemical, biological or radioactive particulate material can cause a local response, or the particles can be swallowed, resulting in a digestive tract or systemic response.

The industrial hygiene community, with their role of monitoring and protecting workers in the workplace, has had a key role in developing standard models of inhalability. One reason is the need to match the performance of personal monitoring sampling devices to human respiratory

function; the American Conference of Governmental Industrial Hygienist (ACGIH) has responsibility for establishing such guidelines. In addition, the International Commission on Radiological Protection (ICRP) has developed mathematical models for use in determining internal dose due to inhaled insoluble radioactive particles.

Discussion

The inhalability of a particle can depend on many factors, including particle size, breathing mode (nasal, oral or a combination of both), breathing rate, ambient wind speed and angle of orientation to the wind. Many early studies in the 1970's and 1980's were performed using mannequins in wind tunnels and found fairly consistent results below ambient wind speeds of 4 m/s (Ogden and Birckett, 1977 and Ogden et al, 1977). At least one study was performed with human subjects using particle sizes of less than 30 microns (Breysse and Swift, 1990). The data indicated that inhalability was 100% at small particle sizes and monotonically decreased with increasing size. The results were consistent for breathing rates up to 20 litres per minute (lpm), regardless of breathing mode. The results of the small particle studies (less than 35 micron data) were used by the International Organization for Standardization (ISO) to develop an empirical model for inhalability for relatively still air (less than 4 m/s), and were extrapolated to 100 microns (ACGIH, 1999).

$$I_{ISO}(d_{ae}) = 1 - 0.15\left[\log_{10}\left(1 + d_{ae}\right)\right]^2 - 0.10\log_{10}\left(1 + d_{ae}\right) \qquad (2)$$

where d_{ae} is given in microns

The results from some larger diameter data sets indicated that the inhalability decreased to about 50% and appeared to stay near 50% up to 100 microns. The ACGIH also developed an empirical model, shown in Equation 3, but were able to include the larger data set. Figure 1 shows an overlay of these two curves.

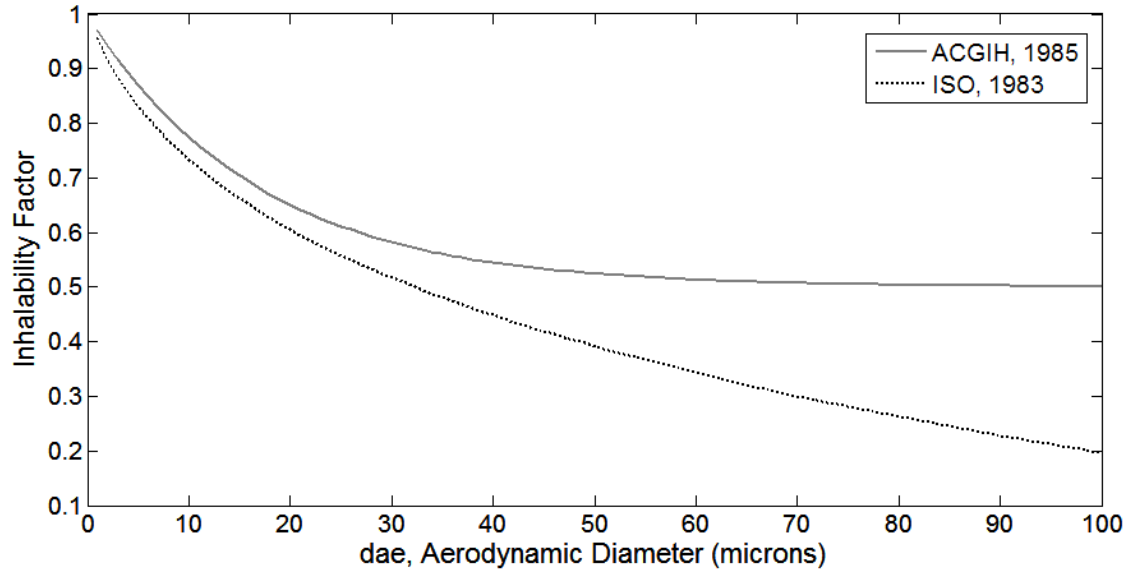$$I_{ACGIH}(d_{ae}) = 0.5\left[1 + \exp(-0.06d_{ae})\right] \qquad (3)$$

4

Figure 1. ISO and ACGIH inhalability curves for still air from equations 2 and 3.

Breysse and Swift studied inhalability in still air (less than 1 m/s); four human subjects volunteered to inhale ^{99m}Tc-labeled pollens with median diameters of 18, 27.5 and 30.5 microns and white pine dust with a median diameter of 24.5 microns (Breysse and Swift, 1990). The breathing mode was nose only. The density of the particles was not measured, but was assumed to be 1.0 g/cm^3, hence the aerodynamic diameter of the particles was equal to the physical diameter (assuming spherical particles). Although the initial curve fit matched the data well (r^2=0.92), the fit resulted in an inhalability of zero for particles larger than 39 microns. Since it was fairly well established that inhalability was greater than zero at particle sizes greater than 40 microns, alternative curve-fit routines were investigated. The data were re-examined and the results fitted with a logistic function. The logistic function mimicked the initial curve fit very well, while establishing non-zero inhalability at larger particle sizes. In addition, both curves exhibit a fundamentally different shape at small to medium particle sizes (concave) than the previously noted functions (convex). Equation 4 shows Menache's logistics function, and Equation 5 shows the equivalent function in an alternate form. Figure 2 shows the initial and recomputed curves. However, while examining Figure 2, the reader is reminded that although the curve is extrapolated to an aerodynamic diameter of 100 microns, the largest data point is 30.5 microns (Menache, et al, 1995).

5

$$I_{Menache} = 1 - \left(\frac{1}{1 + \exp(10.32 - 3.114\ln(d_{ae}))} \right) \qquad (4)$$

$$I_{Menache} = 1 - \left(\frac{1}{1 + 3.033 \cdot 10^4 \, d_{ae}^{-3.114}} \right) \qquad (5)$$
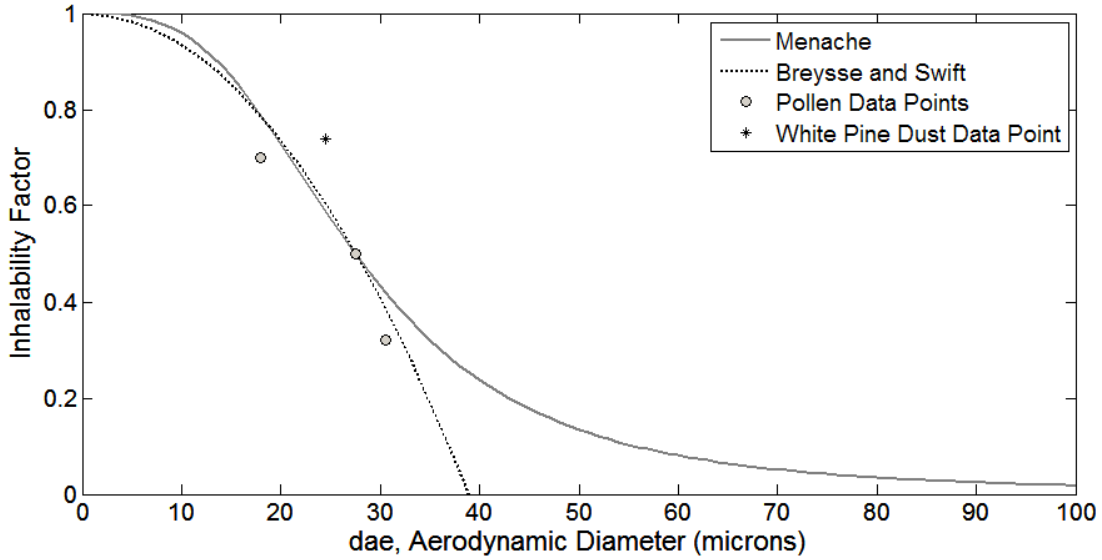

Figure 2. Breysse and Swift data and curve fit compared to Menache's fit for nasal breathing.

A closer examination of the Breysse and Swift data identifies one of the difficulties of these types of studies. Four different particles were used in the study, three pollens and white pine dust. The pollen particles were relatively uniform in size and shape and the geometric standard deviation (σ_g) associated with the log-normal particle size distribution ranged from 1.13-1.16. As a result, it is acceptable to attribute the inhalability for the particular pollens to the median particle size of the distribution. However, the white pine dust was not uniform in either size or shape and the σ_g was 1.92. Figure 3 shows the four particle size distributions; clearly it is not appropriate to assign the inhalability of the white pine dust to the median particle size of 24.5 microns. As a result, a new logistics function fit was calculated using a non-linear least-squares fit routine using the MATLAB® Curve-Fit Toolbox. The new curve is based on the three pollens and omits the data associated with the white pine dust. The new parameters are shown in Equation 6 and a comparison of the new fit and Menache's fit is shown in Figure 4. The figure

6

suggests that Menache's fit may over-estimate inhalability in the 10-30 micron range because a significant amount of the particles in the white pine dust were in fact much smaller than the median value of 24.5 microns. As a result, the inhalability of this particle size distribution is not indicative of the inhalability at the median value of 24.5 microns.

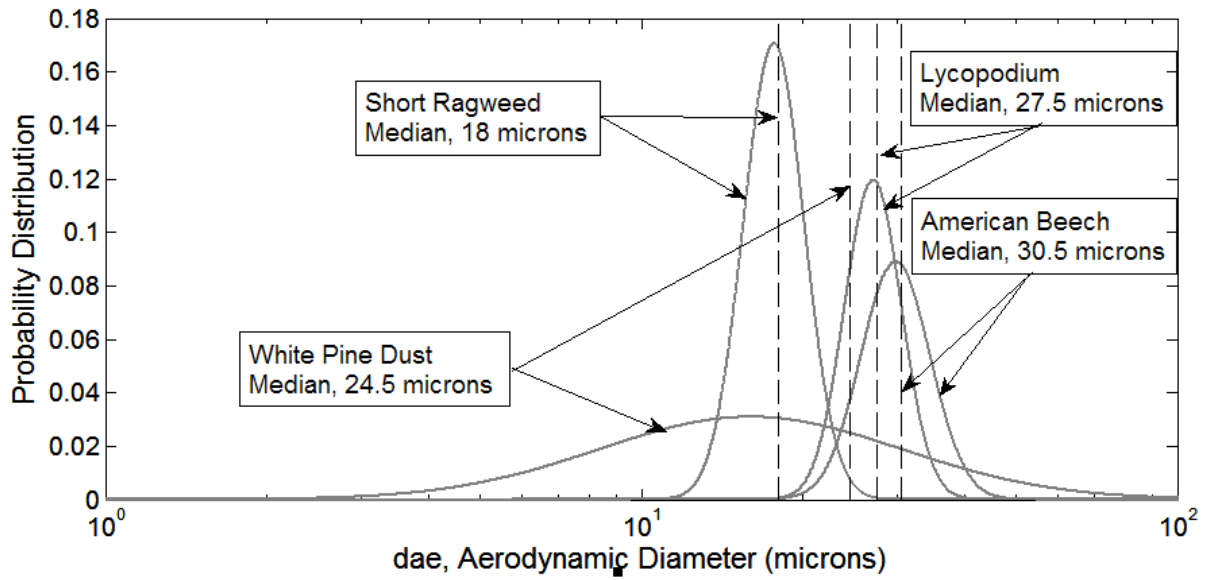$$I_{New} = 1 - \left(\frac{1}{1 + 6.809 \cdot 10^3 \, d_{ae}^{-2.736}} \right) \tag{6}$$

Figure 3. Particle size distributions of the Breysse and Swift particles.

The measurement methods used in inhalation experiments have also evolved. Simply creating monodispersed particles is difficult and often results in large standard deviations associated with particle diameter distributions. In addition, measuring the inhalability of the particles presents a separate set of unique challenges. Aitken conducted an experiment to examine still-air inhalability by utilizing two different laboratories and three different techniques of measuring particulate air concentration to attempt to reduce these errors (Aitken, et al 1999). The experiment utilized a rotating mannequin to minimize the impact of any non-zero horizontal air movement, and examined ten different particle sizes ranging from 6 to 90 microns. Three different breathing rates were used in the experiment and since Aitken claimed that no difference
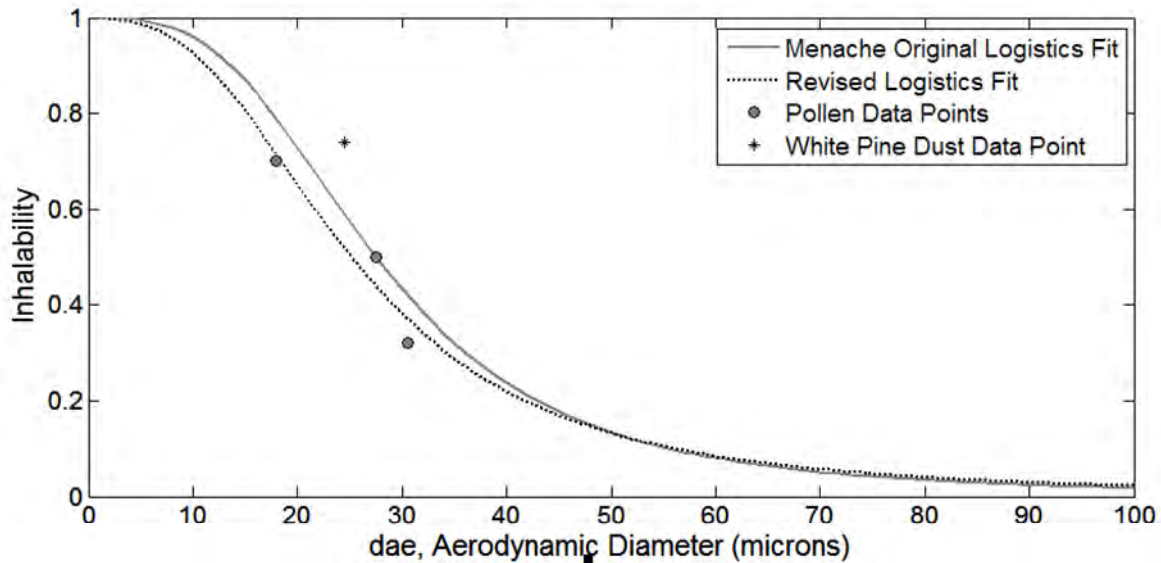
Figure 4. New logistics function fit of Breysse and Swift data.

was seen between oral and oronasal breathing, the final results were based only on oral breathing. Since one would expect oronasal breathing inhalability to be lower than oral breathing alone it is possible that Aitken's data over-estimates inhalability. Figure 5 shows the data, along with the baseline ACGIH curve for comparison. Note that all the data points, with the exception of the largest particle sizes at the lowest breathing rate, are higher than the accepted inhalability curve from the ACGIH. The authors suggested that perhaps the ACGIH curve will actually under-predict inhalation in these still air conditions. The authors further suggested that perhaps the most conservative approach is a linear least-squares fit to the data as shown in Figure 6 (Aitken, et al.1999).

The 20 lpm data from both laboratories were combined to establish the curves shown in Figure 6. Clearly the linear functions provide a reasonable fit to Aitken's data for most regimes, but we have seen no other studies that would suggest a linear fit for inhalability.
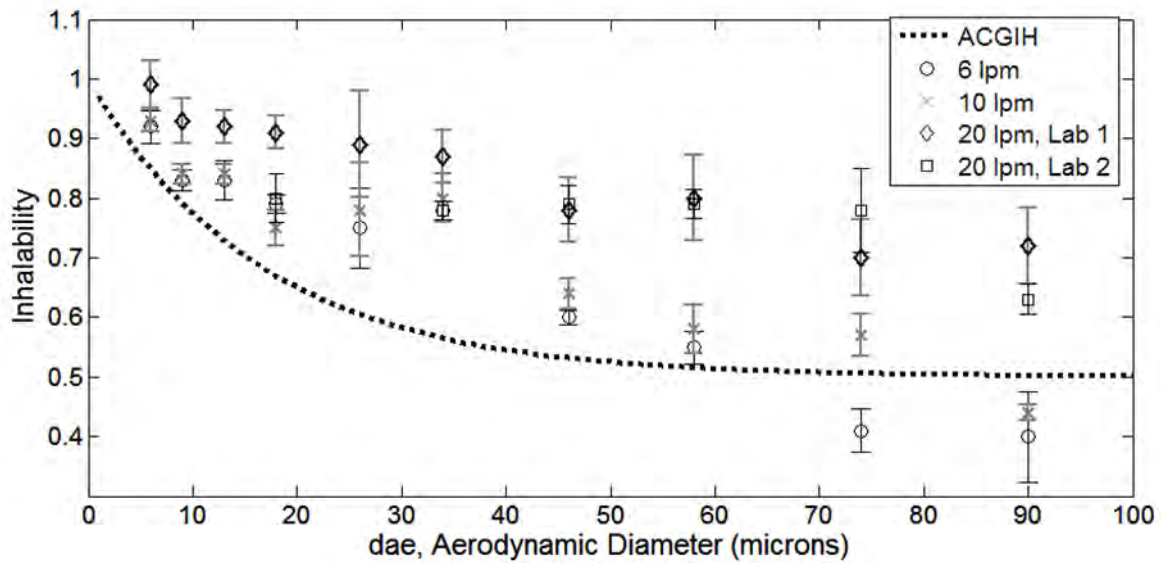
Figure 5. Comparison of ACGIH model to experimentally derived inhalability fractions for varying breathing rates and particle sizes based on Aitken's data.
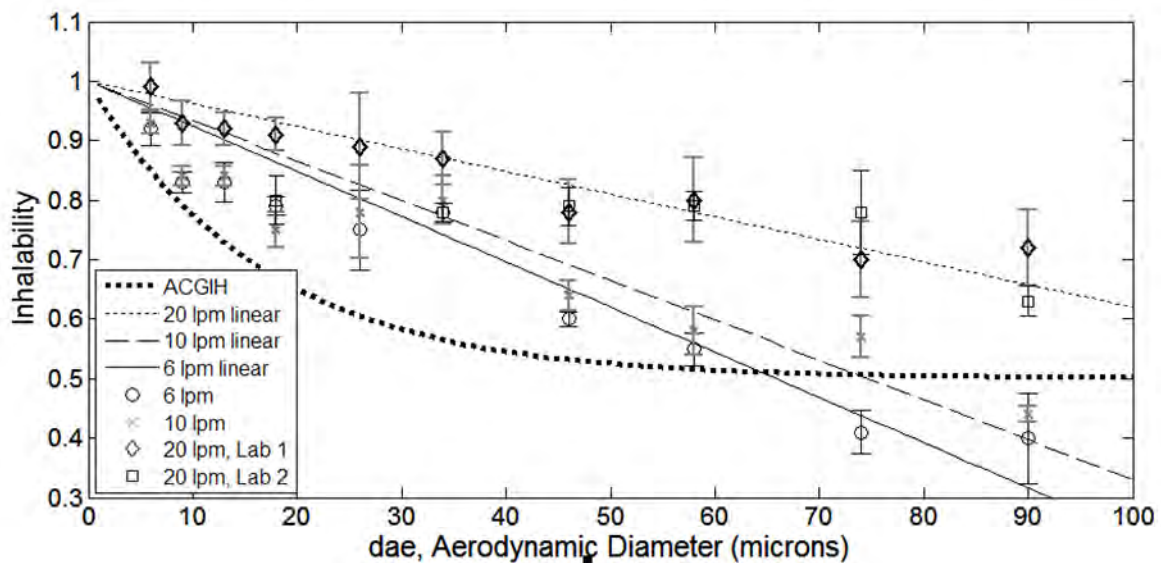
Figure 6. Aitken's data with linear models of inhalability.

Other still-air work with larger particle sizes has been performed (Kennedy and Hinds, 2002, Hsu and Swift, 1999). Hsu and Swift used six different particle sizes, ranging from 13 to 135 microns to provide guidance on inhalability beyond the standard 100 microns. The experiment utilized mannequins representing adults with breathing rates of 8.5, 20 and 35 lpm, and children with breathing rates of 6.3 and 15 lpm. Figure 7 shows Hsu and Swift's data with his

recommended curve fits. Hsu and Swift noted that the inhalability factor showed no dependence on breathing rate at the resting or moderate exercise levels of 8.5 and 20 lpm respectively. Although the children's data is not shown on the graph, Hsu and Swift indicated that there was no difference in inhalability for adults and children. In addition to the data, Figure 7 also contains the curve fit that Hsu and Swift recommended for rest/moderate and heavy breathing rates, a quadratic polynomial of the log of the particle diameter. Although Hsu and Swift did not indicate that his fit was unsuitable for small particles, it is clear from the curve shown in Figure 7 the fit is not representative of physical phenomena for particle sizes lower than the lowest data point of 13.5 microns. Because of the unstable nature of Hsu and Swift's fit at small particle sizes, an alternative fit has been examined here. As noted earlier, Menache used a logistic function and felt that it was appropriately convex at lower particles sizes; therefore, a logistic function was used here to model the Hsu and Swift data. Figure 8 shows the logistic function fit to the data that was calculated using a chi-squared weighting scheme for the combined data set of at-rest and moderate exercise along with Hsu's original fit and the ACGIH model. The logistics function defined in Equation 7 is a reasonable fit to the data and appropriately trends to an inhalability of 1.0 at small particle sizes. Also note that in contrast to the results from Aitken, Hsu and Swift's data suggest an inhalability factor that approaches zero for larger particles. Although Hsu combined the at-rest and moderate exercise data for purposes of developing a curve fit, he notes that for the at-rest breathing rate, the inhalability of the 110 and 135 micron particles is zero, and is small, but non-zero (2.4 and 0.6% respectively) for the moderate exercise rate (Hsu and Swift, 1999).

$$I_{HsuLogistic} = 1 - \left(\frac{1}{1 + 901.4 \cdot d_{ae}^{-2.213}} \right) \qquad (7)$$
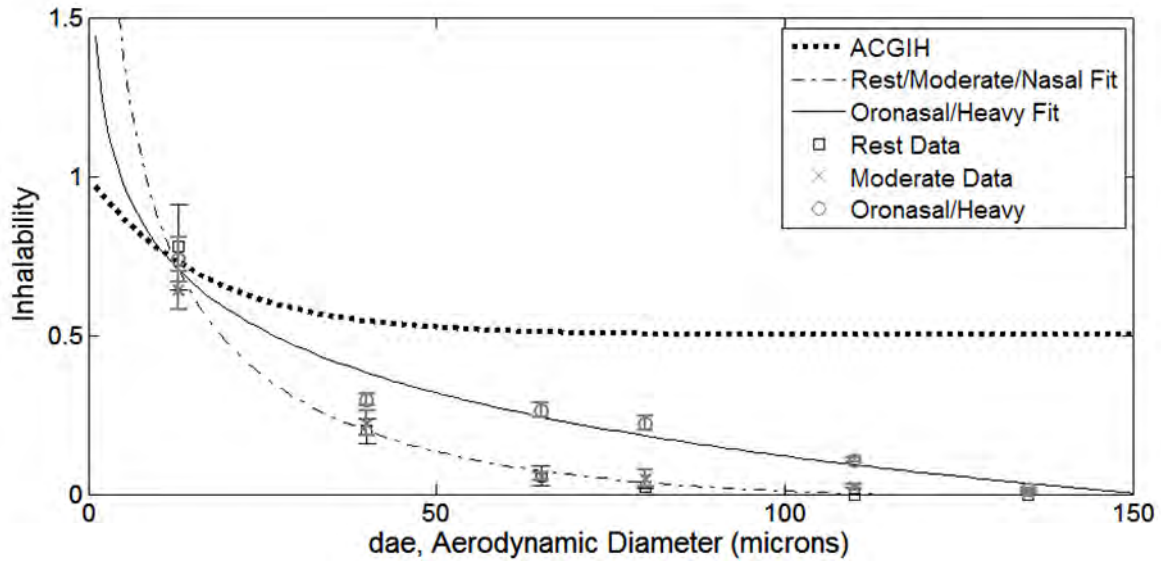
Figure 7. Hsu's data and his original quadratic polynomial curve-fits.
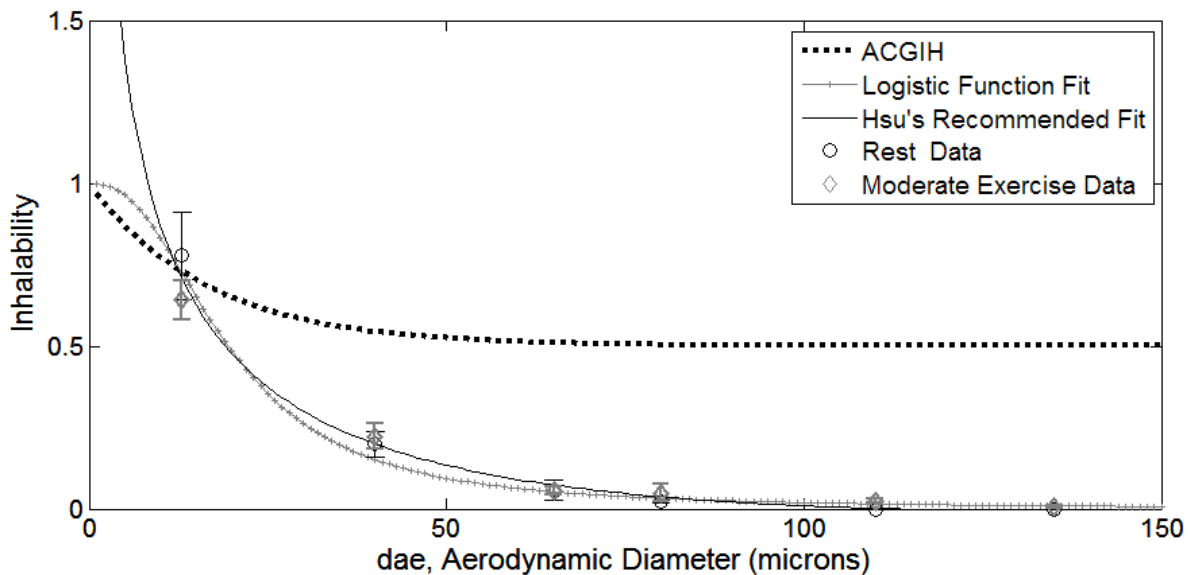

Figure 8. Hsu's data with a weighted logistic function fit.

In another study, previously derived data sets for oral breathing in still air were used to develop mathematical models of aspiration efficiency of blunt and sharp edged round inlets (Brown 2005). The aerodynamic models utilize Stokes number, inlet velocity, ambient wind speed and shape factors to predict the efficiency of particles ability to enter an inlet. Since the shape of the entry to the mouth is between a sharp and blunt inlet, the two resulting models were averaged and fitted with a logistics function, as shown in Equation 8. Figure 9 shows Brown's curve with

11

Aitken's data. Note the fit is particularly good for the 6 and 10 lpm breathing rates. Equation 8 offers an oral complement to Menache's inhalability function for nasal breathing in still air.

$$I_{Brown}(d_{ae}) = \frac{1 + 0.44}{1 + 0.44\exp(0.0195d_{ae})} \qquad (8)$$
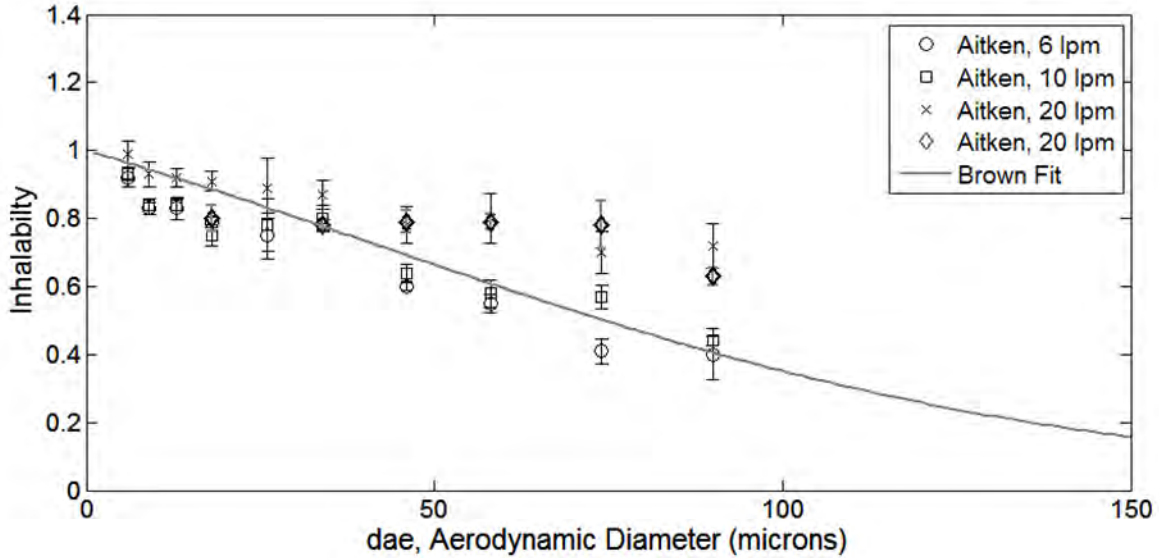
Figure 9. Comparison of Aitken's inhalability data to Brown's oral inhalability equation.

Additional work has been performed to determine the effect of ambient wind speed. In environments with ambient wind speeds greater than 4 m/s, inhalability tends to increase for larger particle sizes and slightly decrease for small particle sizes (Vincent, et al 1999). While many indoor environments can be modeled as "still air", outdoor environments often are not. As a result, the basic inhalability function needs to be modified to include an ambient wind speed term. Obviously the wind speeds to which the oral and nasal cavities are subject depend on the orientation of the wind direction to the individual. Since an orientation dependent wind-speed correction term would be cumbersome to implement, experimental measurements were typically conducted in wind tunnels with rotating mannequins to integrate the measurements over all angles with respect to the ambient wind direction. The resultant wind-speed dependent term was effectively averaged over all orientations and was used to supplement the previously accepted

still-air term (Vincent, et al 1990). The ACGIH based their recommended inhalability function (shown in Equation 9) on their basic still-air function and adding an ambient wind term.

$$I_{ACGIH}(d_{ae}) = 0.5[1 + \exp(-0.06d_{ae})] + 10^{-5}U^{2.75}\exp(0.055 \cdot d_{ae})$$ (9)

where the ambient wind speed U is given in m/s

The range of applicability of this function is for particle sizes less than 100 microns and for wind speeds no greater than 9 m/s.

The ICRP incorporated the ACGIH model in their development of recommendations for human respiratory tract modeling (ICRP, 1994), but felt the ACGIH model underestimated inhalation for smaller particles. As a result, the ICRP developed Equation 10 that utilizes the ambient wind factor term of the ACGIH model, but modifies the first term in the equation.

$$I_{ICRP}(d_{ae}) = 1 - 0.5\left[1 - \frac{1}{7.6 \times 10^{-4}(d_{ae})^{2.8} + 1}\right] + 10^{-5}U^{2.75}\exp(0.055 \cdot d_{ae})$$ (10)

Both ACGIH and ICRP note that there is insufficient data to recommend models for particle sizes greater than 100 microns. Further, they note that their models should not be extrapolated to larger particle sizes. Figure 10 shows the range of ICRP inhalability curves for wind speeds ranging from zero to 9 m/s. Note that inhalability ratios greater than 1.0 have been shown experimentally to occur for large particle sizes and high wind speeds. Vincent attributes the increase in inhalability to the inertial impaction of large particles from the air flowing past the nose and mouth region; the phenomenon is consistent with blunt sampler theory (Vincent, et al 1999).
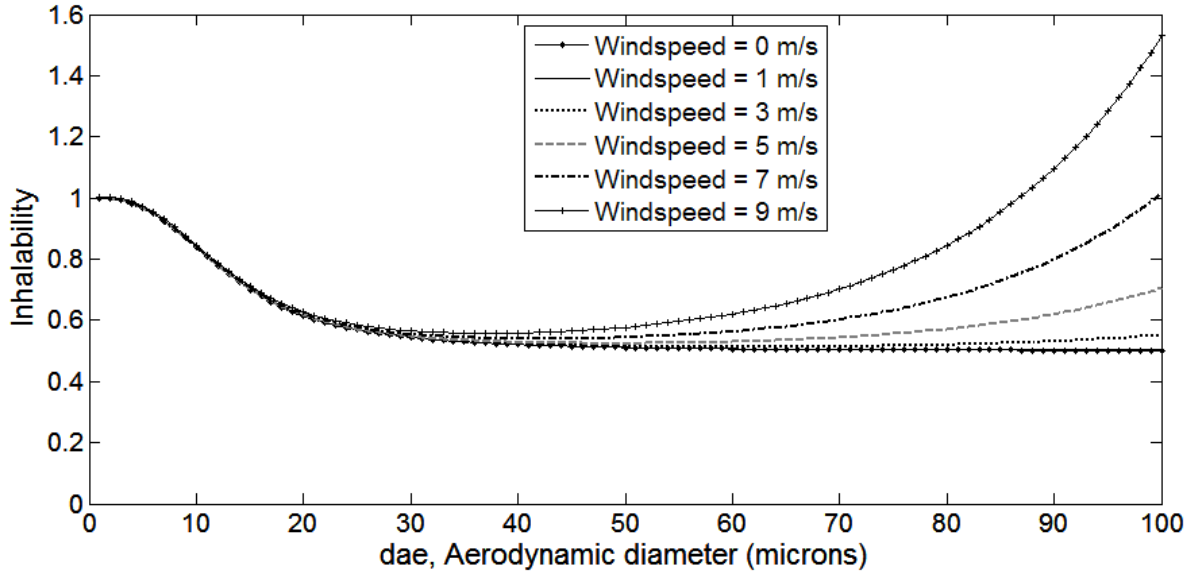
Figure 10. Inhalability as a function of wind speed and aerodynamic diameter based on ICRP recommendations.

Clearly, the ability of airborne particles to penetrate the head is a complicated function of many variables. Many of the differences noted in various studies can be related back to differences in experimental conditions; in other words, the data truly represented differing environmental scenarios. It is obvious that with all these differences the correct model is situation-dependent and it appears that no single model is appropriate for all conditions.

The most significant dependent variables are particle size, wind speed and breathing mode. Data have shown that in still air, inhalability approaches zero as particle size increases; but with an ambient wind, the inhalability approaches 0.5, not zero. Brown recommends a methodology that incorporates two different methods, one for still air conditions of less than 1 m/s ambient wind speed, and another for conditions where the ambient wind speed is greater than 1 m/s. For the still-air condition, data suggest that breathing mode plays a larger role in determining inhalability; the differences in velocity and geometry play a more significant role if there is no contribution from the ambient wind. As such, Brown recommends using Menache's equation to determine the inhalability for nasal breathing and his curve-fit for oral breathing as shown in Equation 11. It is therefore important to know the relative contribution from each breathing mode, which is also a function of breathing rate.

$$I_{Still}(d_{ae}) = f_N \left[1 - \left(\frac{1}{1 + 3.033 \cdot 10^4 d_{ae}^{-3\,114}} \right) \right] +$$
$$f_O \left[\frac{1 + 0.44}{1 + 0.44 \exp(0.0195 d_{ae})} \right] \tag{11}$$

where f_N is the fraction of total breathing from nasal breathing and f_O is the fraction from oral breathing

The breathing fraction has been measured (Niniima, 1981) and a mathematical fit for the data is graphically shown in Figure 11. Note for sleep, rest and light activity, the normal augmenter is 100% nasal breathing. Also, as was noted earlier, we recommend Menache's equations be modified to exclude the use of the white pine dust data, therefore Equation 11 evolves to Equation 12.

$$I_{Still}(d_{ae}) = f_N \left[1 - \left(\frac{1}{1 + 6.809 \cdot 10^3 d_{ae}^{-2\,736}} \right) \right] +$$
$$f_O \left[\frac{1 + 0.44}{1 + 0.44 \exp(0.0195 d_{ae})} \right] \tag{12}$$

The ICRP 66 inhalability function, as described by Equation 10, is best suited for conditions with ambient winds, but the ACGIH suggests that the wind term does not become a factor until 4 m/s. However, if the still air model is used for winds below 4 m/s and the ICRP model is used at 4 m/s and above, a striking, and not very realistic, discontinuity exists as shown in Figure 12.
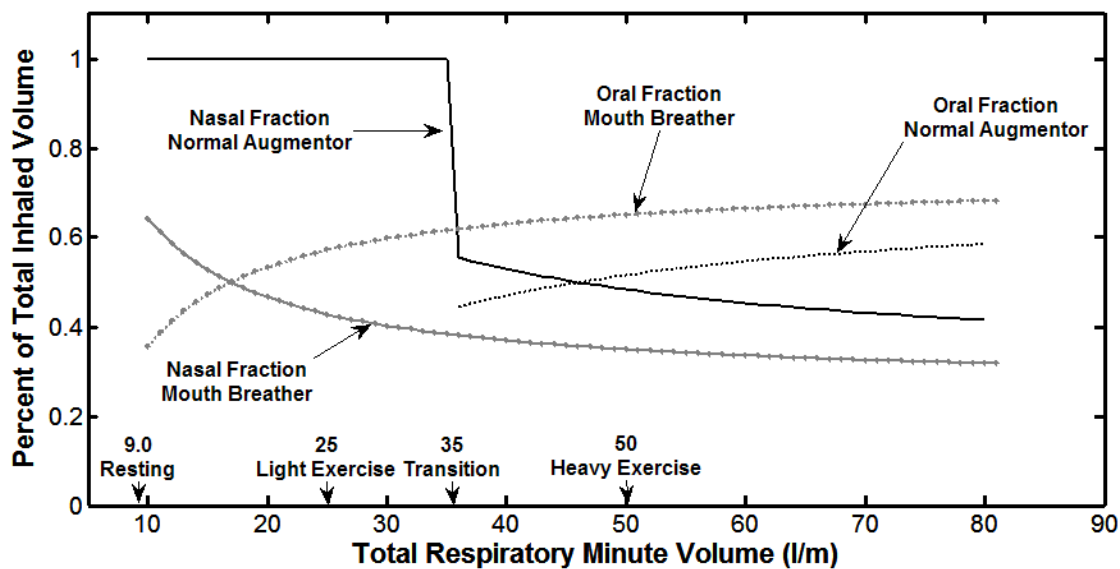
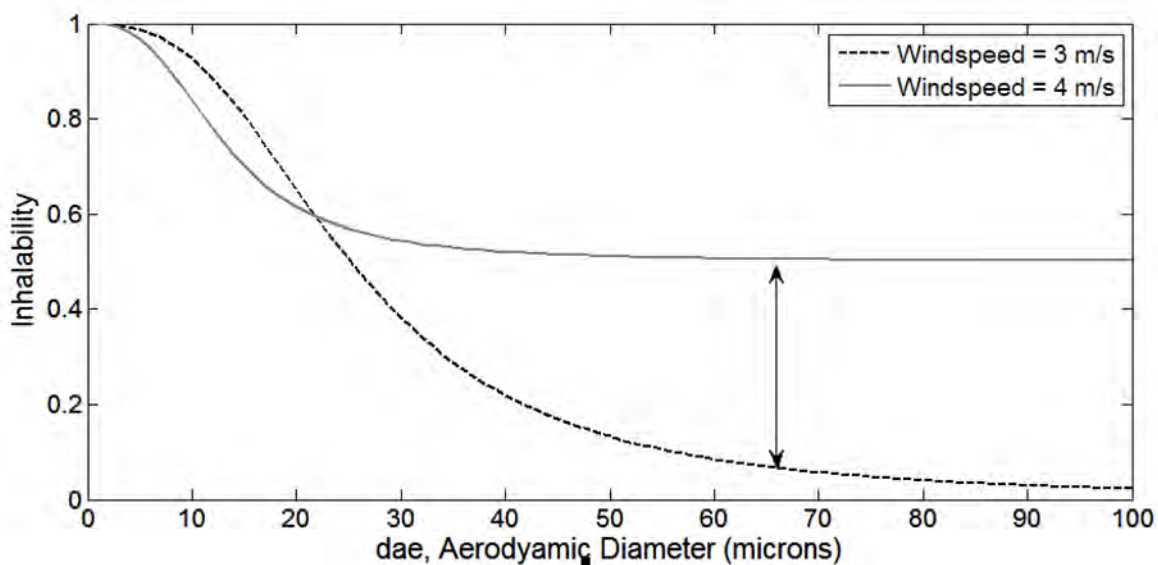Figure 11. Niniima's curve fit for breathing fraction as a function of breathing rate and type.

Figure 12. Discontinuity in inhalability model for wind speeds increasing from 3 to 4 m/s.

An alternative approach to combining the still-air and wind inhalability components is shown in Equation 13.

$$\eta_{U \le 4 m/s} = (1-J)\left\{ f_N \left[1 - \left(1 + \exp\left(8.826 - 2.736 \ln d_{ae}\right)\right)^{-1}\right] + f_o \left[\frac{1.44}{1 + 0.44 \exp\left(0.0195 d_{ae}\right)}\right]\right\}$$

$$+ J\left\{1 - 0.5\left[1 - \left(7.6 \times 10^{-4} (d_{ae})^{2.8} + 1\right)^{-1}\right] + 1 \times 10^{-5} U^{2.75} \exp\left(0.055 d_{ae}\right)\right\}$$

(13)

where: $J = \dfrac{U^{2.75}}{4^{2.75}}$

The suggested model uses the still-air based Equation 12 for wind speeds of 0 m/s and linearly interpolates between Equation 12 and the ICRP model, as shown in Equation 10, for wind speeds greater than 0 and less than 4 m/s. The interpolation scheme is based on $U^{2.75}$, the same power law that is used in the wind driven component of the inhalability function at greater wind speeds. At wind speeds greater than 4 m/s, Equation 10 should be used. Figure 13 shows an example of how this model would look at wind speeds ranging from 0 to 9 m/s for light activity, i.e. nasal breathing only.
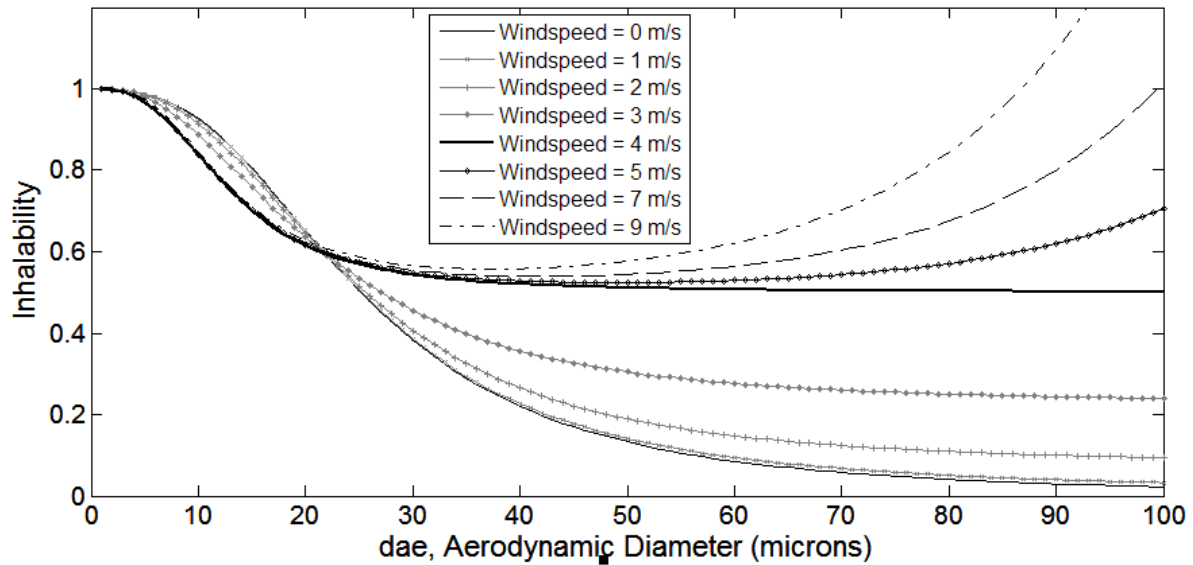

Figure 13. Recommended set of inhalability curves for a normal augmenter at a low breathing rate.

Conclusions and Recommendations

Inhalability is an important parameter in trying to predict the potential effects of aerosol hazards in the form of both small and large particles. Experiments conducted over the last several decades have provided meaningful insights into the process and a variety of mathematical models have been developed from the data. This paper provided an overview of some of the work that has been performed for particles and liquid droplet inhalability and addressed some of the issues that were unresolved. One over-riding issue is that a single function is not appropriate to model inhalability for all situations. For example, eliminating the white pine dust from the Menache model of the Breysse and Swift's experiments provides a better representation of nasal inhalability in still air and Brown established a sound mathematical model of oral inhalability in still air. However, the generalized ICRP and ACGIH models that include still and moving air conditions are well established in their use.

Since a single function is not appropriate to model inhalability for all situations, a stepwise approach was presented. The inhalability function recommended in this paper applies the best models for the appropriate particle size and environmental conditions while minimizing mathematical discontinuities. Although this model is adequate for most conditions, there is a gap in satisfactory modeling for ultra-large particles: none of the data models sufficiently describe inhalability for particles larger than 100 microns. The Menache and Brown equations for still-air conditions tend to zero at larger particle sizes, and the ICRP equations should not be extrapolated beyond 100 microns as they produce unrealistically high inhalability fractions when the wind-driven term is included. The argument may be made that particles of this size have such a limited range that they do not pose a significant health risk. However, conditions can exist that could cause particles this large to be an inhalation hazard. Large particles can remain airborne for significant periods of time either due to very high initial release points or due to significantly turbulent conditions, such as might exist in urban terrain. It is evident that continued experimentation and modeling of varying breathing conditions, environmental scenarios, and particle types will be necessary as new and potentially hazardous situations arise that could impact human health. Standardization of models will be necessary for the development of safety

standards and guidelines in industry, and improved mathematical representations of the data will enhance our ability to model the potential consequences of inhalation hazards.

ACKNOWLEDGMENTS

References

Aitken, R.J., Baldwin, P.E.J., Beaumont, G.C., Kenny, L.C., and Maynard, A.D. (1999). Aerosol Inhalability in Low Air Movement Environments, *J. Aerosol Sci.*, 30:613-626.

American Conference of Governmental Industrial Hygienists (1999) Paricle Size-Selective Sampling for Particulate Air Contaminants, Vincent JH Editor. Cincinnatti, OH: ACGIH Worldwide.

Breysse, P.N. and Swift, D.L. (1990). Inhalability of Large Particles into the Human Nasal Passage: in vivo Studies in Still Air. *Aerosol Science Technology* 13:459-464.

Brown, J.S. (2005). Particle Inhalability at Low Wind Speeds. *Inhalation Toxicology* 17:831-837.

Hsu, D.J. and Swift, D.L. (1999). The Measurement of Human Inhalability of Ultralarge Aerosols in Calm Air Using Mannikans. *J. Aerosol Sci.* 30:1331-1343.

International Commission on Radiological Protection (ICRP) (1994). Human Respiratory Tract Model for Radiological Protection. Publication 66, Pergamon Press, Oxford, United Kingdom, *Annals of ICRP* 24:235.

Kennedy, N.J. and Hinds, W.C. (2002). Inhalability of Large Solid Particles. *J. Aerosol Sci.* 33:237-255.

Menache, M.G., Miller, F.J. and Raabe, O.G. (1995). Particle Inhalability Curves for Humans and Small Laboratory Animals. *Annals of Occupational Hygiene* 39:317-328.

Niinimaa, V. Cole, P., Mintz, S., and Shephard, R.J. (1981). Oronasal Distribution of Respiratory Airflow, *Respiration Physiology*, 43:69-75.

Ogden, T.L. and Birktt, J.L. (1977). The human head as a dust sampler. In *Inhaled Particles IV* (Walton WH, Ed.), pp.93-105 Pergamon Press, Oxford, UK.

Ogden TL, Birkett JL and Gibson J (1977) Improvements to dust measuring techniques, IOM Report No. TM/77/11, pp. 33-41 Institute of Occupational Medicine, Edinburgh, Scotland, UK.

Vincent J.H., Mark, D., Miller, B.G., Armbruster, L., and Ogden, T.L. (1990) Aerosol Inhalability at Higher Windspeeds, *J. Aerosol Sci.*, 21:577-586.

ATTACHMENT 2

(Next Page)

Comparison of Stochastic, Symmetric, and 5-Lobe Asymmetric Lung Models in MPPD

Joshua J. Bergman

Technical Report

15 August 2009

Preface

The research and development work described in this technical report was conducted for Project CB06MSB096 of the Joints Science and Technology Office (JSTO) of the Department of Defense (DoD) Chemical and Biological Defense (CBD) Program. JSTO is also the Chemical/Biological Technologies Directorate (RD-CB) in the Research and Development Enterprise of the Defense Threat Reduction Agency (DTRA). Project CB06MSB096 is titled *Medical Modeling of Particle Size Effects for Inhalation Hazards*.

Table of Contents

List of Tables

List of Figures

INTRODUCTION

Three of the four lung models in the MultiPath Particle Dosimetry (MPPD) software application (Asgharian *et al.*, 2001) were used to determine the bounds of uncertainty for evaluating inhaled particle deposition fractions:

1) Symmetric single-path model,
2) Symmetric multiple-path model – comprised of an asymmetry at the level of the major branching bronchi forming five lobes each with a single-path symmetric branching tree, and
3) Stochastic multiple-path model – comprised of five branching lobes of randomly generated alveolar regions.

The fourth model not considered here consists of ten detailed, stochastic, child-specific lung morphometry models for ages 3 months to 21 years.

There are 10 different stochastic lung models of increasing number of airways provided in MPPD; however, the dimensions of the alveolar sacs have been adjusted to maintain an equal alveolar volume across all lung types. The stochastic lung models are intended to represent the differences in lung structure in the adult human population, and therefore are used in this study to determine the uncertainty of using a single-path or multiple-path symmetric lung model. It should be noted that while the stochastic model potentially provides more accurate results, it is a computationally more expensive simulation than the symmetric models.

METHODS

The normal-augmenter breathing type for four activity levels shown in Table 1 of a healthy, adult male was chosen to represent the single-path symmetric, multiple-path symmetric, and stochastic models. Normal augmenting is the most common breathing mode typified by nasal breathing at minute volumes less than 35.3 L min^{-1}, above which nasal breathing is augmented with oral breathing (57% nasal, decreasing to 40% at a minute volume of 90 L min^{-1}; see Niinimaa, 1981). Functional residual capacity (volume of air remaining in lungs after a tidal expiration) was set to 3300 ml.

Table 1 Selected ICRP-66 respiratory data for healthy adult male (ICRP, 1994).

Activity Level	Tidal Volume (L)	Breathing Rate (min^{-1})	Minute Volume (L min^{-1})
Sleeping	0.625	12	7.5
Resting/Awake	0.750	12	9.0
Light Exercise	1.250	20	25
Heavy Exercise	1.923	26	50

Error-bars were generated for the stochastic model results by averaging the regional deposition fractions of the ten models and calculating the standard deviation. Total deposition uncertainty was calculated by summing the regional averages and propagating the standard deviation using the following formula:

$$\sigma_u^2 = \left(\frac{\partial u}{\partial x}\right)^2 \sigma_x^2 + \left(\frac{\partial u}{\partial y}\right)^2 \sigma_y^2 + \left(\frac{\partial u}{\partial z}\right)^2 \sigma_z^2 + ...$$

where $u=u(x,y,z,...)$ represents the derived quantity and σ^2 is the variance.

Since three quantities of average deposition are summed with their corresponding standard deviations, $u = x+y+z$. The partial derivative of u with respect to x, y, and z is 1, resulting in a total standard deviation of

$$\sigma_u = \sqrt{\sigma_x^2 + \sigma_y^2 + \sigma_z^2} \ ,$$

where x, y, and z, may represent the head, tracheobronchial, and pulmonary regions.

Figures 1 through 4 show the comparison of the symmetric single and multiple-path total deposition fractions compared to the stochastic model for the four activity levels of heavy, light, rest and sleep for a normal augmenter breathing-type in still air. In all cases, the error bars bracket the multiple-path model results for all particle diameters. However, the single-path model at some particle diameters is just above the error bar. This occurs at the smaller diameters; as particle size increases, deposition only occurs in the head and the variation between stochastic models and symmetric models converges to a single value.

Figure 1. Total deposition fraction comparison for symmetric and stochastic models for normal augmenter for sleeping activity.

Figure 2. Total deposition fraction comparison for symmetric and stochastic models for normal augmenter for resting activity.
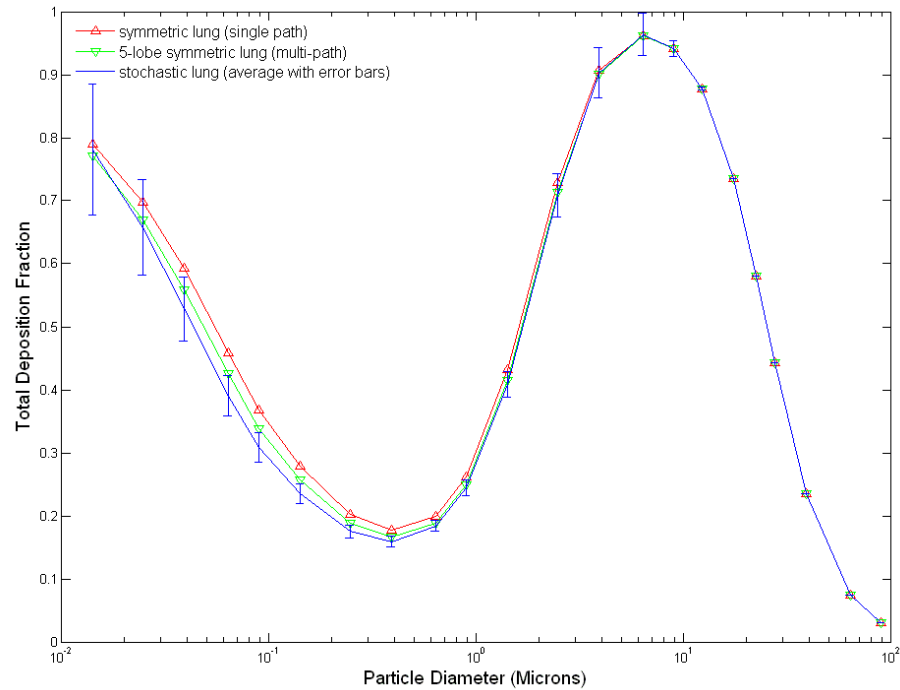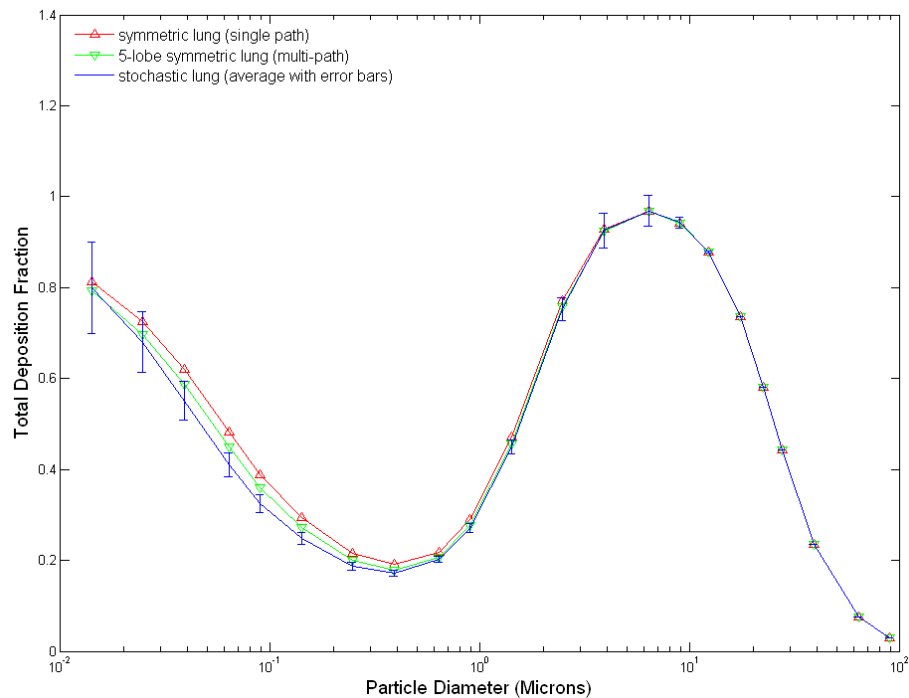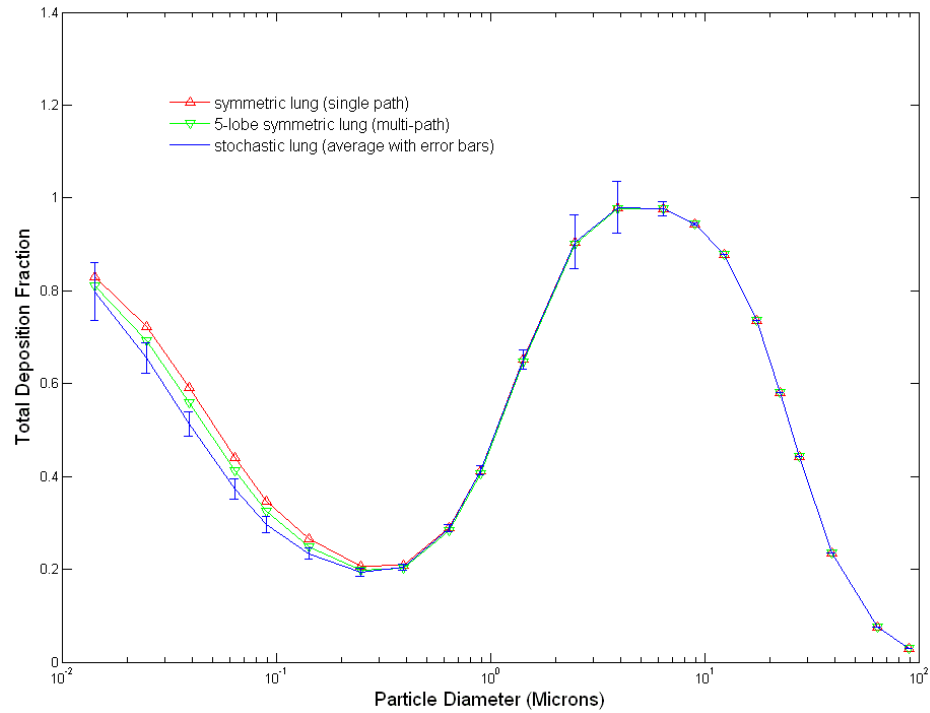
Figure 3. Total deposition fraction comparison for symmetric and stochastic models for normal augmenter for light activity.
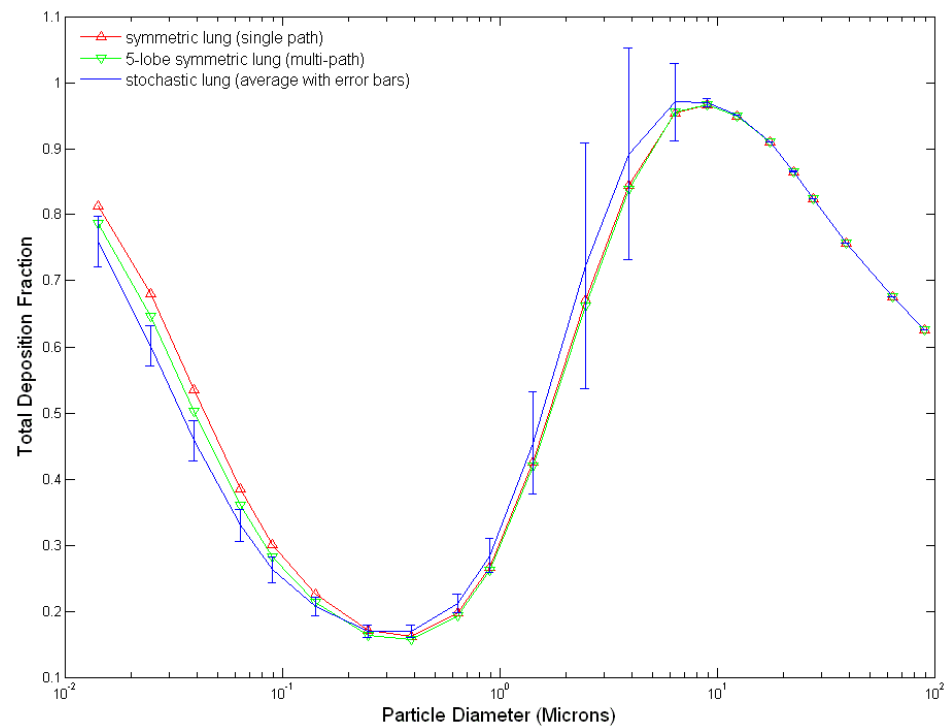

Figure 4. Total deposition fraction comparison for symmetric and stochastic models for normal augmenter for heavy activity.

Comparison of Lung Models in MPPD

Figures 5 through 16 compare stochastic and symmetric models for each activity level and each region: head, tracheobronchial, and pulmonary. As expected, deposition in the head region shows only minor to no fluctuation when comparing symmetric to stochastic models. Differences between sleep and resting activity are also minor across the different respiratory regions.

The significance of comparing stochastic and symmetric model results by lung region is the observation that the multiple-path symmetric model results do not always stay within the error bars of the stochastic model, contrary to what was seen for the most part in Figures 1 through 4 for the single-path model. Between approximately 0.05 microns and 2 microns, deposition fractions in the pulmonary region of the symmetric models consistently remain above the error bars of the stochastic, whereas the tracheobronchial region shows some of the greatest differences between models as compared to other regions. These disparities between symmetric and stochastic models in the tracheobronchial region could be attributed to the random nature of the airway generation in the stochastic model. As mentioned previously, the lobar alveolar sacs' dimensions are adjusted to maintain approximately the same total alveolar lung volume across the ten stochastic lung models (Asgharian *et al.*, 2001). However, the dimensions and volumes of the tracheobronchial region are not adjusted in the model and therefore it is possible for the stochastic models to differ widely in this region. As the number of airways increase, airflow velocity decreases enhancing deposition by diffusion. The ten stochastic models range from a smaller number of airways to a larger number, and as shown in Table 2, the deposition fraction for the particle sizes having the largest error generally decreases with increasing number of airways.

Table 2. Deposition fractions in tracheobronchial region for each stochastic model – particle sizes with largest associated standard deviation for deposition in tracheobronchial region.

Model of Increasing Number of Airways	Particle diameter (microns)		
	1.414214	2.44949	3.872983
	Tracheobronchial region deposition fraction		
Stochastic Model 0	0.3087	0.5943	0.5054
Stochastic Model 1	0.164	0.4253	0.4958
Stochastic Model 2	0.0884	0.1509	0.34
Stochastic Model 3	0.0851	0.1195	0.2455
Stochastic Model 4	0.0858	0.1363	0.2823
Stochastic Model 5	0.0761	0.1017	0.2062
Stochastic Model 6	0.066	0.0764	0.1174
Stochastic Model 7	0.0699	0.0829	0.1328
Stochastic Model 8	0.0642	0.0734	0.1084
Stochastic Model 9	0.0757	0.0962	0.1873

This observation can be attributed to the phenomenon that particle sizes around 2.5 microns are primarily deposited through impaction, especially at higher airflow rates. The magnitudes of the largest error bars indicate that for the stochastic models with the larger number of airways, the deposition fraction decreases for these particles sizes in the tracheobronchial region and that they are most likely being deposited in the pulmonary region via diffusion.
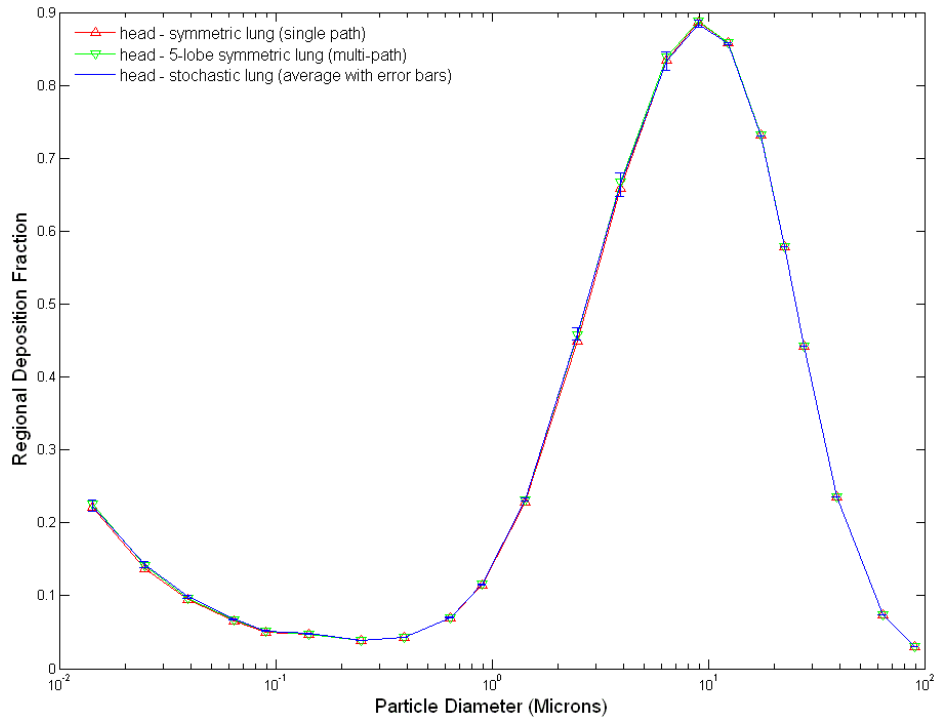
Figure 5. Deposition fraction in head during sleep.
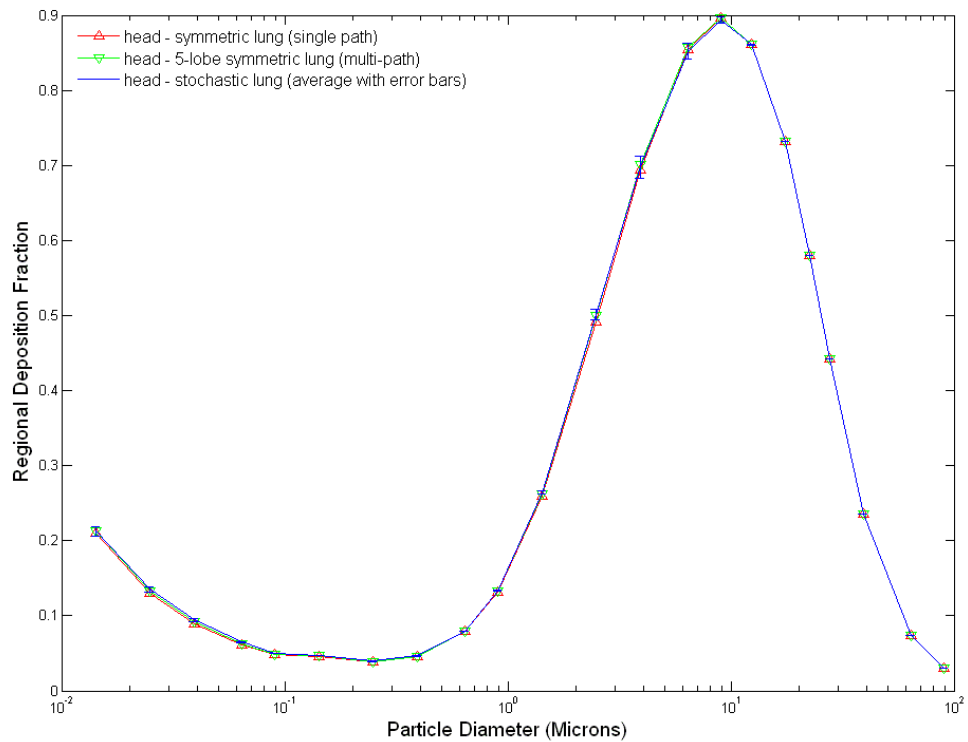
Figure 6. Deposition fraction in head during resting activity.
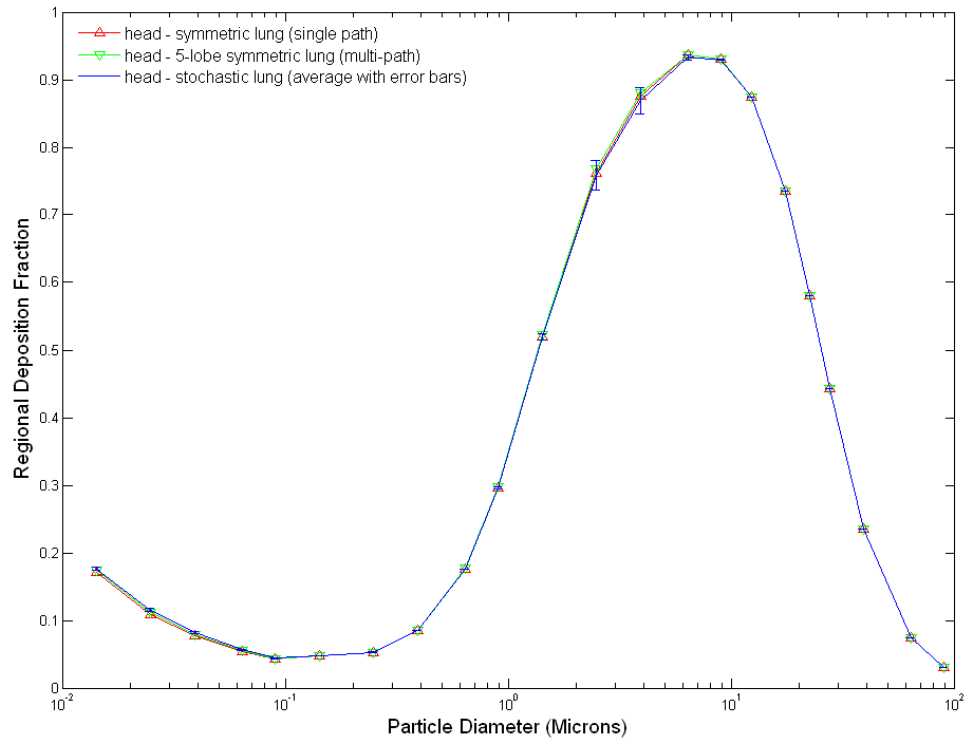
Figure 7. Deposition fraction in head during light activity.
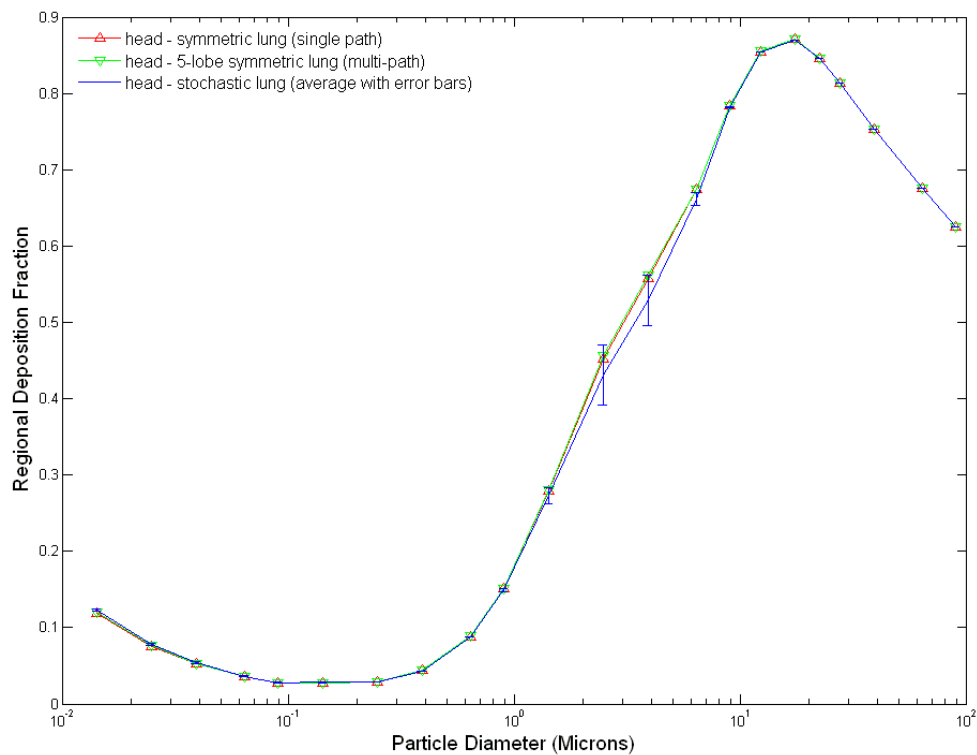
Figure 8. Deposition fraction in head during heavy activity.

Comparison of Lung Models in MPPD
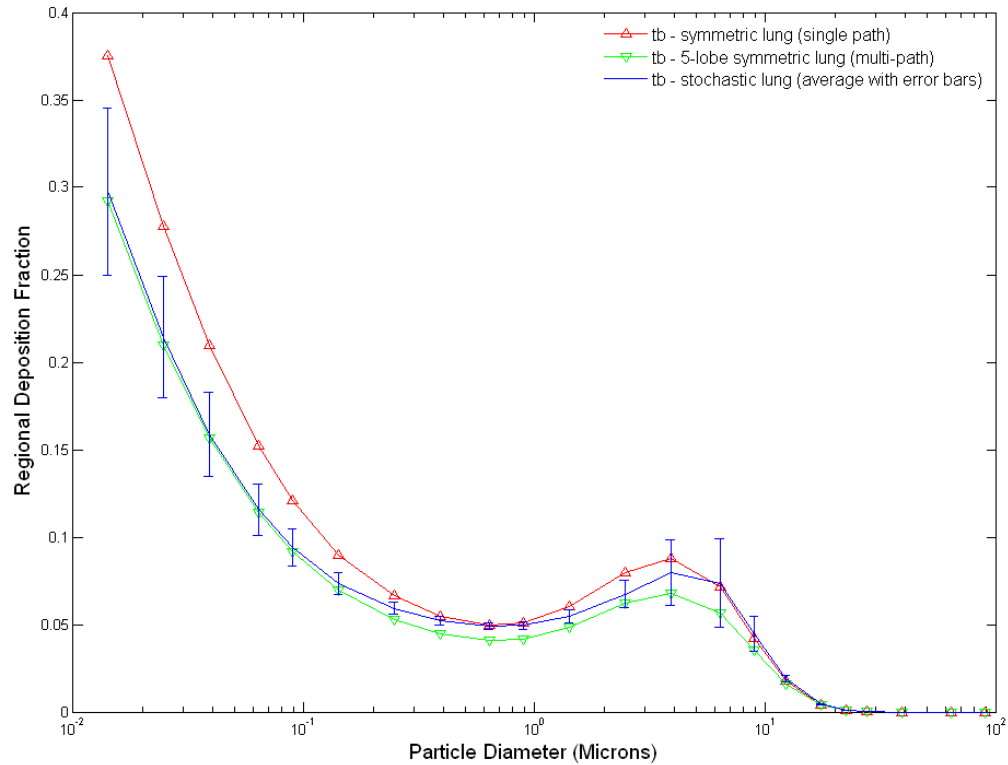
Figure 9. Deposition fraction in tracheobronchial during sleep.
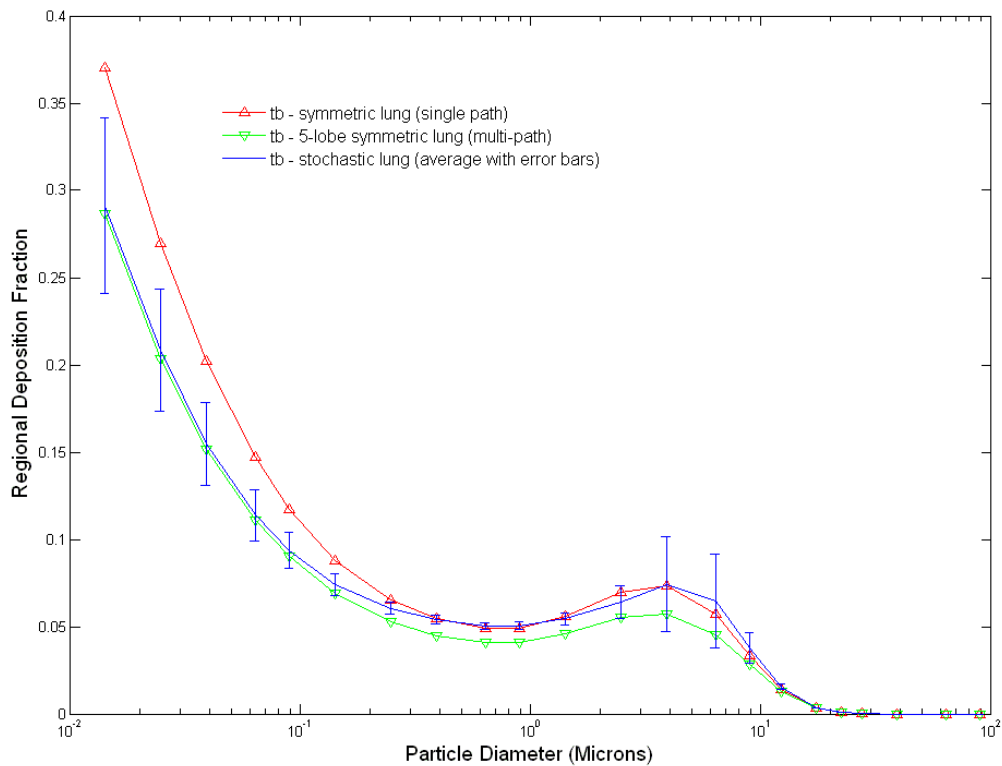
Figure 10. Deposition fraction in tracheobronchial during resting activity.

Comparison of Lung Models in MPPD
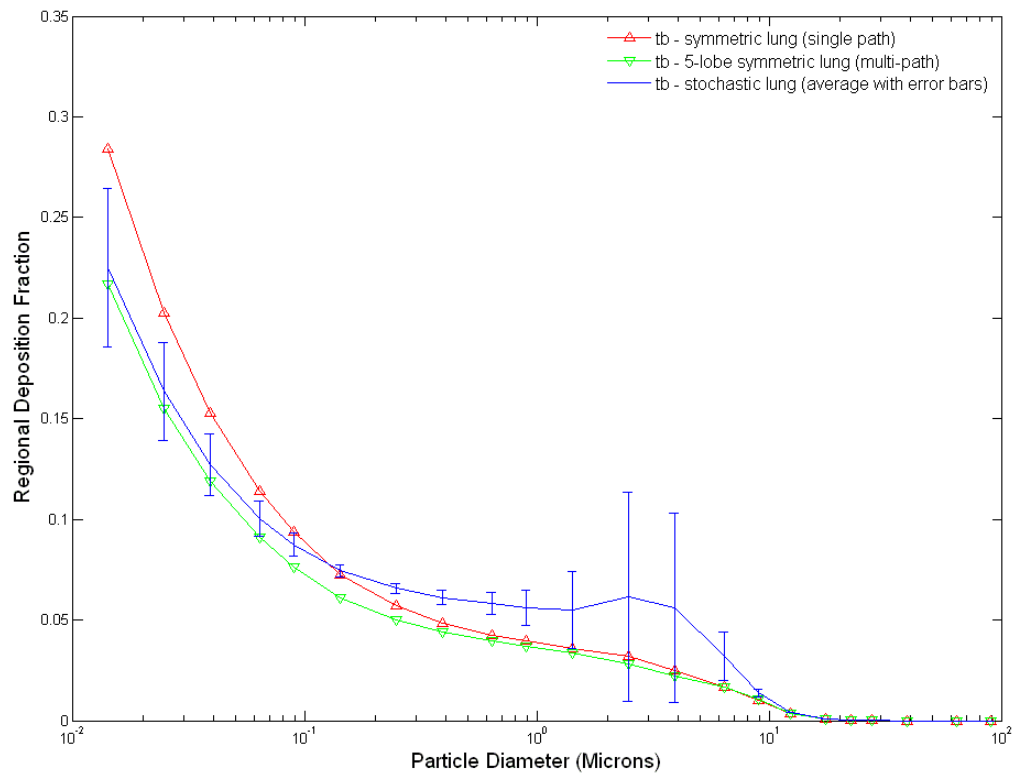
Figure 11. Deposition fraction in tracheobronchial during light activity.
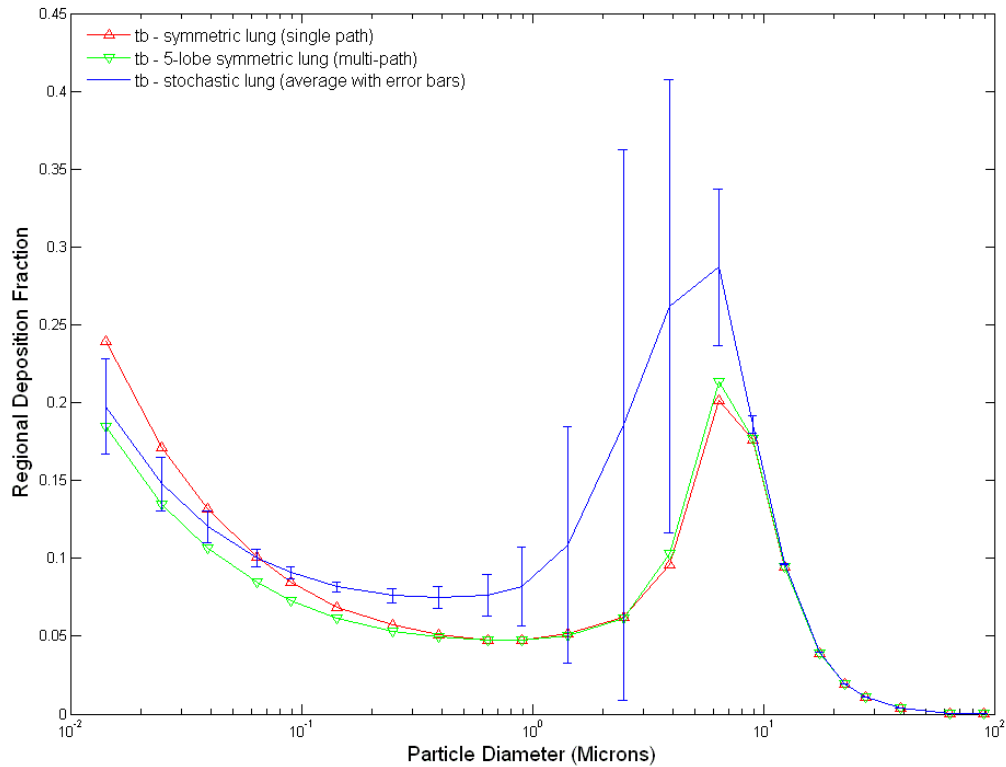
Figure 12. Deposition fraction in tracheobronchial during heavy activity.
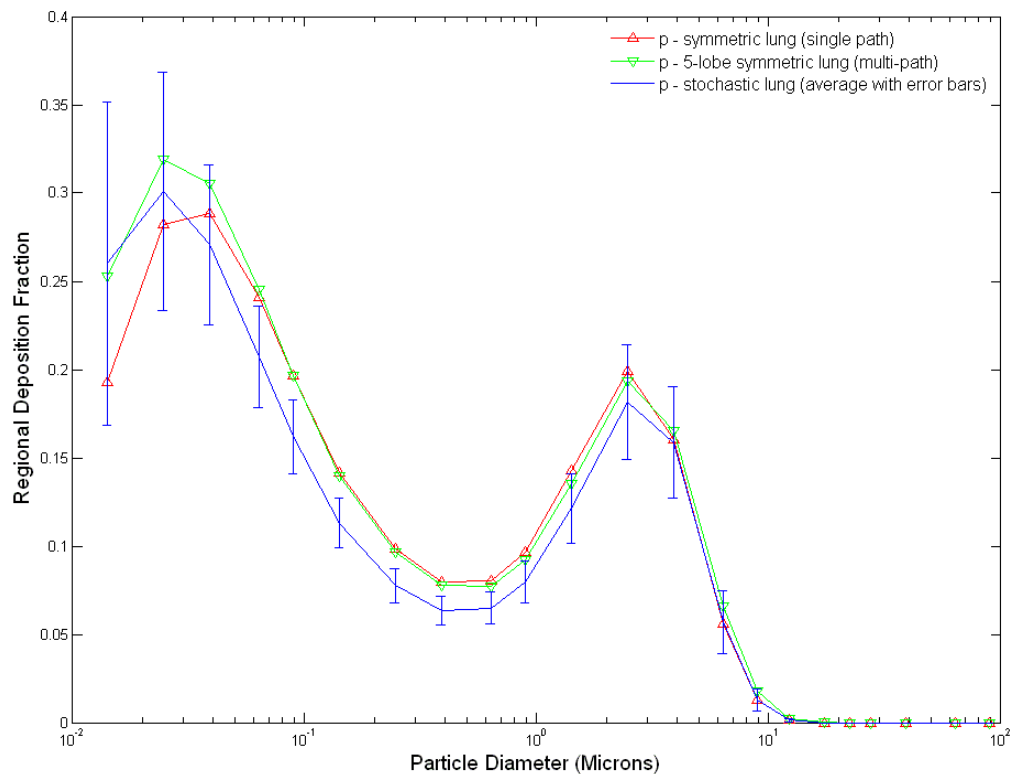
Figure 13. Deposition fraction in pulmonary during sleep.

Comparison of Lung Models in MPPD

11
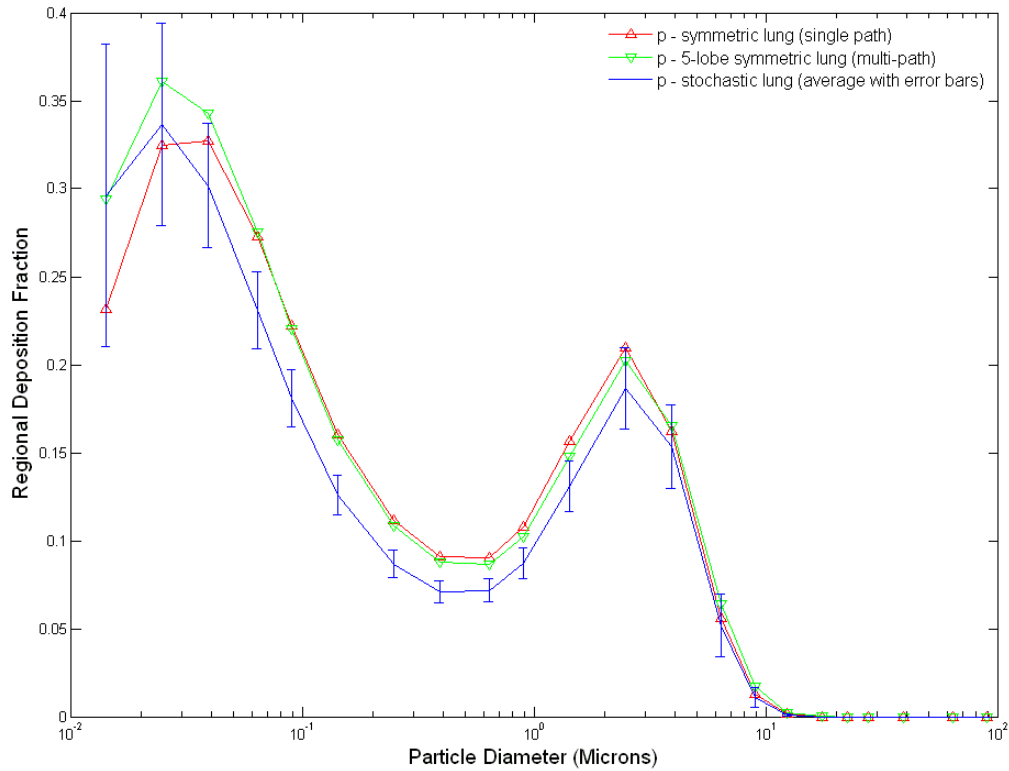
Figure 14. Deposition fraction in pulmonary during resting activity.
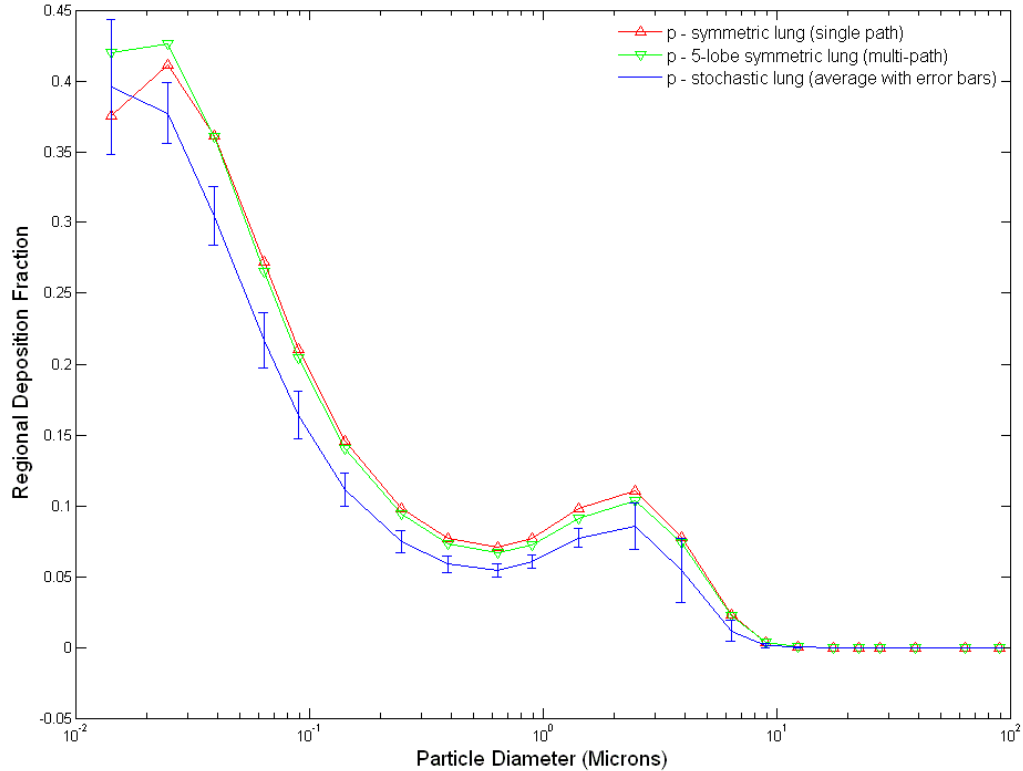
Figure 15. Deposition fraction in pulmonary during light activity.

Comparison of Lung Models in MPPD
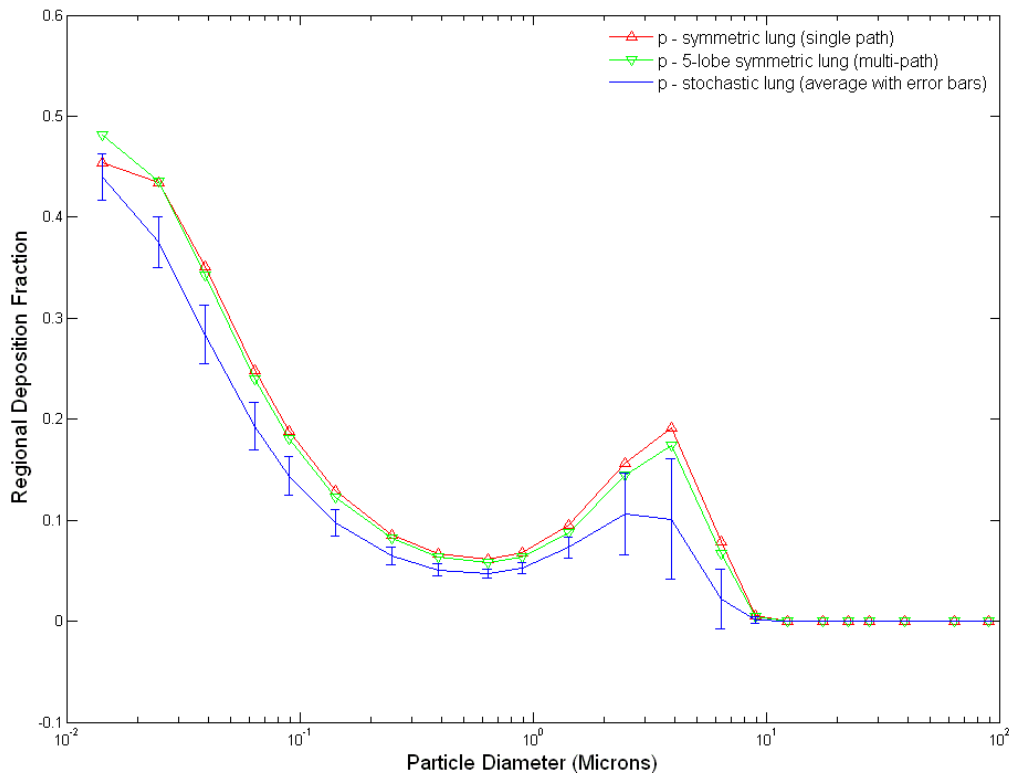
Figure 16. Deposition fraction in pulmonary during heavy activity.

CONCLUSION

A similar study of the uncertainty in MPPD stochastic lung models was done by the developers of the code (Asgharian *et al.*, 2001). The developers concluded that for assessing overall deposition in the lung any of the models would be appropriate for prediction. While they only reported deposition fractions for a particular minute ventilation (equivalent to sleep here), a breathing type which appears to be oral, and particle diameters for deposition to 10 microns, their recommendation is still valid for the breathing type and particle sizes reported in this document.

Comparison of Lung Models in MPPD

REFERENCES

Asgharian B, Hofmann W, Bergmann R., Particle deposition in a multiple-path model of the human lung, *Aerosol Science and Technology* 34:332-339; 2001.

International Commission on Radiological Protection (ICRP). Human respiratory tract model for radiological protection. Oxford: Pergamon Press; ICRP Publication 66, Ann ICRP 24(1-3); 1994.

Niinimaa V, Cole P, Mintz S, Shephard RJ. Oronasal distribution of respiratory airflow. *Respiration Physiology* 43:69-75; 1981.

ATTACHMENT 3

(Next Page)

Effects of Particle Size on Physiological Responses to BW Agent Aerosols

Sharon A. Watson, Scott A. Thornton, Gene E. McClellan, and Kyle K. Millage

Technical Report

30 June 2009

Preface

The research and development work described in this technical report was conducted for Project CB06MSB096 of the Joints Science and Technology Office (JSTO) of the Department of Defense (DoD) Chemical and Biological Defense (CBD) Program. JSTO is also the Chemical/Biological Technologies Directorate (RD-CB) in the Research and Development Enterprise of the Defense Threat Reduction Agency (DTRA). Project CB06MSB096 is titled *Medical Modeling of Particle Size Effects for Inhalation Hazards*.

This review paper is based on many referenced articles. In much of this paper, single paragraphs summarize relevant results from one or two referenced articles. In these cases, the appropriate citation appears at the end of the paragraph rather than in conjunction with each fact quoted in the paragraph.

Table of Contents

List of Figures

List of Tables

Executive Summary

Particle size profoundly affects the regional disposition of an inhaled aerosol and influences the course of development of disease when the aerosol contains an infectious agent. This paper reviews the available literature concerning the relationship between the particle size of inhaled aerosols and the development of respiratory illness. Many of the studies reviewed are concerned with respiratory illness caused by *Francisella tularensis*. This bacterium is listed by the CDC as a Class A biowarfare (BW) agent. It has been observed that the symptoms caused by *F. tularensis* are related to the organism's port of entry into the body. In a BW scenario, the most likely method of exposure is via aerosol inhalation. By this route, very small numbers of bacteria (1-10) are needed to cause severe illness in the alveoli of the lungs. *F. tularensis* causes disease by resisting lysis when engulfed by macrophages, instead, replicating in high numbers and spreading to nearby lymph nodes and throughout the body. It is important to note that other BW agents, such as *Bacillus anthracis, Yersinia pestis, Coxiella burnetti,* and *Brucella spp*, follow a similar strategy in overcoming natural defenses against disease.

The mammalian respiratory system can be physically divided into three regions: 1) the Extrathoracic (ET) region, also called the Nasopharyngeal (NP) region, extending from the nares (or nostrils) to the epiglottis, 2) the Tracheobronchial (TB) region extending from the larynx through the terminal bronchioles, and 3) the Pulmonary (P) region beginning with the respiratory bronchioles and ending with the alveoli. Inhaled particles deposit at various depths in the respiratory system of different mammals. Some BW agents, including *F. tularensis*, *B. anthracis*, and *Y. pestis*, may initiate infection at almost any site of particle deposition. This includes illness in non-respiratory surfaces, such as the conjunctiva and open sores in skin. However, because of effective clearance of deposited particles in the TB region by mucociliary action, respiratory infections occur most often in the NP and P regions, generally referred to as upper and lower respiratory infections, respectively.

Aerosol particles of larger diameter (10 to 100 microns) are influenced more strongly by gravitational and inertial forces and have difficulty negotiating the increasingly narrower respiratory passages during inspiration. These forces usually lead to deposition at sites upstream from the alveoli. Particles of optimal size (3 to 5 microns for bacterial agents) for reaching the P region in humans are also optimal for being exhaled from the body, so that deposition and retention in the P region of these particles is only about 20% of those inhaled.

In general for all mammals studied, inhaled particles of size >10 micron require a much higher dose to initiate illness due to majority deposition in the NP and TB regions. This occurs despite the fact that these larger particles typically each contain many infectious cells, while particles of 1 to 5 micron diameter are more likely to have only one bacterium. The lower number of cells per particle is offset by the lower dose needed to initiate illness when deposited in the alveoli.

This divergence is even more pronounced for small mammals: inhalational exposure with <5 micron mean diameter particles of *F. tularensis* follows a similar clinical course of illness in all mammals, but inhalational exposure with >5 micron particles leads to much less illness in small mammals due to smaller diameter respiratory passages. A macaque monkey model has been used for several years for laboratory studies of tularemia and other BW agents, as the general diameters and layout of the macaque respiratory system, the median infective dose (ID_{50}), symptoms, and aerosol particle deposition closely follow that of humans.

Macaques inhaling particles >10 u in diameter may develop tularemia in sites besides the lungs, such as the lymph-associated tissue of the NP region (oropharyngeal tularemia) and the eyes (ocular tularemia). This difference in location of the infection is due to deposition on those tissues rather than deep in the lungs as seen with small particles. As reviewed in Section 6, macaque monkeys are considered the best available animal model for studying the respiratory effects of tularemia in humans.

This report reviews data on infectious BW agents for several species, including humans, monkeys, guinea pigs, and rats. It reviews data for anthrax, Q fever, plague and VEE, but the primary focus in on tularemia.

In summary, the P region is the most vulnerable target for inhaled *F. tularensis* (due to the organism's efficient defeat and infection of the macrophage removal system); however, other locations also dependent on lymphatic tissue / macrophage defense are also at risk as infection initiation sites. Despite the past focus of professional military scientists to produce efficient weaponized aerosols of 1-5 micron in diameter, it is very likely a terrorist organization without the benefit of modern laboratory facilities may produce and disseminate a coarse preparation including larger particles or a wide range of particle sizes. This report reviews the effects of both smaller and larger aerosol particles in support of the broader objective of this study, which is to develop computational models so that the effects of such a weapon release may be predicted.

1. Introduction - *Francisella tularensis* and Tularemia

The causative agent of the disease tularemia is the bacterium *Francisella tularensis* (formerly *Pasturella tularensis*), a gram-negative, non-spore forming, intracellular pathogen. This disease occurs naturally throughout temperate regions of the Northern hemisphere. There are several subspecies of *F. tularensis* which vary in virulence and distribution. Two subspecies account for the majority of human illness. *F. tularensis subsp. tularensis*, also called Type A, is predominantly found in North America, while *F. tularensis subsp. holarctica* (Type B) is found in Eurasia. *F. tularensis* can remain viable for weeks in water, soil and carcasses and can remain in frozen rabbit meat for years. Type A is one of the most infectious bacterial pathogens known. Because of its environmental hardiness, high infectivity and life threatening effects in humans, Type A was investigated by every country with an offensive biological weapons program as a potential agent. In fact, it was one of the agents given the highest priority in the offensive programs of both the United States and Soviet Union. Today it is considered a potential agent of bioterrorism. As few as 10 organisms (either inhaled or injected intradermally) is the median infective dose (ID_{50}) for humans and macaques. Fortunately, the disease is readily treated with antibiotics and effective vaccines have been developed. (Eigelsbach *et al*. 1968, Sjostedt 2007, USAMRIID 2005).

Natural reservoirs of *F. tularensis* are small mammals, especially rabbits, mice, squirrels, muskrats, voles, and lemmings. Natural human cases are usually acquired during outdoor activity that puts them in these animals' habitats. Tularemia can manifest as several clinical forms, often depending on the point of entry into the human body. Most cases in the United States involve transmission by an arthropod bite in the skin, typically a tick or biting fly. This usually leaves a lesion at the bite site, although the bacteria may have also spread elsewhere in the body. This common form of the disease is called the ulceroglandular form, and is rarely fatal, although the person may get a high fever. The infective site may also be the eyes, causing conjunctivitis (ocular tularemia). The bacteria may be ingested in food or water and cause gastroenteritis, fever, and pharyngeal lesions (oropharyngeal tularemia). This is a common manifestation of Type B strains. The rarest and deadliest form of infection is by direct inhalation of organisms deep into the lungs, which is the primary route of interest in offensive weapons programs. (USAMRIID 2005)

The number of natural tularemia cases in the U.S. has dropped from thousands per year before 1950, to less than 200 per year in the 1990's, with case-fatality rate of 1.4% (Dennis *et al.* 2001). Most human cases are in the Midwestern states, especially Missouri, Arkansas, Kansas, and South Dakota. A foci has existed on the island of Martha's Vineyard, Massachusetts, since 20,000 cottontail rabbits were imported from Missouri for hunting in 1937 (ProMed, 2005a and 2005b). Far more cases occur in Europe, Russia, and some in Iran, many due to water-borne or mosquito-borne outbreaks. This route of infection was a concern to U.S. military personnel deployed to Kosovo, where outbreaks of Type B tularemia occurred from 2000-2002 (ProMed 2002).

Natural inhalational tularemia outbreaks are rare, but Type B has been documented in large-scale hay farming in Vermont and an incident infecting 15/39 (38%) of tourists eating dinner one night at a renovated mill in France (Siret *et al.* 2006). Martha's Vineyard, Massachusetts, is the site of the only two recognized outbreaks of primary pneumonic tularemia in the United States. In the summer of 1978, there were 15 cases of tularemia, including 12 with primary pneumonic presentations. While no definitive source of the outbreak was found, seven cases shared a vacation cottage. Epidemiological investigators indicated that aerosols produced by the family dogs' vigorous shaking of water on their fur contaminated through contact with infected rabbits might have been the source of exposure for these cottage inhabitants. Beginning in 2000 and continuing through 2006, 59 presumed or confirmed tularemia cases were reported from Martha's Vineyard with more than 60% believed to be due to inhalation of the agent. Most of these cases were in landscape workers using lawnmowers and leaf blowers which apparently aerosolized contaminated animal droppings (Matz-Rensing, K *et al.* 2007, Dennis *et al.* 2001, Feldman *et al.* 2003). One case of oropharyngeal tularemia which occurred there was possibly the result of inhaling coarse particles from during handling of a dead rabbit. (ProMed Mail 2005a).

Whatever the site of entry, most bacterial BW agents, such as *F. tularensis, Bacillus anthracis* (causative agent of anthrax), *Coxiella burnetti* (causative agent of Q fever), *Brucella* spp (causative agent of undulant fever) and *Yersinia pestis* (causative agent of plague), are quickly engulfed by phagocytic cells such as macrophages, dendritic cells, monocytes and neutrophils. The phagocytic cells confine foreign particles into vesicles which are soon merged with acidic lysosomes that destroy the foreign particle. The bacterial BW agents use various mechanisms to avoid destruction: *Francisella* quickly breaks out of the vesicle into the macrophage cytoplasm and begins replication, *B. anthracis* spores germinate and then disperse lethal toxins, and *Y. pestis* causes an inflammatory destruction of the macrophage and releases its own lysozymes into surrounding tissue. All these mechanisms cause local lesions, but the more virulent strains may then spread throughout the body via blood or lymph (Celli 2008).

The effects of aerosol exposure to *F. tularensis* were extensively studied in the U.S. Offensive Biological Warfare Program before the program was dismantled in 1969. During the height of program, a 1-million-liter aerosol test chamber was constructed at Fort Detrick, MD to study agent aerosol characteristics under controlled conditions. The 40-foot-high, gas-tight globe was nicknamed the "Eight Ball" (see Figure 1). Enclosed in a 60-by-60-foot laboratory building, the structure had control panels and exposure chambers at the base of the test sphere, as well as catwalks that allowed scientists to observe exploding biological weapons and collect samples from portals. Both animal and human test subjects were exposed to biological aerosols generated in the chamber. Human subjects ascended to specially designed exposure cubicles at equator level. Animals were exposed at other portals. (Perretta 1999, AMEDD 2000, and Jemski 1961)
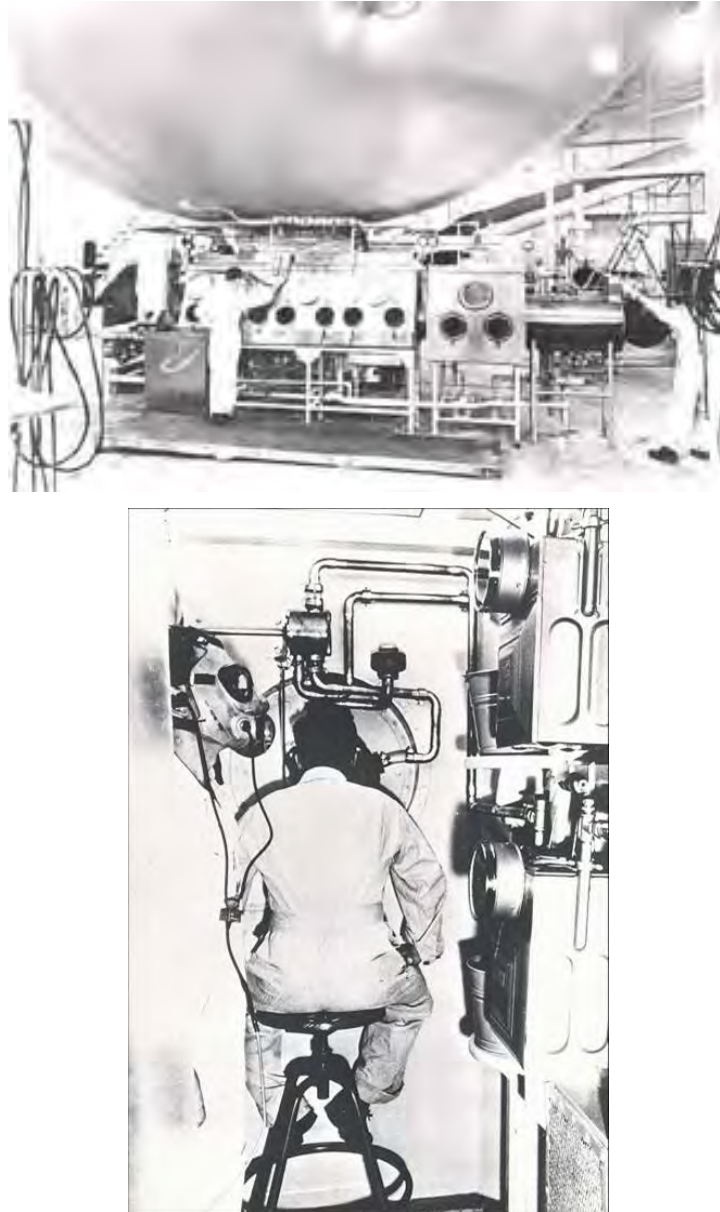
Figure 1. The million-liter aerosol chamber at Fort Detrick was nicknamed the "Eight Ball". The lower picture shows an individual at an exposure port. (AMEDD 2000)

"Operation Whitecoat" was the name given to the series of experiments involving human volunteer test subjects which took place during the period from 1954-1973. Most of the 2300 volunteers were Seventh Day Adventists, conscientious objectors who agreed to be exposed to live agent aerosol clouds in the "Eight Ball" chamber tests and in field tests simulating battlefield deployment of biological agents. At the time, tularemia was regarded as an acceptable prototypical BW agent for these tests since there was effective therapy available as well as adequate animal experimental data on safety and protective

efficacy. Parallel experiments exposed both human and rhesus monkey test subjects to aerosols of *F. tularensis* allowing comparison of data parameters for the two species. (PBS 2009).

During the 1950s and 1960s, the human responses to challenges of *F. tularensis* were studied at several centers in the United States. Over 500 subjects challenged with virulent *F. tularensis* Type A were reported in the accessible medical literature over that time. The majority of volunteers were from one of three groups, prisoners, conscientious objectors, or military personnel. Similar human studies were also performed in the former Soviet Union. (Lyons and Wu 2007)

2.   Lung Structure and Particle Dynamics

The Task Group on Lung Dynamics of the International Committee on Radiological Protection (ICRP) proposed dividing the respiratory system into three parts: Nasopharyngeal (NP), Tracheobronchial (TB), and Pulmonary, or Parenchymal (P) (Task Group on Lung Dynamics, 1966). This division was based on function and clearance mechanisms. The NP region extends from the nares to the larynx. It has a mucociliary system which clears larger particles that deposit there in a half-time of 4 minutes. Most particles deposit in the anterior nares, where they are blown out. Particles in the posterior nares clear down to the throat for swallowing in 6-7 hr half-time. (We note that the NP region is alternatively referred to as the Extra-Thoracic (ET) region.) The TB region begins with the larynx, includes the trachea and bronchioles down through the terminal bronchioles. These are all cleared by the mucociliary system with half-times ranging from 0.5 to 5 hr, depending on distance from the larynx and slowing of mucus secretion in the finer airways. Particles inhaled by mouth breathing tend to go directly to this portion. The P region includes the respiratory bronchioles and alveolar components. None have mucociliary mechanisms and, although the alveoli do have a fluid that washes them (often back up to the respiratory bronchioles). The Task Group recommends clearance half-times of 360 days for insoluble particles (such as bacteria) in the P compartment; however, these particles are usually quickly removed by alveolar macrophages into the lymphatic system. As mentioned above, most BW agents are not killed during this process and in fact, thrive and initiate their pathogenic effect while in presumed confinement by the body's immune system. An average of 10 macrophages is present per alveolar sac in humans, far higher than in rodents. Besides the alveoli, macrophages are found near Mucosa-Associated Lymphoid Tissue (MALT), located in the nasopharyngeal (NALT), gut (GALT), conjunctiva (CALT), larynx (LALT), and tonsils (Cesta 2006). These regions have many B and T lymphocytes ready to react to invaders, and the size and presence of these tissues vary between species (For example: tonsils, probably a major initiation site of oropharyngeal tularemia, are not found in rodents). In the blood, macrophages are replaced by monocytes and neutrophils, which attack and engulf *F. tularensis* injected into the bloodstream by ticks, flies and mosquitoes.

Much work on the physical nature of particle deposition in the animal or human respiratory system has been performed with non-toxic substitutes. Also, the objects of the studies are often non-viable compounds found in occupational environments, such as fumes, soot or radioactive particles. As these objects cannot replicate, the focus of these studies was on the amount of substance inhaled and deposited in the lungs. While inhalation of living disease agents does require a certain minimum number of organisms (which varies widely among species), the ability of disease-causing organisms to replicate inside the host is a major feature of pathogenicity.

Production of aerosol particles of specific sizes has been a challenge, with early attempts making particle groups with specific median diameters, but clearly each with a

range of sizes. This project is concerned with the effect of different particle sizes, some much larger than ideal for deep lung penetration, and almost certainly is affected by the requirement of macrophage uptake for many BW agents to cause illness. Holma has suggested the optimal particle size for macrophage uptake to be 1.5 µm (slightly larger than the *F. tularensis* bacterium), with a maximum size of only 8 µm (Holma 1967, Phalen and Raabe 1974).

Harper and Morton were among of the first to study particle size and deposition of bacterial aerosols in the respiratory tract. They exposed guinea pigs and monkeys (presumably rhesus macaques) to radio-labeled *Bacillus subtilis* spores (similar in diameter to *B. anthracis*). (See Table 1.) The 1 micron particles were generated using a Collison atomizer discharging into a closed circuit fed with dry air. They adjusted the concentration and flow so that they achieved an aerosol consisting almost entirely (90%) of single "dry" spores of about 1 micron each in diameter. For the Collison atomizer, no particles exceeded 3 microns. (Harper and Morton 1953)

Table 1. Immediate distribution of retained aerosol (radio-labeled *B. subtilis* spores). Data consolidated from Harper and Morton, 1953.

Species	Particle Diameter (microns)	%Head	%Trachea	%Lungs
Guinea Pig	1	37.0	11.0	52.0
Guinea Pig	2.5	54.8	17.7	27.5
Guinea Pig	3.8-4	66.3	14.8	18.9
Guinea Pig	5.7	94.2	4.2	1.6
Guinea Pig	6.1	87.8	6.6	5.6
Guinea Pig	8.4	96.5	3.2	0.3
Guinea Pig	10	98.2	1.2	0.6
Monkey	1	25.8	0.9	73.3
Monkey	3.8-4	43.6	7.8	48.6
Monkey	5.8	51.0	13.1	35.9
Monkey	8.1	48.2	4.2	47.6
Monkey	11.8	84.7	3.5	11.8

For the data in Table 1, particles of 2.5 to 12 microns in diameter were generated using a spinning disk apparatus. In analyzing the results, they used a head-trachea-lungs grouping. Note the trend towards more product remaining in the head region as the particle size increases, however, also note the monkey retains more in the lungs even at larger particles. This is presumably due to the larger diameter of the monkey bronchiole passages (Harper and Morton 1953)

Table 2 lists other studies in which the deposition of various small particles is measured as percentage found in the P region. No species was specified for the monkey data. (Snipes 1989).

Table 2. Pulmonary deposition for selected laboratory animal species and humans by particle size (Snipes 1989).

Species	*Body Mass (kg)*	*0.5 microns (%)*	*1 microns (%)*	*2 microns (%)*	*5 microns (%)*
Rat	0.25	10	7	7	ND
Guinea Pig	0.7	35	20	30	ND
Monkey	2.4	40	30	20	10
Human	70	15	25	25	10

Cheng and coworkers exposed cynomolgus monkeys (*Macaca fascicularis)* to aerosols of radio labeled particles that were 2 and 5 micron in diameter. The aerosol solutions were generated from a Vero cell supernatant tagged with a Tc-99m radiolabel. Collison and Retec nebulizers were used to generate small and large particles, respectively. The animals were anesthetized, placed in a plethysmograph box, and exposed to the aerosol. The deposition pattern was determined using a gamma camera. The amount of particles remaining in the "head" region (= NP) was 39% for the smaller particle and 59% in the larger ($p<0.05$), and the "lung" deposition (= TB and P) was 12.2% and 8%, respectively (NS). (See Table 3.) These are similar to human deposition, except the human would have somewhat higher percentage of the smaller particle in the TB/P.   Using the non-invasive gamma camera method made it difficult to determine the amount of particles deposited in the TB vs. P regions. (Cheng *et al.* 2008)

 Table 3. Percent deposition of inhaled radio-labeled particles in long-tailed macaque monkeys.

Particle Size μ	% Head	%Lung
2.3	39	12.2
5.1	59	8

Thomas studied particle deposition and infection in a BALB/c mouse model, with emphasis on new equipment to produce large particles. Small particles (1 to 4 μm) were generated by the Collison nebuliser and Henderson apparatus. Large particles (12 μm) were produced by the flow-focusing aerosol generator (FFAG) developed by Ingeniatrics Technologies. In Table 4, note the larger numbers of large particles remaining in the NP region, although the numbers in the P region are rather high compared with Harper and Morton (Table 1). (Thomas 2008)

Table 4. Regional deposition of inhaled *E. coli* MRE 162 in BALB/c Mice.

Particle Size μ	No. in NP	No. in TB	No. in P
1 to 4	6×10^2	2×10^2	8×10^3
12	3×10^4	6×10^2	1×10^3

3.   Tularemia Respiratory Illness in Animals and Humans

F. tularensis infection has been identified in over 300 species of mammals . However, scientists working on the pathogenesis of *F. tularensis* in the early years felt that a human model was the only valid way to study *F. tularensis*. Therefore, much of the early literature examines the response to *F. tularensis* delivered by a variety of routes to human volunteers. As research methodology developed, other species, including mice, rats, guinea pigs, dogs, and monkeys were used to investigate all aspects of infection. The non-human primate model is currently the animal model that best recapitulates the human disease. (McCrumb 1961, Lyons and Wu 2007)

Tularemia is rarely seen naturally in monkeys, as few inhabit the cooler endemic areas of the organism and its reservoirs. One outbreak occurred in an outdoor exhibit of long-tailed macaques in a zoo in Germany. This area of Germany has never reported a human or animal case of tularemia. Eighteen of the 35 monkeys were clinically infected with a regional Type B strain. Five young and one adult animal died of systemic infection, with oropharyngeal lesions predominant in all deaths, leading to speculation that contaminated food or water was the source (Matz-Rensing *et al.* 2007). The rest of the adults became ill with a milder disease as typically observed in humans. Another outbreak in non-macaque monkeys at a Canadian zoo was determined to be caused by wild ground squirrels entering the exhibit and introducing infected fleas (Matz-Rensing *et al.* 2007).

Studies have shown that macaques have very similar susceptibility and clinical responses to Type A *F. tularensis* exposure as humans, especially with the highly virulent strain SCHU S4. This was true whether the bacterium was introduced by aerosol, oral solution, or injection. Macaques also have similar clinical results with Type B *F. tularensis*, with somewhat higher mortality in untreated pneumonic forms, but still having a median lethal dose (LD_{50}) >10^6 inhaled organisms of strain 425 (Schricker *et al.* 1972). Replication in the lung region seems to occur much faster with Type A, with 10^5 more organisms than the inoculum found within 2 days and death in 3 days (Eigelsbach *et al.* 1961). Type B had only a 10^3 increase above the already high inoculum after 6 or 7 days and death, if any, occurred later (Schricker *et al.* 1972). Type B effects were usually limited to the lungs, while Type A would spread systemically before death. See Table 5 (Data summarized from Eigelsbach *et al.* 1961 and Eigelsbach *et al.* 1968)

Table 5. Respiratory virulence and infectivity of *Francisella tularensis* SCHU S4 (Type A) in Rhesus Macaque and Man (Eigelsbach *et al.* 1961 and Eigelsbach *et al.* 1968).

Dose (Organisms)	Macaque Ill / Exposed	Macaque Deaths	Human Ill / Exposed
9-18	19/23 (83%)	9 (39%)	6/8 (75%)
20-52	30/35 (86%)	20 (57%)	10/12 (83%)
132-180	11/11 (100%)	10 (91%)	ND
750*	7/8 (88%)	7 (88%)	ND

*Challenge with SCHU S**5** for controls in vaccine trial

Schricker *et al.* investigated the effects of aerosol exposure of a Type B strain in macaques. Strain 425 aerosols were generated in a large sphere from liquid suspensions with a nebuliser producing particles primarily in the range of 1 to 5 μm in diameter. The aerosols were allowed to equilibrate at 21 °C and 85% relative humidity before the animals were exposed (whole body). Results are shown in Table 6. Significant illness occurred, although the strain was not as virulent as SCHU S4. The pattern of dissemination, multiplication, and clearance of strain 425 in monkeys was dose-related. Incubation periods were shorter, and the illness was longer and more severe with increasing inhaled numbers of organisms. Throughout all doses, the incubation period and duration of acute illness were generally 3 to 7 days and 1 to 3 weeks, respectively. (Schricker *et al.* 1972)

Table 6. *F. tularensis* 425 (Type B) Infection in Rhesus Macaques Following Respiratory Exposure

Dose (Organisms)	% Mild or Moderate Illness	% Severe Illness	% Fatal
10	70	0	0
10^2	95	5	0
10^3	97	0	3
10^4	80	13	7
10^5	80	12	8
10^6	55	27	18

McCrumb vaccinated human volunteers with either an attenuated live vaccine (presumably the LVS strain) or a cell wall antigen vaccine, and then challenged them with various doses of aerosolized virulent strain (see Table 7). Even though all were vaccinated (except the controls), a considerable amount of dose-related illness followed. Two moderate and all severe illness cases were treated with antibiotic. Note all unvaccinated controls were severely ill. (McCrumb 1961)

Table 7. Results of virulent *F. tularensis* aerosol challenge to vaccinated volunteers (McCrumb 1961).

Vaccine	Dose	Asymptomatic	Mild	Moderate	Severe
Cell Wall	200	3	0	2	1
Cell Wall	2000	0	1	1	1
Live Vaccine	200	5	1	0	0
Live Vaccine	2000	3	1	1	0
Live Vaccine	2×10^4	0	0	2	1
Control	200	0	0	0	4
Control	2000	0	0	0	4
Control	2×10^4	0	0	0	2

Sawyer summarized several trials of testing the effect of "aged" aerosols on rhesus macaques and volunteers. Aerosols were generated using a 2-fluid nozzle to disseminate liquid containing 30×10^9 viable cells per milliliter. Aerosol clouds were created and held in a 1,000,000-liter spherical static chamber ("Eight Ball") in the absence of sunlight; the temperature was 24 °C, and the relative humidity was 85%. Biological decay was similar in all tests, 1.5 to 2% per minute. Desired aerosol concentrations were achieved by adjusting the amount of culture disseminated and by diluting the aerosol with clean air equilibrated with chamber conditions. At the time of each exposure, at least 65% of the viable organisms were contained in particles 5 micron or less in diameter. To estimate the distribution of organisms in particles, the GP20 sampler , a non-discriminatory total collector, was employed in addition to the AGI30 with preimpinger. Enumeration of *F. tularensis* was accomplished by serial dilution and plating. Caged monkeys were placed in the test chamber at the equator for 3 or 10 min. A tightly fitting face mask connected to the chamber at the equator was used for human exposure. Subjects inhaled through the nose and exhaled through a mouthpiece connected to filters and an air flow meter. Prescribed volunteer exposure was 10 breaths of 1 liter in 60 seconds. The product of (i)

the duration of exposure, (ii) the respiratory minute volume, and (iii) the concentration of viable organisms in particles 5 microns or less in diameter was taken as the inhaled dose. The effect of aerosol age on infectivity of airborne *F. tularensis* for man and monkey was similar (see Table 8, data summarized from Sawyer *et al.*). Infectivity of aerosols aged 30 and 60 min was comparable to that of dynamic aerosols but was reduced when the clouds were aged 120 or 180 minutes. Neither the incubation period nor the severity of the clinical illness, however, varied with the age of the aerosol. Onset of illness was usually abrupt, and the predominant manifestations were fever, headache, myalgia, anorexia, and retrosternal discomfort. Because human volunteers and monkeys were exposed simultaneously to the same aerosols, a direct comparison of susceptibilities could be made (see Table 9, data summarized from Sawyer *et al.*). Because of their lower respiratory volumes, monkeys exposed for 10 min inhaled approximately the same number of organisms as men exposed for 1 min. (Sawyer *et al.* 1966)

Table 8. Infectivity of aged aerosols of Francisella tularensis for rhesus macaques and human volunteers (Sawyer *et al.* 1966).

Species	*Dose*	*No. Ill / No. Exposed 60 Min*	*No. Ill / No. Exposed 120 Min*	*No. Ill / No. Exposed 180 Min*
Macaque	50	7/8	1/8	1/19
Macaque	150	7/8	10/12	2/20
Macaque	350	12/12	12/12	1/16
Macaque	750	12/12	7/8	3/8
Macaque	2000	4/4	8/8	24/24
Macaque	6500	8/8		28/28
Macaque	25,000	4/4	8/8	20/20
Man	80		0/4	
Man	150	3/4		0/8
Man	350		1/4	0/4
Man	750	4/4		0/4
Man	7500		8/8	8/8
Man	12,500			3/4
Man	50,000		7/8	10/12

Table 9. Direct comparison of susceptibilities of man and monkey to *F. tularensis* (Sawyer *et al.* 1966).

Species	Dose	No. Ill / No. Exposed 60 Min	No. Ill / No. Exposed 120 Min	No. Ill / No. Exposed 180 Min
Man	80-180	3/4	0/4	0/8
Monkey	80-180	7/8	1/4	0/8
Man	700-1000	4/4	1/4	0/4
Monkey	700-1000	8/8	4/4	0/4
Man	5000-15,000		8/8	11/12
Monkey	6000-15,000			12/12

4. Tularemia; Ulceroglandular, Oropharyngeal, Ocular and Enteric Illness in Animals and Humans

In nature, the ulceroglandular form of tularemia is the most common presentation. This infection usually occurs as a consequence of a bite from an arthropod vector which has previously fed on an infected animal. Some human cases occur following the handling of infected meat, with infection occurring via cuts or abrasions. An ulcer develops at the site of infection and the local lymph nodes are enlarged. The lymph nodes are painful, swollen, and may rupture and ulcerate. The ulcer may last from 1 week to several months. With glandular presentation, there is no apparent primary ulcer, but there are one or more enlarged lymph nodes. Ulceroglandular and glandular presentations account for 75-85% of naturally occurring tularemia cases. (USAMRIID 2005)

Oropharyngeal tularemia is a common manifestation in Europe and Asia when patients have drunk contaminated water. Rarely are cases with inflammation of the intestines or mesenteric lymph nodes seen, probably due to the higher doses required. (Kandemir *et al.* 2007 and Hornick *et al.* 1966)

When virulent Type A strains of *F. tularensis* were injected intragastrically into mice, an LD_{50} of 10^6 organisms was noted (1000X more than by inhalation or intradural administration). The initial infection, as with humans, was the mesenteric lymph nodes. The injection bypassed the oropharyngeal region in order to eliminate the chance for inhalation exposure, so no oropharyngeal lesions were noted. (KuoLee *et al.* 2007)

Oral *F. tularensis* infection in humans occurred with 10^9 organisms ingested but not with 10^6 organisms. Illness resembled aerosol challenge and GI symptoms were minimal. No pharyngeal lesions occurred. (Hornick *et al.* 1966).

Oral ID_{50} in rhesus is listed as about 10^7, while for man is similar, but less data is available: $>10^6 <10^8$. Oral LD_{50} for rhesus is about 10^8. All monkeys died after drinking 10^{10} SCHU cells (Hornick *et al.* 1966). All five human volunteers who gargled 10^{10} SCHU developed large painful cervical nodes (oropharyngeal tularemia) which had to be treated immediately with streptomycin. Three of the five drinking 10^{10} of the attenuated LVS also developed cervical adenopathy, but it was much milder. This type of infection did not occur in those taking a capsule of bacteria or in previous aerosol challenges. See Table 10. (Hornick *et al.* 1966 and Tulis *et al.* 1969)

A large outbreak of tularemia occurred in Kosovo in 1999-2000. Epidemiologic and environmental investigations identified sources of infection and modes of transmission. Case and control status was verified by enzyme-linked immunosorbent assay, Western blot, and microagglutination assay. A total of 327 serologically confirmed cases of tularemia pharyngitis and cervical lymphadenitis were identified in 21 of 29 Kosovo municipalities. Matched analysis of 46 case households and 76 control households suggested that infection was transmitted through contaminated food or water and that the source of infection was rodents. Generalized symptoms of tularemia typically included

---

sudden onset of illness, often with high fever, chills, fatigue, headache, pharyngitis, sore joints, chest discomfort, dry cough, vomiting, abdominal pain, and diarrhea. The usual incubation period is 3 to 5 days, although it can be as long as 21 days. An ulcerating lymphadenitis due to tularemia is shown in Figure 2. (Reintjies *et al.* 2002)

Table 10. Oral infectivity of *F. tularensis* SCH S4 for rhesus macaques (Hornick *et al.* 1966).

Dose	Infected (%)	Died (%)	Mean Day of Death
10^4	0	0	--
10^6	100	100	18
10^6	25	25	18
10^8	100	63	11
10^{10}	100	100	5

Figure 2. Ulcerating lymphadenitis caused by F. tularensis *(Reintjies* et al. *2002).*

The oculoglandular form of tularemia is rare and occurs when the conjunctiva becomes infected. This may occur either by rubbing the eyes with contaminated fingers or by splashing contaminated materials in the eyes. Cleaning carcasses or rubbing the area of a tick bite and then the eye can result in this form of tularemia. Clinical presentation involves initial flu-like signs with conjunctivitis and painful swelling of the regional lymph nodes. In severe forms, the conjunctiva may be ulcerated and ocular discharge may be present This phenomenon was observed experimentally in 7 monkeys exposed to aerosols of 12.5 and 24.0 micron particles containing *F. tularensis*. The animals developed severe conjunctivitis accompanied by a purulent discharge from the nose and eyes, a rise in rectal temperature, and an increase in the number of bacteria in the blood. The monkeys that developed conjunctivitis died between 10 to 21 days after exposure. (Day and Berendt 1972)

The typhoidal form of tularemia involves systemic infection and can develop from the oropharyngeal form.

5.   Particle Size Dependence of Infection in Animals and Humans

Much work has been done with particle size effects for different bacterial, viral, and toxin agents on various experimental mammals. All showed a definite trend towards an increasing amount of agent needed as the particle size increases, in other words, smaller particles are much more efficient in causing illness and death. Necropsy studies indicate smaller particles caused more pathogenesis in the P region, as would be expected. Larger particles led to more lesions occurring in the NP and TB regions, as well as more conjunctivitis. Results from some smaller animals, especially the guinea pig, do not correlate well with primates on susceptibility of some agents, regardless of particle size.

Druett *et al.* was one of the first research groups to attempt to produce homogenous batches of aerosol particles of various sizes. They exposed rhesus macaques and guinea pigs to aerosol clouds of *B. anthracis* spores, *Y. pestis* organisms, and *Brucella suis* organisms. Data for guinea pigs are summarized in Table 11. This data is reported in terms of exposure (note that the abbreviation LNt_{50} has the same meaning as LCt_{50}, which is more commonly used today) rather than in terms of dose since the breathing rate of the animals was not determined in the experiments. Furthermore, estimates of retained dose by region of the animal respiratory tract would require either measurement by some method or careful calculations of respiratory mechanics. Druett *et al.*provide further information on the number of organisms per particle for the different particle sizes that would provide a basis for further analysis. (Druett *et al.* 1953, 1956a, and 1956b).

Table 11. LNt_{50} (median lethal concentration-time integral in units of *org-min/l*) for bacterial agents of large and small particles in guinea pigs (Druett *et al.* 1953, 1956a, and 1956b).

Agent	1-micron particles	12-micron particles
Bacillus anthracis spores	0.34×10^6	5.7×10^6
Yersinia pestis	5×10^4	11×10^4
Brucella suis	1.9×10^2	1.2×10^5

Druett *et al.* noted how the majority of lesions were found in the lower lungs with smaller particles, and in the upper respiratory tract with larger particles. In monkeys, aerosols of single spores of anthrax were 14 times more efficient than aerosols of 12 micron particles as compared to 17 times more efficient for guinea pigs as shown in Table 11. Monkeys exposed to clouds of 12 micron particles often developed massive

edema of the face and head but this phenomenon was not observed in monkeys exposed to single spores. (Druett *et al.* 1953)

Table 12 provides further data on particle size effects in guinea pigs. Note how larger doses are needed with larger particles.

Table 12. Average number of particles of each diameter needed to cause effect in guinea pigs after aerosol exposure (Day *et al*. 1960a).

Agent	Parameter	Very Small (1-2 μ)	Small (5-8 μ)	Intermed. (10-12 μ)	Large (18-24 μ)
B. anthracis	LD$_{50}$	2.3 x 10^4	2.2 x 10^5	7 x 10^5	Not determined (ND)
Y. pestis	LD$_{50}$	1.2 x10^4	2.5 x 10^5	4.5 x 10^5	ND
VEE	ID$_{50}$	20	1.9 x 10^4	2.8 x 10^5	ND
C. burnetti	ID$_{50}$	1x 10^6	3.2 x 10^7	2.5 x 10^9	ND

Ongoing work by Thomas has shown that the LD$_{50}$ for *Y. pestis* pneumonic plague in the BALB/c mouse is about 600 cells for 1 to 4 micron diameter particles and about 3000 cells for 12 micron particles (Thomas 2008).

Data from studies of aerosol exposure of various animals and human volunteers to different particle sizes of *F. tularensis* are summarized in the following tables. Table 13 begins with a summary of the number of organisms in particles of four size ranges corresponding to the LD$_{50}$ or the ID$_{50}$ in three species.

In Day and Berendt's (Day and Berendt 1972) study on various particle sizes containing *F. tularensis* organisms, 96 rhesus macaques were exposed to aerosol particles with median diameters of 2.1, 7.5, 12.5, or 24.0 microns. Aerosol particles with diameters ranging from 1 to 5 micron were disseminated with a University of Chicago Toxicity Laboratories (UCTL)-type atomizer fitted with an aerotec tube. Dissemination of relatively homogeneous aerosols of particles larger than 5 microns was carried out with a spinning-top device. The particle size distribution produced by this disseminator was controlled by regulating the speed of the rotor with compressed air. Microscopic sizing and counting of particles, as well as the counting of cells within particles, was carried out with a phase microscope fitted with an eyepiece graticule. Animals exposed to particles whose median diameters were either 2.1 or 7.5 micron were all infected and showed

extensive infection of the lower respiratory tract. Death occurred in these animals 4 to 8 days after exposure. Monkeys exposed to 12.5 or 24.0 micron median diameter particles presented upper respiratory infections with involvement of the cervical and mandibular lymph nodes, evidenced by swelling and abscess formation. Thirty-eight of the 45 animals in this group were infected. Those animals not surviving died from 8 to 21 days after exposure. Seven monkeys exposed to the 12.5 and 24 micron particles developed severe conjunctivitis (ocular tularemia), with a purulent discharge for eyes and nose, fever, and increased bacteremia. All seven of these monkeys died between 10 and 21 days after exposure. As with Druett's work, larger lesions were noted in the lower respiratory system with smaller particles, while larger particles led to smaller lesions, mostly in the NP or TB regions.

Table 13. Range of number of *F. tularensis* cells in particles of four size ranges needed to cause effect after aerosol exposure (Day *et al.* 1960b, Eigelsbach *et al.* 1968, Day and Berendt 1972).

Species	*Parameter*	*Very Small (1-2 µ)*	*Small (5-8 µ)*	*Intermediate (10-12 µ)*	*Large (18-24 µ)*
Guinea Pig	LD_{50}	2-32	$4.7\text{-}8.7 \times 10^3$	$17\text{-}27 \times 10^3$	$125\text{-}230 \times 10^3$
Macaque Monkey	LD_{50}	7-27	50-630	250-1,500	1,600-8,500
Macaque Monkey	ID_{50}	<5	<240	<556	340
Human	ID_{50}	10-52	14-162	ND (<49,000)	ND

Griffith reported some additional data with *F. tularensis* particles in animals using only illness and death as endpoints. Table 14 summarizes the data. No pathology was reported. Larger doses were used with larger particles. Note that only one guinea pig died.

Table 14 Response to intermediate and large *F. tularensis* particles in aerosol exposures on various animals (Griffith 1962)

Species	*Particle Diameter (µ)*	*Dose (cells)*	*No. ill / exposed*	*No. dead / exposed*
Guinea Pig	7	200-2000	ND	1/30

Monkey	8	70	8/12	7/12
Monkey	8	250	19/20	15/20
Monkey	18	1×10^4	3/4	3/4
Chimpanzee	19	7×10^4	2/2	0/2

Table 15 shows similar data obtained with rhesus macaques exposed to the SCHU S4 strain of Type A *F. tularensis*. Larger doses were needed with the larger particles to achieve the same effect.

Table 15. **Response to various sizes of particles containing *F. tularensis* in aerosol exposure on rhesus macaques (Day and Berendt 1972)**

Particle Diameter µ	Dose	No ill/ exposed	No dead / exposed
2.1	5	6/6	1/6
2.1	11	6/6	3/6
2.1	32	6/6	4/6
2.1	65	6/6	6/6
7.5	240	6/6	3/6
7.5	720	6/6	4/6
7.5	2208	6/6	6/6
7.5	4416	6/6	6/6
12.5	556	5/6	3/6
12.5	1141	6/6	5/6
12.5	2745	7/7	6/7
12.5	2.9×10^4	3/3	3/3
24.0	146	2/6	0/6
24.0	873	4/6	1/6
24.0	2315	6/6	2/6
24.0	1.1×10^4	5/5	4/5

Table 16 shows data from human experiments conducted on volunteer inmates of the Ohio State Penitentiary, where respiratory exposures were conducted in a trailer-mounted Henderson-type apparatus. Aerosol concentrations of approximately 1 to 5 cells per liter were employed. Volunteers were exposed to 10 liters of air through masks on ports in the exposure tube. No volunteer was exposed for more than 90 seconds or more than 18 respirations.

Table 16. Volunteer Study with Aerosolized F. tularensis Particles (Saslaw et al. 1961 and Griffith *et al*. 1963).

Particle Diameter μ	Dose	No ill/ exposed
1.0-4.0	10-52	16/20
8.3	14	3 / 4
8.3	162	1 / 2
8.3	983	2/2
8.8	3.4×10^4	2/7
9.6	1.4×10^3	0/8
10.5	4.9×10^4	6/6

Anno and coworkers reviewed and extracted body temperature and symptomatology data from the clinical records of 118 volunteers undergoing medical testing after inhaling various doses of viable, highly virulent *F. tularensis* (SCHU-S4 strain). The individuals were the controls in a series of studies performed to determine the efficacy of LVS vaccine against a variety of challenge inhalation doses ranging from 10 to 62,000 organisms. Table 17summarizes the clinical case data sources utilized in the analysis. (Anno *et al.* 1998)

Table 17. Clinical case records of human aerogenic challenge with F. tularensis (reviewed and analyzed by Anno *et al*. 1998)

Source of Data	Number of Cases	Dose Range (Number of Organisms)
CONTROLS		
Ohio State University	22	10 TO 52
University of Maryland	23	2,100 TO 62,000
U.S. Army Medical Unit Ft. Detrick	73	315 TO 37,663
Total (Controls)	*118*	*10 to 62,000*

The dose response function of tularemia infection for individuals exposed to known amounts of inhaled *F. tularensis* pathogens was calculated based on the 118 clinical cases. Table 18 gives the quantal responses: 0 = no infection or 1 = infection. The criteria applied to the data in order to identify infected individuals were based on temperature measurements normally made every 6 hours. An individual was considered to have a febrile infection when 3 or more sequential body temperature measurements occurred at or above a level of 100 °F. Based on this criterion, Table 18 shows that only 6 individual exposures of the 17 in the dose range of 10 to 45 organisms did not produce infection; all of the cases ranging in dose from 46 to 62,000 organisms produced infection. (Anno *et al.* 1998)

Table 18. 118 clinical case tularemia incidence data aerogenic (SCHU-S4) challenge (from Anno *et al*. 1998).

Individual Dose (Organisms)	Response*
10	0
10	0
10	1
12	0
13	1
13	1
14	1
16	1
17	0
18	1
20	0

20	1
23	1
23	1
25	1
30	1
45	0
≥46**	1

* 0= No, 1 = Yes, **101 cases

6.   The Macaque Monkey as a Respiratory Model

 Macaque monkeys (Genus *Macaca*), especially the rhesus macaque (*M. mulatta*) and the cynomolgus or long-tailed macaque (*M. fascicularis*), have long been used in non-human primate studies. They are common, have a wide range of habitat in the wild, and co-exist well with humans. They are mid-sized for their genus, with the rhesus typically weighing from 2.5 – 5.7 kg for males and 4.7 – 8.3 kg for females, and the long-tailed ranging from 4.4 – 10.9 kg for males and 5.6 – 10.9 kg for females. Experiments usually list somewhat smaller sizes (4-5 kg) and thus are probably not fully grown individuals. Recently, the long-tailed macaque, usually denoted by its confusing nickname, cynomolgus or "dog-milker", has become the monkey model of choice compared to the rhesus. A few laboratories have also worked with the African green monkey, or vervet (*Chlorocebus aethiops*), a similar-sized monkey much studied for viral infections (Layton *et al.* 2008).

 Studies have shown the respiratory system of the macaque to be very similar to humans. However, there are some differences. The tube diameters are about half that of humans, and there is a difference in the number of generations in the lung. In addition, macaques breathe more rapidly than humans.

 The optimal animal model for tularemia should parallel the human infection model as closely as possible. Salient features of human tularemia infections include: (1) type A strain is the most virulent whereas type B strain typically does not cause significant morbidity or mortality in humans; (2) primary organs involved include liver, spleen, and lung; (3) humans are very resistant to live vaccine strains (LVS) and vaccination with LVS by scarification or aerosol delivery results in protection against intradermal and aerosol challenge with virulent strains. With Type A tularemia in humans, a dose of 10 organisms and 15 organisms was adequate for inducing infection via subcutaneous and pulmonary routes, respectively. The incubation period and clinical course of the infection were very reproducible among volunteers. (Lyons and Wu 2007).

 White *et al.* (1964) used primates to evaluate primary pulmonary tularemia infection by aerosols. Deaths occurred with as few as nine organisms, although only 30–50% of primates died when doses were between 9 and 49 organisms. In contrast, 95% of the primates died after an inhalation dose in the range of 132 to 180 organisms. This range of infectivity is similar to studies in human volunteers, all of whom were rescued, of course, with antibiotics. Pathological findings in the monkeys included observable lesions in the lung, spleen and liver at 72 hours post exposure and tracheobronchial lymph nodes were enlarged. (White *et al.* 1964) The time to onset of symptoms (3-7 days) and duration of illness (1-3 weeks) is similar in primates and humans. The primate model also recapitulates the human disease with respect to LVS-induced protection against type A strains. (Lyons and Wu 2007)

Particles in the P region of the respiratory system are removed to the Lung-Associated Lymph Nodes (LALN) at the same rate for humans, dogs, and monkeys, but more slowly in guinea pigs and rats (Snipes 1989).

Monkeys responded well to treatment with either streptomycin or chloratetracycline following illness with *F. tularensis,* SCHU S4 strain, with all 41 treated monkeys surviving vs. none of 9 control monkeys (Eigelsbach *et al.* 1968).

Lyons and Wu completed an extensive review of the literature in order to define the most optimal model(s) for *F. tularensis* infection. . In his review, Lyons summarizes and compares the clinicopathologic changes induced by *F. tularensis* in different species but points out that significantly more information is needed on how various species (particularly the rat, rabbit, and guinea pig) respond to *F. tularensis* infection. Table 19 represents the opinions of Lyons and Wu on the advantages and disadvantages of the models currently known. These authors caution that it is important to remember that the "optimal" animal model may not exist either for tularemia or for many emerging infections. With that possibility in mind, they suggest that we need to consider other options and approaches for improving the methods we have for comparing the responses among species, "potentially through computational strategies that can create correlative algorithms using both positive and negative aspects of the host response." (Lyons and Wu 2007)

Table 19 Advantages and disadvantages of various models for *F. tularensis* infection by the inhalation route as summarized by Lyons and Wu, 2007.

Model	Advantages	Disadvantages
Human	Primary target of new therapeutics and vaccines. Historically reproducible model.	Public perception of high risk
Monkey	LVS vaccine protection is similar to human	High cost and maintenance. Resistance to Type B is low.
Mouse	Low cost. Genetically manipulated strains available. Tools for dissecting the mechanisms of the host immunological response readily available.	Very sensitive to LVS challenge and poor LVS induced protection to virulent strains. Short lived LVS induced protection.
Rat	LVS induced protection similar to man.. Low doses for infection like man.	High survival resistance to LVS and SCHU S4
Rabbit	Sensitive to SCHU S4 and more resistant to Type B	Limited studies available. No immunological tools to define host response available yet.

Guinea Pig	Sensitive to SCHU S4	Limited studies available. No immunological tools to define host response available yet.

7. References

AMEDD 2000, *Cutting Edge: A History of Fort Detrick, Maryland*, Chapter 7 "Opening the Gates", U.S. Army Medical Department (AMEDD), October 2000. www.detrick.army.mil/cutting_edge/chapter07.cfm

Anno,G.H., et al. 1998. Consequence Analytic Tools for NBC Operations Volume 1-Biological Agent Effects and Degraded Personnel Performance for Tularemia, Staphylococcal Enterotoxin B (SEB) and Q Fever, DSWA-TR-97-61-V1, Contract No. DNA 001-94-C-0024.

Celli, J 2008. *Francisella tularensis*. In, *Dangerous Liaisons: The Interaction of Macrophages with Biowar Agents*. Invited Presentation, American Society for Microbiology 6th Biodefense and Emerging Diseases Research Meeting, Baltimore, MD, 24-27 Feb 2008.

Cesta, MF 2006. Normal Structure, Function, and Histology of Mucosa-Associated Lymphoid Tissue. Toxicol Pathol 34:599-608.

Cheng, Y *et al*. 2008. *Aerosol Deposition in Monkeys*, Poster 231, American Society for Microbiology 6th Biodefense and Emerging Diseases Research Meeting, Baltimore, MD, 24-27 Feb 2008.

Day, WC, *et al*. 1960a. The Influence of Aerosol Particle Size on Respiratory Infectivity. I. Exposure of Guinea Pigs to Aerosols of *Pasturella tularensis, Pasturella pestis, Bacillus anthracis, Coxiella burnetii,* and the Virus of Venezuelan Equine Encephalitis. Army Biological Labs, Fort Detrick, Frederick, MD, BL Tech Memo 9-17, ADC322395.

Day, WC, *et al*. 1960b. The Influence of Aerosol Particle Size on Respiratory Infectivity. II. Exposure of Rhesus Monkeys to Aerosols of *Pasturella tularensis*. Army Biological Labs, Fort Detrick, Frederick, MD, BL Tech Memo 9-20.

Day, WC, and RF Berendt, 1972. Experimental Tularemia in *Macaca mulatta*: Relationship of Aerosol Particle Size to the Infectivity of Airborne *Pasturella tularensis*. Infec Immun 5:77-82.

Dennis, DT *et al*, 2001. *Tularemia as a Biological Weapon: Medical and Public Health Management*, for the Working Group on Civilian Biodefense. JAMA 285:2763-2773

Druett, HA, *et al*. 1953. Studies on Respiratory Infection. I. The Influence of Particle Size on Respiratory Infection with Anthrax Spores. J Hyg 51:359-371

Druett, HA, *et al*. 1956a. Studies on Respiratory Infection. II. The Influence of Aerosol Particle Size on Infection of the Guinea Pig with *Pasturella pestis*. J Hyg 53:37-48.

Druett, HA, *et al*. 1956b. Studies on Respiratory Infection. III. Experiments with *Brucella suis*. J Hyg 54 (1):49-57.

Eigelsbach, HT, *et al*. 1961. Aerogenic Immunization of the Monkey and Guinea Pig with Live Tularemia Vaccine. Proc Soc Exp Biol Med 123:732-734.

Eigelsbach, HT *et al*. 1968. Tularemia: The Monkey as a Model for Man. In H. Vagtborg (ed.), Use of NonHuman Primates in Drug Evaluation, A Symposium, Southwestern Foundation for Research and Education, San Antonio, TX. pp 230-248

Feldman, KA *et al*. 2003. Tularemia on Martha's Vineyard: Seroprevalence and Occupational Risk. Emerg Infect Dis. 9:350-354

Griffith, WG. 1962. Infectivity of Large Diameter (8 and 19 Microns) Homogenous Particles of *Pasturella pestis* in Guinea Pigs, Monkeys, and Chimpanzees. Conference on Aerosol Stability and Infectivity, p 63-67. US Army Biological Laboratories, Fort Detrick, MD, Sep 1962.

Griffith, WG, *et al.* 1963. Experimental Tularemia in Man Effect of Particle Size on Airborne Infection. Presented at Quadripartite Chemical-Biological-Radiological Joint Meetings, Conference on Biological Basic Research, Naval Biological Laboratories, Oakland, CA. 7-10 Oct 1963.

Harper, GJ, and JD Morton 1953. The Respiratory Retention of Bacterial Aerosols: Experiments with Radioactive Spores. J Hyg 51:372-385.

Holma, B 1967. Lung Clearance of Mono-and Di-Disperse Aerosols Determined by Profile Scanning and Whole-Body Counting, Acta Medica Scand. Supp 473.

Hornick, RB, *et al*. 1966. Oral Tularemia Vaccination in Man. Antimicrob Agents Chemother. 6:11-14.

Jemski, JV 1961. Respiratory Virulence of *Pasturella tularensis*, SCHU-S4 Strain, for Man. TE-1462.

Kandemir, B, *et al*. 2007. Tularemia Presenting with Tonsillopharyngitis and Cervical Lymphadenitis: Report of Two Cases, Scand J Infect Dis 39:620-622.

KuoLee, R, X Zhao, J Austin *et al.* 2007. Mouse Model of Oral Infection with Virulent Type A *Francisella tularensis*. Infec Immun 75:1651-1660.

Layton, RC, *et al*. 2008. Comparison of Two Nonhuman Primates Primary Pneumonic Plague Models. Poster 045, American Society for Microbiology 6th Biodefense and Emerging Diseases Research Meeting, Baltimore, MD, 24-27 FEB 2008.

Lyons, C. R., and T. H. Wu, 2007. "Francisella Tularensis: Biology, Pathogenicity, Epidemiology, and Biodefense", Ann. N.Y. Acad. Sci. 1105: 238-265

Matz-Rensing, K *et al*. 2007. Epizootic of Tularemia in an Outdoor Housed Group of Cynomolgus Monkeys (*Macaca fascicularis*), Vet Pathol 44:327-334.

McCrumb, FR, 1961. Aerosol Infection of Man with *Pasturella tularensis*.Bacteriol Rev. 25:262-267.

PBS 2009. The American Experience "The Living Weapon", Public Broadcasting System (PBS) Transcript, Chapter 8.
http://www.pbs.org/wgbh/amex/weapon/program/weapon_08.html

Perretta, B. 1999 "Historic Structure Stands as Reminder of Biological Warfare" Capital News Service, Maryland NEWSNET newsnet.umd.edu/history/warstructure04.htm

Phalen RF and OG Raabe 1974. *Aerosol Particle Size as a Factor in Pulmonary Toxicity*, Air Force Technical Report 74-125.

ProMED Mail 2002. Tularemia – Kosovo. ProMED-Mail; 06 Feb: 20020206.3498 <http:promedmail.org>. Accessed 12 Mar 2008.

ProMED Mail 2005a. Tularemia, Oropharyngeal – USA (Massachusetts). ProMED-Mail; 8 Jul: 20050711.1971 <http:promedmail.org>. Accessed 12 Mar 2008.

ProMED Mail 2005b. Tularemia – USA (Massachusetts). ProMED-Mail; 19 Aug :20050819.2438 <http:promedmail.org>. Accessed 12 Mar 2008.

Reintjies, R, *et al.* 2002. Tulareimia Outbreak Investigation in Kosovo: Case Control and Environmental Studies , Emerging Infectious Diseases 8 (1) . www.medscape.com/viewarticle/423528

Roy, CJ, M Hale, JM Hartings *et al*. 2003. Impact of Inhalation Exposure Modality and Particle Size on the Respiratory Deposition of Ricin in BALB/c Mice. Inhal Toxicol 15:619-638.

Saslaw, S., *et al*. 1961. Tularemia Vaccine Study: II – Respiratory Challenge. Arch Ind Med 107:134-146.

Sawyer, WD, JV Jemski, AL Hogge *et al*. 1966. Effect of Aerosol Age on the Infectivity of Airborne *Pasturella tularensis* for *Macaca mulatta* and Man. J Bact 91:2180-2184.

Schricker, RL *et al*. 1972. Pathogenesis in Monkeys Aerogenically Exposed to *Francisella tularensis* 425. Infect Immun 5:734-744.

Siret, V *et al.* 2006. An Outbreak of Airborne Tularaemia in France, August 2004. Eurosurveillance 11:58-60.

Sjostedt, A. 2007. Tularemia: History, Epidemiology, Pathogen Physiology, and Clinical Manifestations, Ann NY Acad Sci 1105: 1–29.

Snipes, MB 1989. Species Comparisons for Pulmonary Retention of Inhaled Particles. (Chapter 7). In *Concepts in Inhalation Toxicology*, pp 193-227.

Task Group on Lung Dynamics 1966. Deposition and Retention Models for Internal Dosimetry of the Human Respiratory Tract, Health Phys. 12:173-208.

Thomas, RJ 2008. *Small and Large Particle Infections of Yersinia pestis.*Poster 151, American Society for Microbiology 6th Biodefense and Emerging Diseases Research Meeting, Baltimore, MD, 24-27 FEB 2008.

Tulis, JJ, *et al.* 1969. Oral Vaccination against Tularemia in the Monkey. Proc Soc Exp Biol Med. 132:893-897.

USAMRIID 2005, "USAMRIID's Medical Management of Biological Casualties Handbook" Sixth Edition, U.S. Army Medical Research Institute of Infectious Diseases, Fort Detrick, Frederick, Maryland, April 2005.
http://www.usamriid.army.mil/education/bluebook.html

White, JD, *et al*. 1964. Pathogenesis of Experimental Tularemia in Monkeys. J Infect Dis 114:277-283.

ATTACHMENT 4

(Next Page)

FXCODA: Tularemia and Ricin Models with Regional Particle Deposition

Darren R. Oldson, Kyle K. Millage, and Gene E. McClellan

Technical Report

2 September 2009

Prepared by:

Applied Research Associates, Inc.
Health Effects and Medical Response Group
801 N. Quincy St.
Arlington, Virginia 22203

Prepared for:

Defense Threat Reduction Agency
Attn: Dr. Christopher Kiley, RD-CBI
8725 John J. Kingman Road
Fort Belvoir, VA 22060-6201

Contract Number: DTRA01-03-D-0014-0025

JSTO Project: CB06MSB096

Preface

The research and development work described in this technical report was conducted for Project CB06MSB096 of the Joints Science and Technology Office (JSTO) of the Department of Defense (DoD) Chemical and Biological Defense (CBD) Program. JSTO is also the Chemical/Biological Technologies Directorate (RD-CB) in the Research and Development Enterprise of the Defense Threat Reduction Agency (DTRA). Project CB06MSB096 is titled *Medical Modeling of Particle Size Effects for Inhalation Hazards*.

Contents

List of Tables

List of Figures

1 Introduction

We have added three new models to FXCODA: a tularemia infection model, a tularemia fatality model, and a ricin fatality model. Each of these models includes a regional particle deposition model based on MPPD (Multiple–Path Particle Dosimetry Model). This technical report describes these models.[1]

2 Regional Particle Deposition Model

FXCODA now includes a particle deposition model that calculates conversion factors for mapping presented dosage to the following four quantities:

1. number of agent–containing particles deposited in the pulmonary region

2. number of agent–containing particles deposited in the extrathoracic region

3. mass of agent deposited in the pulmonary region

4. mass of agent deposited in the extrathoracic region.

Overview of Calculation of Conversion Factors First, FXCODA calculates particle diameters to associate with the given material's particle size bins. If d_i, $i = 0, 1, \ldots n$, are the particle diameters being used as particle size distribution boundaries (shown in the HPAC Material Editor), FXCODA uses

$$g_i = \sqrt{d_{i-1} \cdot d_i}$$

to represent bin i, $i = 1, 2, \ldots n$; i.e., in FXCODA, and in the discussion below, "bin i" refers to particles with diameter g_i. Second, FXCODA calculates constants that relate the presented dosage associated with bin i to the following quantities: (1) number of agent–containing particles (ACPs) deposited in the pulmonary and extrathoracic regions, and (2) mass deposited in the pulmonary and extrathoracic regions.

1. Let D_i denote presented dosage associated with bin i and let $DACP_i^{pul}$ and $DACP_i^{et}$ denote the number of deposited ACPs, associated with bin i, in the pulmonary and extrathoracic regions (respectively). FXCODA uses the following model:

$$DACP_i^{pul} = c_i^{pul} D_i$$
$$DACP_i^{et} = c_i^{et} D_i$$

where

---

[1] The HPAC GUI (Output button → Plot → Custom ... → Class) implies that FXCODA provides a Probability of Illness class for ricin. This class is incomplete (it always returns probability 0). The Probability of Illness class was included for technical reasons regarding the generation of casualty tables.

(1)

$$c_i^{pul} = \text{(number of inhaled ACP, per unit presented dosage, associated with bin } i)\cdot$$
$$\text{(pulmonary deposition fraction for bin } i)$$

(2)

$$c_i^{et} = \text{(number of inhaled ACP, per unit presented dosage, associated with bin } i)\cdot$$
$$\text{(extrathoracic deposition fraction for bin } i)$$

2. Let D_i again denote presented dosage associated with bin i and let m^{pul} and m^{et} denote the deposited mass, associated with bin i, in the pulmonary and extrathoracic regions (respectively). FXCODA uses the following model:

$$m^{pul} = c_i^{pul} D_i$$
$$m^{et} = c_i^{et} D_i$$

where

(3)

$$c_i^{pul} = \text{(number of inhaled particles, per unit presented dosage, associated with bin } i)\cdot$$
$$\text{(pulmonary deposition fraction for bin } i) \cdot \text{(particle mass)}$$

(4)

$$c_i^{et} = \text{(number of inhaled particles, per unit presented dosage, associated with bin } i)\cdot$$
$$\text{(extrathoracic deposition fraction for bin } i) \cdot \text{(particle mass)}$$

Calculation of Conversion Factors Below we describe how FXCODA calculates the right–hand sides of Eqs. 1–4. In these equations, $d = g_i$ for particle size bin i.

- Particle mass (M):

$$M = \frac{4}{3}\pi \left(\frac{d}{2}\right)^3 \rho$$

where d is the particle diameter and ρ is the particle density.

- Number of inhaled particles per unit presented dosage (N):

$$N = \left(\frac{\dot{V}}{M}\right) \cdot I$$

2

where $\dot{V}$ is the respiratory minute volume and I is the inhalability fraction ($\dot{V}/M$ is the number of particles per unit dosage). The inhalability fraction I is defined by

$$I = \begin{cases} I_1(d, U, \dot{V}) & 0 \leq U \leq 4 \\ I_2(d, U) & 4 < U \leq 9 \\ I_2(d, 9) & U > 9 \end{cases}$$

$$I_1(d, U, \dot{V}) = (1 - J)\left(f_N(\dot{V}) \left(1 - \frac{1}{1 + \exp(8.826 - 2.736 \ln d)} \right) + \right.$$

$$\left. f_O(\dot{V}) \frac{1.44}{1 + 0.44 \exp(0.0195d)} \right) +$$

$$J \left(1 - 0.5 \left(1 - \frac{1}{7.6 \times 10^{-4}(d)^{2.8} + 1} \right) + 10^{-5} U^{2.75} \exp(0.055d) \right)$$

$$I_2(d, U) = 1 - 0.5 \left(1 - \frac{1}{7.6 \times 10^{-4}(d)^{2.8} + 1} \right) + 10^{-5} U^{2.75} \exp(0.055d)$$

$$J = \frac{U^{2.75}}{4^{2.75}}$$

$$f_O(\dot{V}) = 1 - f_N(\dot{V})$$

$$f_N(\dot{V}) = \begin{cases} 1 & \dot{V} \leq 35.3 \\ \frac{0.29\dot{V} + 9.9}{0.98\dot{V} + 1.4} & \dot{V} > 35.3 \end{cases}$$

where d is the particle diameter measured in microns, U is the ambient wind speed (in m/s), $\dot{V}$ the respiratory minute volume (in liters/min), and f_N the nasal breathing fraction.

- Number of inhaled ACP per unit presented dosage (N_{ACP}):

$$N_{ACP} = N \cdot \left(1 - \exp\left(-\bar{C}M \right) \right)$$

where $\bar{C}$ is the number of organisms per unit mass.

- Pulmonary and extrathoracic deposition fractions: Given the respiratory minute volume $\dot{V}$ and particle diameter d, FXCODA calculates the pulmonary and extrathoracic deposition fractions using lookup tables generated by MPPD and bilinear interpolation. Graphs of the pulmonary and extrathoracic deposition fractions, for $\dot{V} = 0.015$ m^3/min and $\dot{V} = 0.075$ m^3/min, are shown in Fig. 1.

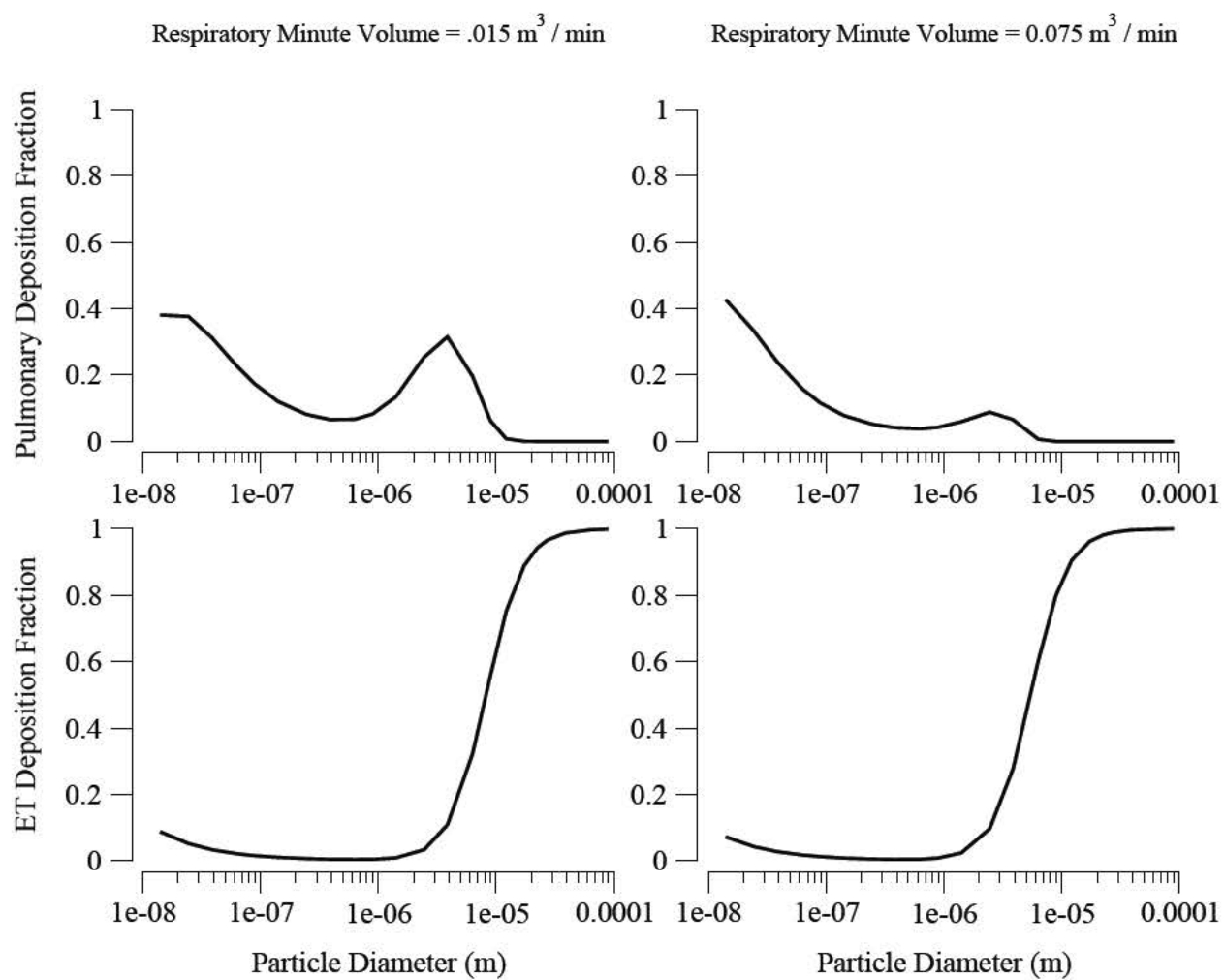Figure 1: Pulmonary and extrathoracic deposition fractions for $\dot{V} = 0.015$ m^3/min and $\dot{V}$ = 0.075 m^3/min.

3 Tularemia Model

3.1 Infection

Overview FXCODA computes the probability of infection P_i by combining the probability of pulmonary infection and the probability of extrathoracic infection. Specifically, given dosage information from HPAC, FXCODA calculates

$$P_i = P_i^{pul} + P_i^{et} - P_i^{pul} P_i^{et},$$

where P_i^{pul} is the expected probability of pulmonary infection and P_i^{et} is the expected probability of extrathoracic infection.

Probability of Pulmonary Infection For a given presented dosage, FXCODA calculates the probability of pulmonary infection, p_i^{pul}, by (1) converting the presented dosage to x, the number of agent–containing particles deposited in the pulmonary region (where x denotes a value of the random variable X), and then (2) calculating $p_i^{pul}(x)$ with a probit model. Given the expected value and variance of the presented dosage (the dosage parameters provided by HPAC), FXCODA calculates the expected value of p_i^{pul} by integrating p_i^{pul} with respect to the distribution of X.

Probability of Extrathoracic Infection Similarly, for a given presented dosage, FXCODA calculates the probability of extrathoracic infection, p_i^{et}, by (1) converting the presented dosage to y, the number of agent–containing particles deposited in the extrathoracic region (where y denotes a value of the random variable Y), and then (2) calculating $p_i^{et}(y)$ with a probit model. Given the expected value and variance of the presented dosage (the dosage parameters provided by HPAC), FXCODA calculates the expected value of p_i^{et} by integrating p_i^{et} with respect to the distribution of Y.

3.2 Fatality

Overview Given dosage information from HPAC, FXCODA computes the probability of fatality P_f by combining the infection model described in Section 3.1 with the original FXCODA tularemia infection and fatality models. Specifically, FXCODA

1. calculates the expected probability of infection P_i as described in Section 3.1

2. calculates an "equivalent" exposure e, where e represents an expected dosage and dosage variance (5 micron particles), such that the original FXCODA tularemia model returns the same infection probability P_i

3. calculates $P_f(e)$ using the original FXCODA tularemia fatality model.

3.3 Casualty Table

Table 1 shows the probability values a_{jk} on which tularemia casualty tables are based.

Table 1: Tularemia casualty table entries (probability values) returned to HPAC.

	Pulmonary	Extrathoracic	All
Fatalities	$a_{11} = P_f \cdot \frac{P_i^{pul}}{P_i}$	$a_{12} = P_f \cdot \frac{P_i^{et}(1-P_i^{pul})}{P_i}$	$a_{13} = P_f$
Injuries	$a_{31} - a_{11}$	$a_{32} - a_{12}$	$a_{33} - a_{13}$
Casualties	$a_{31} = P_i^{pul}$	$a_{32} = P_i^{et}(1 - P_i^{pul})$	$a_{33} = P_i^{pul} + P_i^{et}(1 - P_i^{pul})$

4 Ricin Model

4.1 Fatality

For a given presented dosage, FXCODA calculates the probability of fatality, p_f, by (1) converting the presented dosage to x, the number of micrograms of ricin deposited in the pulmonary region per kilogram of body mass (where x denotes a value of the random variable X) and then (2) calculating $p_f(x)$ with a probit model. Given the expected value and variance of the presented dosage (the dosage parameters provided by HPAC), FXCODA calculates the expected value of p_f, P_f, by integrating p_f with respect to the distribution of X.

ATTACHMENT 5

(Next Page)

Respiratory Effects of HD Exposure in Humans

Sharon A. Watson

Technical Report

15 December 2008

Prepared by:

Applied Research Associates, Inc.
Health Effects and Medical Response Group
801 N. Quincy St.
Arlington, Virginia 22203

Prepared for:

Defense Threat Reduction Agency
Attn: Dr. Christopher Kiley, RD-CBI
8725 John J. Kingman Road
Fort Belvoir, VA 22060-6201

Preface

The research and development work described in this technical report was conducted for Project CB06MSB096 of the Joints Science and Technology Office (JSTO) of the Department of Defense (DoD) Chemical and Biological Defense (CBD) Program. JSTO is also the Chemical/Biological Technologies Directorate (RD-CB) in the Research and Development Enterprise of the Defense Threat Reduction Agency (DTRA). Project CB06MSB096 is titled *Medical Modeling of Particle Size Effects for Inhalation Hazards*.

This report provides a brief review of the effects of sulfur mustard (HD) on the human respiratory system.

Table of Contents

List of Tables

Introduction

On July 12, 1917 on a World War I battlefield near Ypres, Belgium, the German Army delivered artillery shells containing sulfur mustard (HD) resulting in more than 20,000 casualties. Mustard agents accounted for 80% of the chemical casualties in World War I. In 6980 recorded cases of World War I mustard burns, the location of the lesions were as follows:

- eyes   86%
- respiratory   75%
- scrotum   42%
- face   27%
- anus   24%
- legs   11%
- buttocks   10%
- hands   4%
- feet   1.5%.

Less than 5% of mustard casualties who reached medical treatment died, but the mustard injuries were slow to heal and necessitated an average convalescent period of more than 6 weeks. (Dire 2007)

It is important to note that mustard binds irreversibly to tissue within several minutes after contact but the clinical effects of mustard are delayed. Mustard causes tissue damage within several minutes after contact without causing any concomitant clinical effects such as burning or erythema. Because of the lack of immediate symptoms, the exposed person is often unaware of the exposure. Signs and symptoms may appear as early as two hours after a high-dose exposure, but typically there is a latent or asymptomatic period extending to 24 hours at lower doses. Though extremely rare, there are a few reports of individuals exposed to very large amounts of mustard who died within hours. The onset of signs and symptoms are typically between four and eight hours. The ambient atmospheric concentration (C) of mustard vapor, the duration (t) of exposure, the weather conditions, and the body site exposed are the important factors in the onset time. (USMRICD 1995)

Respiratory Effects

Some of the earliest effects from mustard involve the nose, the sinuses, and the pharynx. Respiratory effects develop slowly and usually take several days to reach maximal severity. Symptoms occur first in the upper airways and progress to the lower

airways, most likely because concentration of HD vapor in the inhaled air decreases by absorption as it flow to the lower airways. There may be irritation or burning of the nares, epitasis, sinus pain or irritation, and irritation or soreness of the pharynx at low concentrations. Mucous membrane hyperemia, edema, and necrosis occur after moderate acute exposure. There may be profuse, thin, mucopurulent rhinorrhea and sinusitis developing later. Mucosal findings can range from small discrete ulcerations to extensive sloughing. (USMRICD 1995 and Dire 2007)

Pharyngitis usually appears 1-3 days after inhalation exposure and may occur with nasal involvement. The palate, uvula, tonsils, and pharynx may appear hyperemic and edematous. Multiple whitish ulcerations appear next and vary in size according to severity of the exposure. As the dosage increases other effects occur including laryngitis with voice changes and a nonproductive cough. Laryngeal involvement often resembles that of the pharynx. Edema and necrosis may lead to airway obstruction. Hoarseness is almost always present and may last 3-6 weeks or longer. As shown in Table 1, tissue damage begins in the upper airways and descends to the lower airways in a dose-dependent manner. Damage to the trachea and upper bronchi leads to a cough with production of sputum. Lower airway involvement causes dyspnea as well as an more severe cough and increased quantities of sputum. Necrosis of the airway mucosa with resulting inflammation can cause pseudomembrane formation. Pseudomembranes may occur from the most proximal parts of the airways to the most distal portions. These membranes may cause local airway obstruction at the sites of formation, and detachment may lead to obstruction of lower airways. Usually, the terminal airways and alveoli are affected only for fatal exposures. According to the *Medical Management of Chemical Casualties Handbook,* "terminally, there may be necrosis of the smaller airways with hemorrhagic edema into surrounding alveoli. This hemorrhagic pulmonary edema is rarely a feature unless tissue damage is severe and dosage was high."   (USMRICD 1995, Dire 2007)

The cause of death in mustard poisoning is commonly respiratory failure. Mechanical obstruction by pseudomembranes may be a cause, but more usually deaths result from secondary bacterial pneumonia caused by bacterial invasion of denuded respiratory mucosa and necrotic debris. In World War I, early mortality occurred in slightly more than 2% of US troops exposed to mustard and was caused almost entirely by pulmonary complications. Suppurative bacterial bronchitis and bronchopneumonia are frequent complications. Agent-induced bone marrow suppression is also a contributory factor in later, septic deaths from pneumonia. During the Iran-Iraq War, approximately 10% of the Iranian casualties treated in western European hospitals showed progressive stenosis of the tracheobronchial tree. (USMRICD 1995, Dire 2007).

Table 1. Effects of sulfur mustard (HD) on the respiratory system.

Note: This table was generated primarily from data previously collected in Dire 2007; USAMRICD 1995, Kehe *et al.* 2008, and Veterans at Risk 1993.

Dosage mg-min/m^3 (Ct)	Effect	Time of Onset	Reference
1.0-2.0	Barely detectable odor		Vedder, E.B. 1925, Requena, L. C. *et al.* 1988, Unde and Dunphy 1944
12-70*	Irritated nasal mucosa, hoarse	2hr- 2days	Wachtel 1941,OSRD 1946, PCS 1946
58.5	Nasopharynx membrane exfoliation with no pulmonary symptoms		Sim, V.M. 1971
70-120	Mild inflammation of nose and throat	1-3 days	Henry, M.C. 1991
100	laryngitis, non-casualty		Henry, M.C. 1991
100	Injury to respiratory membrane		US Army 1974
100	Severe effects		NAS 1977
100-250	Mild symptoms		Kadivar, N. and Adams, S.C. 1991
120-200	Hyperemia, hoarse, cough, slight necrosis of membrane	1-3 days	Henry, M.C. 1991
150	ICT50 , sneezing, lachrymation, nose bleed, sore throat		US Army 1990
200	Sneezing, epitasis, sore throat, hoarse, tracheitis,bronchitis, hack, pseudo membrane, pulmonary edema, bronchopneumonia	4-6 hours , bronchial effects in 36-48 hours	PCS 1946
225	incapacitation		Stroykov, Y.N. 1973
240	Damage to respiratory organs		Neyrinck, B. *et al.* 1986
250-500	Severe laryngitis, membrane inflation		Kadivar, N. and Adams, S.C. 1991
133-600	Tracheobronchitis, cough, pseudomenbrane, fever	4-6 hours	OSRD 1946
200-600	Membrane inflation, hyperemia, necrosis with pseudomembrane, aphonia , cough	1-3 days	Henry, M.C. 1991
360	Lung injury		Unde and Dunphy 1944
390	Occasional severe lung injury		Gates and Moore 1946 Norris, G.W. 1918
400-660	Vomiting, frequent and prolonged		Norris, G.W. 1918
360-900	Serious lung injury, pulmonary edema, pneumonia	4-6 hours	Wachtel C., ed., 1941
900	Revised LCT50		NAS 1997
1000	Congested parenchyma, edema emphys, severe bpn	2 days	Gates and Moore 1946
1500	LCT50 respiratory failure, delayed death	4-6 hours	US Army 1990 **

* No significant effect reported at 60 and <70 *mg-min/m^3* by Henry 1991 and Sinclair 1949, respectively

** Numerous studies estimate the LCt$_{50}$ to be between 1000-2100 *mg-min/m^3*.

Toxicokinetics, Mechanism of Action and Pathophysiology

Because mustard agents are very lipophilic, they are absorbed readily across intact skin and mucous membranes. Moisture and heat enhance the penetration. Approximately 20% of HD is absorbed by the skin, while the remainder evaporates. Of the absorbed HD, 10-50% binds to the skin as reacted (fixed) mustard, and the remaining 50-90% is widely distributed in the circulation as unreacted (free) mustard. However, systemic effects of this circulating HD are observed only at high doses. Mustard is eliminated from the body through urination as a by-product of alkylation. (Dire 2007)

After decades of research, no single mechanism or clear understanding has been discovered for the biological damage caused by mustard agents. The toxic effects of mustards depend on their rapid covalent binding to a large number of biological molecules as well as in the formation of a reactive cyclic ethylene sulfonium ion. Mustard agent molecules are highly reactive, containing contain 2 reactive binding groups. Mustards can bind to the base components of nucleic acids and to sulfur in SH-groups in proteins and peptides. Mustards can alkylate DNA, leading to DNA strand breaks and apoptosis. Mustards also bind to cellular glutathione, a very important small peptide crucial to many biochemical reactions as a major free radical scavenger. Glutathione depletion con have a variety of effects including inactivation of enzymes, loss of calcium homeostasis, lipid peroxidation, cellular membrane breakdown, and cell death. According to Dire, individual cell death has been demonstrated in animal models within 2 hours of vapor exposure and general cell necrosis within 12 hours. (Dire 2007)

In general, HD-induced damage of the human respiratory tract is characterized by edema, inflammation and cell death of the airway epithelial lining. Only scarce data are available concerning the effects at the microscopic level. Data are available only from patients who died several days or weeks after exposure. Thus, primary damage and secondary effects are difficult to distinguish. The pathological findings in casualties from lethal gassing during World War I and the Iraq-Iran War are very similar. (Kehe *et al.* 2008, Pappenheimer 1926, Hochmeister and Vycudilik 1989)

HD affects primarily the upper part of the respiratory tract and only persons exposed to severely high dosage show signs of deep pulmonary damage. Most cases show formation of pseudomembranous laryngotracheitis. Pseudomembranes were composed of fibrin and cell debris derived from infiltrating leukocytes and necrotic epithelium. The pseudomembranous laryngotracheitis was characterized by diphtheria-like inflammation with fibrinous deposits. Mucus was observed in the upper respiratory tract: nose, throat, larynx, glottis, and upper parts of the trachea. Paranasal sinuses were affected with varying degree. The epithelial lining of the upper respiratory tract showed signs of necrosis. During days 3–6, necrotic cells appeared in the whole upper respiratory tract. A thick continuous membranous layer was observed lining the uvula, tonsils, epiglottis,

pharynx, larynx, and bronchi. Massive leukocyte infiltration was described leading to bronchial obstruction. Usually the lungs show few or no signs and symptoms. A prominent feature was the engorgement of the blood vessels. The alveoli exhibited signs of emphysema. Only severely intoxicated patients showed signs of lung edema. (Heitzmann 1921, Winternitz and Finney 1920, Kehe *et al.* 2008)

Conclusions

The most serious and debilitating effects of mustard intoxication are its effects on the respiratory tract. This brief literature review was undertaken to collect available data to provide insight concerning mustard's respiratory effects as an aid to development of enhanced predictive modeling of the consequences of mustard exposure, whether accidental or in the event of terrorist attacks.

One finding based on this review is that vapor effects deep in the lungs occur as a primary effect only at very high doses. This finding implies that mustard vapor is absorbed efficiently as gases move into the respiratory track during inspiration, so that very high exposures are required to get significant amounts of vapor deep in the lungs. Thus, an accurate estimation of regional deposition of vapor requires a dynamic calculation of removal of HD from vapor as it passes through the airway generations. Then, estimation of regional deposition of HD due to inhaled aerosols will require a dynamic model of the evaporation of HD droplets as they are inhaled in addition to the calculation of deposition processes for the droplets themselves.

References

Dire, D.J. 2007. CBRNE – "Vesicants, Mustard: Hd, Hn1-3, H" in *Emedicine* from WEBMD, the Continually Updated Clinical Reference. http://www.emedicine.com/emerg/topic901.htm

Gates, M., and Moore, S. 1946. Mustard Gas and other Sulfur Mustards, Chapter 5 pp30-58 in *Chemical Warfare Agents and Related Chemical Problems*, Parts I-II, Washington, D.C.: Office of Scientific Research and Development, National Defense Research Committee. DTIC AD 234270

Heitzmann, O. 1921. Ü̈ber Kampfgasvergiftungen. VIII. Die pathologisch-anatomischen Vera�水nderungen nach Vergiftung mit Dichlordï̈athylsulfid unter Ber̈ucksichtigung der Tierversuche. Z Gesamte Exp Med.1921;13:484–522.

Henry, M.C. 1991. *Literature Review of Sulfur Mustard*. USAMRIID TR-91-01, January 1991

Hochmeister, M, and Vycudilik, W., 1989. *Morpho-toxicologic findings following war gas effect (S-Lost)*. Beitr Gerichtl Med. 1989;47:533–8.

Kadivar, N., and Adams, S.C. 1991. "Treatment of Chemical and Biological Warfare Injuries: Insights Derived from the 1984 Iraqi Attack on Majnoon Island. *Military Medicine*, 156 (4) 171-177

Kehe *et al.*, 2008 "Sulfur Mustard Research—Strategies for the Development of Improved Medical Therapy" Open Access Journal of Plastic Surgery. Eplasty. 2008; 8: e32. Published online 2008 June 10. http://www.pubmedcentral.nih.gov/articlerender.fcgi?artid=2431646

NAS (National Academy of Sciences) 1997, National Research Council, Committee on Toxicology, Subcommittee on Toxicity Values for Selected Nerve and Vesicant Agents, *Review of Acute Human-Toxicity Estimates for Selected Chemical-Warfare Agents*, Washington, D.C.: National Academy Press, 1997.

Neyrinck, B., Wauters, A. Hendrickx, A. 1986. "Treatment of Intoxicated Soldiers by War Gases" pp.539-541. in *Proceedings of the Second World Congress on New Compounds in Biological and Chemical Warfare: Toxicological Evaluation*, Ghent Belgium August 24-27 1986

Norris, G.W. 1918. "Toxic Gases in Modern Warfare" *Journal Am Med Assoc* 71:1822-1825.

OSRD 1946. *Chemical Warfare Agents and Related Chemical Problems*, Parts I-II, Washington, D.C.: Office of Scientific Research and Development, National Defense Research Committee.

Pappenheimer, A.M., 1926. *Pathological action of war gases.* In: Lynch C, ed.Medical Aspects of Gas Warfare. Washington, DC: US Government Printing Office; 1926:87–249.

PCS (Project Coordination Staff) 1946. *Technical Aspects of Chemical Warfare in the Field. Part 2 Discussion of Experimental Data.* Chemical Warfare Service, Washington DC

Requena, L.C. *et al.* 1988. "Chemical Warfare, Cutaneous Lesions from Mustard Gas" J. Am. Acad. Dermatol., 19: 529-536

Sim, V.M. 1971. "Chemicals Used as Weapons in War" In *Drill's Pharmacology of Medicine* 4th Edition McGraw-Hill Book Co. New York

Sinclair, D.C. 1949. "The Clinical Reaction of Skin to Mustard" *Br. Journal of Dermatol. Syph.* 61:113-125.

Stroykov, Y.N. 1973. Medical Aid for Toxic Agent Victims US Army Foreign Science and Technology Center, FSTC-HT-23-1074-73.

Unde, G. and Dunphy, E.B. 1944. *The Effect of Oily Drops on Eyes Exposed to Mustard Vapor.* Porton 2800, Porton Down, England . August 9, 1944

US Army 1974. "Treatment of Chemical Agent Casualties and Conventional Military Chemical Injuries" Chapter 4 1-12, Chapter 5 1-9, Army TMB-285, May 1974

US Army 1990. *Potential Military Chemical/Biological Agents and Compounds*, FM 3-9, NAVFAC P-467, AFR 355-7, December 12, 1990.

USMRICD 1995. "Vesicants" *Medical Management of Chemical Casualties Handbook,* 2nd Edition, US Army Medical Research Institute of Chemical Defense. http://www.fas.org/nuke/guide/usa/doctrine/army/mmcch/index.html

Vedder, E. B. 1925. "The Vesicants" in *The Medical Aspects of Chemical Warfare.* Williams and Wikins Company, Baltimore, Maryland

"Veterans at Risk: The Health Effects of Mustard Gas and Lewisite Chapter 7 Nonmalignant Respiratory Effects of Mustard Agents and Lewisite." 1993 http://books.nap.edu/openbook.php?record_id=2058&page=112

Wachtel C., ed., 1941. *Chemical Warfare*, Brooklyn, NY: Chemical Publishing Co., Inc., 1941.

Winternitz, M.C., and Finney, W.P., 1920, *The pathology of mustard poisoning.* In: Winternitz MC, Milton C, ed. Collected Studies on the Pathology of War Gas Poisoning. New Haven, Conn: Yale University Press;1920:101–13.

DEPARTMENT OF DEFENSE

DEFENSE TECHNICAL INFORMATION CENTER
8725 JOHN J. KINGMAN ROAD, SUITE 0944
FT. BELVOIR, VA 22060-6218
        ATTN: DTIC

QUANTERION SOLUTIONS, INC.
1680 TEXAS STREET, SE
KIRTLAND AFB, NM 87117-5669
        ATTN: DTRIAC

JOINT PROJECT MANAGER INFORMATION SYSTEMS (JPM IS)
JOINT PROGRAM EXECUTIVE OFFICE FOR
    CHEMICAL BIOLOGICAL DEFENSE (JPEO-CBD)
301 PACIFIC HIGHWAY
SAN DIEGO, CA 92110

DEFENSE THREAT REDUCTION AGENCY
8725 JOHN J. KINGMAN ROAD
FT. BELVOIR, VA 22060-6201
        ATTN: DR. CHRISTOPHER KILEY /J9CBA

DEFENSE THREAT REDUCTION AGENCY
8725 JOHN J. KINGMAN ROAD
FT. BELVOIR, VA 22060-6201
        ATTN: MR. RICHARD FRY /J9CBI

DEFENSE THREAT REDUCTION AGENCY
8725 JOHN J. KINGMAN ROAD
FT. BELVOIR, VA 22060-6201
        ATTN: DR. ERIN REICHERT/J9CBM

DEFENSE THREAT REDUCTION AGENCY
8725 JOHN J. KINGMAN ROAD
FT. BELVOIR, VA 22060-6201
        ATTN: DR. RON MERIS /J9ISR

DEFENSE THREAT REDUCTION AGENCY
8725 JOHN J. KINGMAN ROAD
FT. BELVOIR, VA 22060-6201
        ATTN: DR. AIGUO WU /J9ISR

GREAT BRITAIN

DEFENCE SCIENCE AND TECHNOLOGY LABORATORY
CB HAZARD ASSESSMENT,
DETECTION, A117, BUILDING 7,
PORTON DOWN, SALISBURY, WILTS, SP4 0JQ
        ATTN: MR. RICHARD BEEDHAM

DEPARTMENT OF DEFENSE CONTRACTORS

APPLIED RESEARCH ASSOCIATES, INC
SECURITY ENGINEERING AND APPLIED SCIENCES
119 MONUMENT PLACE
VICKSBURG, MS 39180-5156
        ATTN: MR. JOSEPH L. SMITH